

https://dspace.org/

Optimization of the synthesis and performance of Nanocomposite Sodalite/Ceramic membrane for Pre-Combustion CO2 capture

Eterigho-Ikelegbe, Orevaoghene

2020

University of the Witwatersrand, Johannesburg

https://hdl.handle.net/10539/31357

Eterigho-Ikelegbe, Orevaoghene. (2020). Optimization of the synthesis and performance of Nanocomposite Sodalite/Ceramic membrane for Pre-Combustion CO2 capture. [Master's dissertation, University of the Witwatersrand, Johannesburg]. WIReDSpace. https://hdl.handle.net/10539/31357

Downloaded from a DSpace repository. https://dspace.org/

UNIVERSITY OF THE WITWATERSRAND, JOHANNESBURG

Optimization of the Synthesis and Performance of Nanocomposite Sodalite/Ceramic Membrane for Pre-Combustion CO_2 Capture

Orevaoghene ETERIGHO-IKELEGBE

(1794557)

A Dissertation Submitted to the Faculty of Engineering and the Built Environment, University of the Witwatersrand, Johannesburg, in Fulfilment of the Requirements for the Degree of Master of Science in Engineering.

Supervisor: Prof. Michael O. Daramola

Co-supervisor: Dr. Samson Bada

January 2020

Declaration

I, Orevaoghene Eterigho-Ikelegbe (1794557) declare that this dissertation is my unaided work. It is being submitted for the degree of Master of Science in Engineering to the University of Witwatersrand, Johannesburg, South Africa. It has not been submitted before for any degree or examination to any other University.

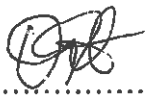

.....

Signature of Candidate

.....24th..... day of ...January.... year ...2020...

Abstract

It is generally accepted by the scientific community that CO_2 is a major greenhouse gas responsible for global warming, marked by an increase in global temperature. Amongst other sequestration options to minimize the impact of CO_2 on the environment, carbon capture and storage (CCS) is essential. The technology already implemented and validated for separating CO_2 from other gases on an industrial scale is the absorption technology using aqueous amine. However, the use of amine scrubbing is a costly operation. Membrane technology is one of the best separation processes adopted for liquid separation, a cost-effective method and is considered for gas separations as the technology is expected to deliver lower energy penalties.

Zeolite-based membranes that can withstand aggressive chemicals, high temperatures and pressure operations are very appealing for use in pre-combustion CO_2 capture. However, zeolite membranes synthesized with zeolite crystals coated on the surface of the support, otherwise known as "thin-film" supported membranes are prone to defects. This leads to loss of selectivity of the membrane. Moreover, the formation of cracks is promoted when thin-film zeolite membranes are exposed to high temperatures, which occur as a result of the huge difference in thermal expansion of the supports in comparison to the zeolite crystals. Nanocomposite zeolite membrane prepared by embedding zeolite crystals within the pores of the support, yields remarkably thermally and mechanically stable nanocomposite membranes.

In this study, sodalite crystals were prepared via the pore-plugging hydrothermal (PPH) synthesis protocols. After evaluating the sodalite crystals, the PPH protocols that yielded high-quality sodalite crystals were then utilized for the synthesis of high-quality nanocomposite sodalite membranes supported on α-Al_2O_3 ceramic tubes. The as-synthesized sodalite crystals were evaluated using techniques such as scanning electron microscopy (SEM) for checking the surface morphology of the as-synthesized sodalite crystals. X-ray diffraction (XRD) was used to check the crystallinity and purity of sodalite crystals, while Fourier transform infrared spectroscopy (FTIR) was used to evaluate the surface chemistry of the as-synthesized sodalite crystals. The quality of the as-synthesized membranes was evaluated using single gas permeation (H_2, CO_2, N_2) and for separating H_2 from H_2/CO_2 in the context of pre-combustion CO_2 capture.

The main findings of the research revealed that the quality of the as-synthesized sodalite crystals can be positively or negatively impacted by adjusting PPH synthesis conditions such as ageing, pre-interruption and post-interruption time. Furthermore, during single gas permeation test of membranes prepared by the best PPH synthesis protocols compared to membranes synthesized via the direct hydrothermal synthesis method, membrane prepared via PPH synthesis using two interruption steps displayed the best performance. The nanocomposite membrane displayed H_2 permeance of 7.97×10^{-7} mol.s^{-1}.m^{-2}.Pa^{-1} at 100 °C and a feed pressure of 0.48 MPa. Consequently, the H_2/CO_2 ideal selectivity at these conditions was 8.76. Regarding H_2/CO_2 mixture, the permeance of H_2 reduced from 8.03×10^{-7} mol.s^{-1}.m^{-2}.Pa^{-1} to 1.06×10^{-7} mol.s^{-1}.m^{-2}.Pa^{-1} when tested at 25 °C and a feed pressure of 0.18 MPa. Also, in the presence of CO_2, nanocomposite sodalite membrane selectivity (i.e. separation factor) reduced to 4.24 at 25 °C and a feed pressure of 0.48 MPa.

Even though adjusting PPH synthesis protocol of sodalite crystal preparation before synthesis of sodalite membrane produced membrane with interesting results, optimizing the PPH synthesis in the presence of the support might yield better results as the support could play a role during sodalite crystal growth to reduce defect formation. The encouraging results as documented in this dissertation provide a platform for further investigation on sodalite/ceramic nanocomposite membrane for efficient pre-combustion CO_2 capture.

Dedication

In memory of my late aunty – Mrs Anna Ono Obrifor (1949-2013)

Acknowledgement

I appreciate God, for, without Him, this work wouldn't see the light of day. The road was rough, but His love for me even when I do reject him kept me going. Thank you for making my life so beautiful. Your Grace is amazing. Oghene doh!

Special thanks to Engr. Ajirioghene E. Agbada and family for giving this dream financial lift. I do appreciate all the love and support. I will not fail to acknowledge the prayers and support of my family – (Mr Patrick, Mrs Regina, Mr Oghenekaro, Dr Omamuzo, Miss Okeoghene, Mr Akpololohor) Eterigho-Ikelegbe. To Mr Okeoghene Obrifor, thank you for always checking and sending messages of hope and encouragements. To my friends Oghenetega U. and Michael A, God bless you guys for epitomizing Proverbs 18:24. I couldn't have asked for more.

To my supervisor, Prof. Michael O. Daramola, thank you for giving this research meaning. Thank you for your patience and guidance throughout the preparation of this dissertation. I am most grateful. To my co-supervisor, Dr Samson Bada, thank you for always checking to make sure the work was progressing. Special thank you to Prof. Falcon Rosemary for her constant encouragements. My appreciations are in order for assisting to support the research financially through the DSI/NRF grant-holder linked bursary.

To Every Nation (EN) Rosebank Church, EN Transformation Vrededorp youth leaders, Thank You. To Prof. Adeshola Ilemobade, thank you for receiving me with open arms, for all the times we spent together, for all the prayers we prayed together and for always reminding me of who I am – God's man.

I thank the Department of Science and Innovation (DSI)/National Research Foundation (NRF) through the South Africa Research Chairs Initiative (SARChI) Clean Coal Technology Grant (Grant Number: 86421) for the financial support received for this research. Opinions, findings and conclusions expressed are those of the author and are not necessarily to be attributed to the NRF.

My sincere gratitude to every researcher of the Sustainable Energy and Environment Research Unit (SEERU), the Clean Coal Technology (CCT) research group, collaborators, and administrative staffs of the School of Chemical and Metallurgical Engineering for their generous

assistance. The Microscopy & Microanalysis Unit (MMU) of the University of the Witwatersrand is also well acknowledged for training and utilization of microscopy instruments.

siyabonga!!!

Publication and Presentation

The following journal articles and conference presentations emerged from this study.

Journal Articles

1. O. Oloye, **O. Eterigho-Ikelegbe**, M.O. Daramola. Synthesis and evaluation of a nanocomposite hydroxy sodalite/ceramic (HS/ceramic) membrane for pre-combustion CO_2 Capture: characterization and permeation test during CO_2/H_2 separation. Journal of *Materials Science for Energy Technologies*. https://doi.org/10.1016/j.mset.2019.10.005.

2. **Orevaoghene Eterigho-Ikelegbe**, Samson Bada, Rosemary Falcon, Michael O. Daramola. Development of pore-plugging hydrothermal synthesis protocol for the synthesis of hydroxy sodalite nanoparticles: Effect of synthesis parameters on crystallinity, seed size and morphology of sodalite crystals. Journal of *Applied Nanoscience* (Submitted).

3. **Orevaoghene Eterigho-Ikelegbe**, Samson Bada, Michael O. Daramola. Performance evaluation of sodalite/ceramic membranes prepared via pore-plugging hydrothermal synthesis method (Prepared).

4. **Orevaoghene Eterigho-Ikelegbe**, Michael O. Daramola. Membranes for CO_2 capture in power plants - opportunity and challenges (In Preparation).

Conference Presentations (Poster and Oral)

1. **Orevaoghene Eterigho-Ikelegbe**, Christin-leigh Eden, Michael O. Daramola., Development of the pore-plugging hydrothermal synthesis protocol for the synthesis of hydroxy sodalite/ceramic membrane for pre-combustion CO_2 capture: Effect of synthesis parameters on crystallinity, *The 10th Trondheim Conference on CO_2 Capture, Transport and Storage (TCCS-10);* Trondheim, Norway, 17 - 19 June 2019 (**Poster presentation)**.

2. **Orevaoghene Eterigho-Ikelegbe,** Michael O. Daramola., Development of pore-plugging hydrothermal synthesis protocol for the synthesis of hydroxy sodalite/ceramic membrane for

pre-combustion CO_2 capture: Effect of synthesis parameters on crystallinity, *8th International Zeolite Membrane meeting, IZMM;* Lulea, Sweden, 16 - 20 June 2019 (**Oral presentation)**.

3. **Orevaoghene Eterigho-Ikelegbe,** Michael O. Daramola., Optimizing pore-plugging hydrothermal synthesis protocol for the synthesis of pure hydroxy sodalite crystals – use of SEM imaging, *Microscopy in Material Science Workshop Programme*; University of the Witwatersrand, Johannesburg, South Africa, 3 December 2018 (**Poster presentation)**.

4. **Orevaoghene Eterigho-Ikelegbe,** Michael O. Daramola., Developing pore-plugging hydrothermal synthesis protocol for the synthesis of defect-free hydroxy/sodalite ceramic membranes for H_2/CO_2 separation, *9th Cross Faculty Postgraduate Symposium*; University of the Witwatersrand, Johannesburg, South Africa, 29-30 October 2018 (**Poster presentation)**.

5. **Orevaoghene Eterigho-Ikelegbe,** Michael O. Daramola., Enhancement of the quality of nanocomposite hydroxy sodalite/ceramic membranes for H_2/CO_2 separation, *DST-UNESCO National Engineering Student Conference;* The Cape Peninsula University of Technology, Symphony Way Bellville, Cape Town, 17 September 2018 (**Oral and Poster presentation)**.

6. **Eterigho-Ikelegbe, O**., Daramola, M.O., Optimization of the synthesis and performance of nanocomposite sodalite ceramic membrane for pre-combustion CO_2 capture, *Carbon Energy and the Environment National Student Colloquium 2018;* North-West University, Northwest Province, South Africa, 21 June 2018 (**Oral presentation)**.

Table of Contents

Declaration ..... **i**
Abstract ..... **ii**
Dedication ..... **iv**
Acknowledgement ..... **v**
Publication and Presentation ..... **vii**
Table of Contents ..... **ix**
List of Figures ..... **xiii**
List of Tables ..... **xvi**
Nomenclature ..... **xvii**
Chapter 1: Introduction **1**
1.1 Motivation and Background 1
1.2 Problem Statement 6
1.3 Research Questions 7
1.4 Research Aim and Objectives 8
1.5 Dissertation Outline 8
Chapter 2: Literature Review **10**
2.1 Fossil Fuel, Carbon Dioxide Emissions and Global Warming 10
2.2 Renewable Energy 15
2.3 Carbon Capture and Storage (CCS) 16
2.3.1 CO_2 transportation and storage 17
2.3.2 CO_2 utilization 18
2.3.3 CO_2 capture 19
2.3.3.1 Post-combustion CO_2 capture 20
2.3.3.2 Oxyfuel Combustion CO_2 capture 21
2.3.3.3 Pre-combustion CO_2 capture 22
2.4 Separation Techniques Considered for Pre-combustion CO_2 Capture 25
2.4.1 Adsorption-based technique for CO_2 capture 25
2.4.2 Membrane-based technique for CO_2 capture 27
2.5 Membranes for CO_2 capture 29

2.5.1 Organic Membrane 29
2.5.2 Mixed Matrix Membrane 30
2.5.3 Metal-Organic Framework Membrane 32
2.5.4 Inorganic Membrane 33
2.5.4.1 Zeolite membrane 36
2.6 Transport Mechanisms in Zeolite Membranes 40
2.6.1 Molecular sieving mechanism 41
2.6.2 Adsorption mechanism 41
2.6.3 Diffusion mechanism 42
2.6.4 Knudsen diffusion mechanism 43
2.7 Synthesis Strategies for Zeolite Membranes 44
2.7.1 Direct hydrothermal synthesis method 45
2.7.2 Secondary seeded growth (SSG) hydrothermal synthesis method 45
2.7.3 Pore-plugging hydrothermal synthesis method 47
2.8 Reported Zeolite Membranes for H_2/CO_2 Separation 48
Concluding Remarks 51
Chapter 3: Experimental Procedures and Analysis 52
3.1 Experimental 52
3.1.1 Chemicals and materials 53
3.1.2 Experimental equipment 54
3.1.3 Description of the membrane module 55
3.1.4 Membrane gas separation equipment 56
3.2 Synthesis of SOD Crystals 57
3.3 Synthesis of SOD/Ceramic Membrane 57
3.4 Membrane Characterization Techniques 58
3.4.1 X-ray diffraction (XRD) 59
3.4.2 Scanning electron microscopy (SEM) coupled with energy-dispersive x-ray spectroscopy (EDS) 60
3.4.3 Fourier transform infrared (FT-IR) 60
3.4.4 Thermogravimetric analysis (TGA) 60
3.5 Membrane Performance Evaluation 61

3.5.1 Single gas permeation 61
3.5.2 Mixture gas separation 63
Concluding Remarks 65
Chapter 4: Development of Pore-Plugging Hydrothermal Synthesis Protocol for the Synthesis of Hydroxy Sodalite Nanoparticles: Effect of Synthesis Parameters on Crystallinity, Seed Size and Morphology of Sodalite Crystals 67
4.1 Introduction 67
4.2 Experimental 69
4.3 Results and Discussion 71
4.3.1 Crystallinity 71
4.3.2 Crystal particle size 74
4.3.3 Morphology of as-synthesized SOD crystals 75
4.3.4 FTIR characterization 78
4.3.5 Thermal stability 79
Concluding Remarks 80
Chapter 5: Preparation and Performance Evaluation of Nanocomposite Sodalite/Ceramic Membranes 81
5.1 Introduction 81
5.2 Membrane preparation, characterization and performance evaluation 82
5.3 Results and Discussion 83
5.3.1 Membrane synthesis and characterization 83
5.3.2 Single gas permeation 87
5.3.3 Mixture gas separation 99
Concluding Remarks 103
Chapter 6: Conclusions and Recommendations 104
6.1 Overall Conclusions 104
6.2 Recommendations 105
References 107
Appendix A: Experimental Equipment 136
Appendix B: Membrane Equipment Process Flow Diagram 140
Appendix C: Procedures for Operating the Membrane Gas Separation Equipment .. 144

Appendix D: Published Works 146
Appendix E: Plagiarism Report 148

List of Figures

Figure 2. 1 World energy demand projections (Adapted from IEA, 2011) 10
Figure 2. 2 Major greenhouse gases (Adapted from IEA, 2018).....12
Figure 2. 3 World CO_2 emission by sector in 2013 (Adapted from IEA, 2015) 13
Figure 2. 4 Rising global temperature and CO_2 (Source: https://www.climatecentral.org/.....14
Figure 2. 5 Carbon capture and storage chain 17
Figure 2. 6 Schematic of post-combustion capture process (Modified from Merkel et al., 2010; Favre, 2011; Rubin et al., 2012) 21
Figure 2. 7 Schematic of oxy-fuel combustion capture process (Modified from Merkel et al., 2010; Favre, 2011; Rubin et al., 2012) 22
Figure 2. 8 Schematic of pre-combustion capture process (Modified from Merkel et al., 2010; Favre, 2011; Rubin et al., 2012) 23
Figure 2. 9 Schematic of a gas separation membrane.....28
Figure 2. 10 Typical ranges of selectivity and H_2 permeance for the three main types of H_2 separation membrane, including carbon molecular sieves (CMS). 1 gas permeation unit (GPU) = 1×10^{-6} cm^3/cm^2 s cm Hg = $3.3e^{-10}$ mol (STP)/m^2/Pa/s. (Adapted from Ku et al., 2011) 35
Figure 2. 11 Representation of each term of the general zeolite expression (Georgiev et al., 2009) 37
Figure 2. 12 Primary building unit of zeolite (left), corner-shared primary building blocks of zeolite (right).....37
Figure 2. 13 (a) molecular sieving (b) Knudsen diffusion (c) convective flow (Adapted from Shao et al., 2009; Al-Mufachi et al., 2015).....44
Figure 2. 14 Nanocomposite architecture versus thin-film architecture membrane.....48
Figure 3. 1 Summary of experimental procedure 52
Figure 3. 2 Picture of typical tubular support (pictures not to scale).....53
Figure 3. 3 Cross-section of the tubular support.....54
Figure 3. 4 Picture of the membrane module used in this study showing graphite seals below (picture not to scale).....55

Figure 3. 5 Schematic of membrane module inside which the synthesized tubular membrane sits in (Modified from Miachon et al., 2007).....56
Figure 3. 6 Illustration of sodalite crystal synthesis with ageing (left) and sodalite/ceramic membrane synthesis 58
Figure 3. 7 Process Flow Diagram (PFD) of the permeation set-up employed for single gas permeation 62
Figure 4. 1 Pore-plugging protocol to produce SOD-a and SOD-b.....70
Figure 4. 2 Pore-plugging protocol to produce SOD-c and SOD-d.....70
Figure 4. 3 Pore-plugging protocol to produce SOD-e and SOD-f 70
Figure 4. 4 Pore-plugging protocol to produce SOD-g and SOD-h 71
Figure 4. 5 Pore-plugging protocol to produce SOD-i and SOD-j 71
Figure 4. 6 X-ray diffraction patterns of as-synthesized SOD-a to SOD-d 73
Figure 4. 7 X-ray diffraction patterns of as-synthesized SOD-e to SOD-j 74
Figure 4. 8 SEM images of the as-synthesized SOD-a to SOD-d 76
Figure 4. 9 SEM images of the as-synthesized SOD-e to SOD-j 77
Figure 4. 10 FT-IR spectra of the as-synthesized SOD-a to SOD-j.....78
Figure 4. 11 TGA curves of SOD nanoparticles of SOD-a, SOD-e, and SOD-i.....80
Figure 5. 1 (a) XRD patterns of membrane M1, M2, M3, M4 (b) XRD patterns of membrane B1, B2 84
Figure 5. 2 SEM micrographs of (a) support top view, (b) support inner layer, (c) support cross-section.....85
Figure 5. 3 SEM micrographs of (a) SOD crystals collected from the bottom of the autoclave, (b) membrane surface (M1), (c) membrane cross-section (M1) 86
Figure 5. 4 SEM micrographs of (a) SOD crystals collected from the bottom of the autoclave, (b) membrane surface (B1), (c) membrane cross-section (B1).....87
Figure 5. 5 Relationship between permeance and kinetic diameter.....89
Figure 5. 6 Relationship between permeance and kinetic diameter.....90
Figure 5. 7 Effect of permeation temperature on H_2, CO_2, and N_2 permeance 91
Figure 5. 8 Effect of permeation temperature on H_2, CO_2, and N_2 permeance 92
Figure 5. 9 H_2, CO_2, and N_2 permeances as a function of feed pressure at 25 °C.....93
Figure 5. 10 H_2, CO_2, and N_2 permeances as a function of feed pressure at 25 °C (B1, B2) 94

Figure 5. 11 Ideal selectivity of H_2/CO_2 as a function of feed pressure 95
Figure 5. 12 Ideal selectivity of H_2/CO_2 as a function of temperature at 0.18 MPa.....96
Figure 5. 13 Ideal selectivity of H_2/CO_2 as a function of temperature at 0.48 MPa.....97
Figure 5. 14 Pressure dependence of permeance through SOD membrane M4 in H_2/CO_2 mixture at 25 °C.....99
Figure 5. 15 Pressure dependence of permeance through SOD membrane B1 in H_2/CO_2 mixture at 25 °C.....100
Figure A. 1 A 45 mL capacity autoclave (left) and LABOTEC EcoTherm® oven (right) 136
Figure A. 2 A 250 mL capacity autoclave.....136
Figure A. 3 Membrane testing rig (a) front view (b) side view.....137
Figure A. 4 Picture of feeding cylinders to the membrane gas separation testing rig 138
Figure A. 5 Picture of Bruker 430-GC used in this study.....139
Figure B. 1 Detailed process flow diagram with component list 140

List of Tables

Table 2. 1 Properties of common hydrogen-selective membranes (Adhikari and Fernando, 2006; Ockwig and Nenoff, 2007) 36
Table 2. 2 Typical pore sizes of zeolites (Petrov and Michalev, 2012; Mohammadi and Maghsoodloorad, 2013) 38
Table 2. 3 Selected results of some inorganic zeolite membrane 50
Table 3. 1 Property of raw support 54
Table 3. 2 Properties of gases used in this study (Shao et al., 2009; Ghadimi et al., 2014; Kosinov et al., 2016) 61
Table 4. 1 Estimated SOD crystal sizes 75
Table 5. 1 Conditions for synthesis of SOD/ceramic membrane 83
Table 5. 2 Permeation results at 25 °C and 0.18 MPa 88
Table 5. 3 Comparison of membranes tested in this work compared to literature under relatively similar test condition 98
Table 5. 4 H_2/CO_2 mixture separation factor of sodalite membrane M4 and B1 100
Table 5. 5 Comparison of mixture gas separation data of the SOD membrane in this study with other membranes in the literature 102

Nomenclature

List of Abbreviations

Abbreviation and acronyms	Full Meaning
CCS	Carbon capture and storage
FTIR	Fourier transmission infra-red
SEM	Scanning electron microscopy
XRD	X-ray diffraction
EOR	Enhanced oil recovery
GHG	Greenhouse gas
NO_2	Nitrogen dioxide
SO_2	Sulphur dioxide
H_2	Hydrogen
CO	Carbon monoxide
WGS	Water gas shift
IGCC	Integrated gasification combined cycle
ASU	Air separation unit
PPH	Pore-plugging hydrothermal
SOD	Sodalite
IEA	International energy agency
IGCC	Integrated gasification combined cycle
AGR	Acid gas removal
BP	British petroleum
CCU	Carbon capture and utilization
PCC	Post-combustion capture
GCI	Global CCS institute
DH	Direct hydrothermal
SSG	Secondary seeded growth
IEAGHG	IEA Greenhouse gas R&D programme

Abbreviation and acronyms	Full Meaning
MOF	Metal organic framework
MMM	Mixed matrix membrane
ZIF	Zeolitic-imidazolate framework
DDR	Deca-dodecasil 3R (DD3R)
TMP	Trans-membrane pressure
TGA	Thermogravimetric analysis
IS	Ideal selectivity
SF	Separation factor

Units of measure / Symbols

Symbols	Meaning
°C	degree centigrade
KPa	kilopascal
nm	nanometer
y	mole fraction
P	pressure
p	partial pressure
A	membrane area
%	percentage
s	second
n	amount of gas
mol	mole
t	permeation time period
g/mol	molecular weight
f	molar flow rate
F	flux
ml/min	milliliter/min
S	selectivity
Q_{stp}	flow rate at standard temperature and pressure
ΔP_{in}	logarithmic mean pressure

Notations

Greek letters

Π	permeance ($mol.s^{-1}.m^{-2}.Pa^{-1}$)
α-Al_2O_3	alpha-alumina

Subscript

i	specie i
j	specie j
f	feed side
p	permeate side
r	retentate side

Chapter 1: Introduction

In this chapter, the motivation and background of the study are clearly presented. The aim, research questions, and structure of the dissertation are also outlined.

1.1 Motivation and Background

The intergovernmental panel on climate change (IPCC, 2018) considers carbon dioxide (CO_2) as a major greenhouse gas responsible for global warming. The combustion of fossil fuel to produce electrical energy is the principal anthropogenic source of CO_2, which accounts for about three-quarter of total anthropogenic emissions of CO_2 worldwide (Rubin et al., 2012; Hammond and Spargo, 2014). According to the international energy agency report (IEA, 2019), coal remains a major component of global fossil fuel supplies, accounting for 27 % of all energy used worldwide and makes up 38 % of electricity generation. This is unlikely to change significantly in the coming decades (EIA, 2016), despite its serious impacts on our health and environment.

Renewable biomass, solar, wind energy, nuclear, hydrogen fuel and carbon sequestration have been identified as techniques for stabilizing greenhouse gas (GHG) concentration in the atmosphere. Carbon sequestration, otherwise known as carbon capture and storage (CCS) is a clean coal technology, which enables the continued use of fossil fuel sources (Daramola et al., 2017). The CCS technology when added to other GHG emission strategies can lower the cost of mitigating climate change. It is also regarded as the only technology option capable of significantly reducing CO_2 emissions from coal power generation plants (IEA, 2013a, b). The capturing of CO_2 from coal-derived power generation plant or large point sources is achieved under three technological pathways – post-combustion, pre-combustion and oxyfuel combustion (Gibbins and Chalmers, 2008). For traditional coal-fired plants, coal is combusted with air to give a flue gas consisting mainly of CO_2 and nitrogen (N_2). Because CO_2 is captured at the end of the combustion process, it is referred to as post-combustion. Capturing CO_2 via the pre-combustion pathway occurs by converting syngas produced from gasification to CO_2 and hydrogen (H_2). By so doing, CO_2 from the syngas stream can be captured before combustion of the H_2 rich gas for use in the gas turbine. Pre-combustion capture pathway applies to the integrated gasification combined cycle (IGCC) plant, in which chemicals, hydrogen, different fuels, along with syngas can be co-produced

from coal and coal/biomass-mixtures in an environmentally responsible manner (Schwartz and Makuch, 2013). Pre-combustion capture is also applicable to steam reforming of natural gas where pure hydrogen is needed to drive fuel cell applications. Various developmental IGCC technology projects have demonstrated the production of high-pressure syngas where CO_2 capture technology can be applied relatively easier (Figueroa et al., 2008). If a specific technology can produce H_2 and CO_2, significant savings can be earned from avoiding recompression costs and plant economics would be further enhanced. For carbon storage that requires very high compression of the CO_2, it will be of huge benefit.

The technology already implemented and validated for separation of CO_2 is the absorption technology (Albarracin Zaidiza et al., 2015; Zhao et al., 2016). Absorption is very effective for post-combustion CO_2 capture. However, when integrated with a power plant, the efficiency of the plant decreases by 8-14 % points due to high energy requirements for solvent regeneration (Wang et al., 2015a; Zhao et al., 2016). The acid gas removal (AGR) process uses a solvent to absorb flue gas followed by regenerative stripping of the CO_2-rich solvent to release CO_2 is applied to capture CO_2 under pressure (Gazzani et al., 2014). The challenge of using chemical solvents in the AGR process is that it requires a large amount of steam-heat for solvent regeneration (Figueroa et al., 2008). Because of the high partial pressure of CO_2 available for gasification and in IGCC, physical solvent is the preferred solvent to capture CO_2. Physical solvents dissolve acid gases without a chemical reaction, preferentially with increasing pressure (García et al., 2011). However, the use of physical solvents generally results in a higher capital cost and work best when the operating temperature is low, below 40 °C (Davidson, 2011). By applying the AGR process for high-temperature processes like IGCC plant, it is therefore required that syngas be cooled. By cooling the syngas, water condenses from it which goes along with loss of energy and mass. If the AGR process could be achieved at the temperature of the outlet of the shift reactor (i.e. high temperature), the energy losses would be lower and the gas approaching the gas turbine will have more motive mass (GCI, 2012). Also, by using either chemical or physical solvents to capture CO_2 via pre-combustion, compression energy is required in raising the pressure of CO_2 for storage (GCI, 2012, Rubin et al., 2012).

The cost of installing a full CCS facility to generate electricity from a fossil power plant, for example, is dominated by the cost of capture (IPCC, 2005). Budinis et al. (2018) identified this as

a major barrier to CCS adoption. The cost of capture according to the IEA (2013) report, constitute between half and two-thirds of the total cost of CCS. Using conventional regenerative amine scrubbers, avoided cost of CO_2 capture is around $57 - 60/tonne (D'Alessandro et al., 2010). Thus, the major drive in research, development and demonstration (RD&D) for IGCC designs with capture is to reduce this energy penalty and cost through material development.

Membrane-based separation is a niche separation technology which is expected to deliver lower energy penalties, cost and smaller carbon footprint (Lin et al., 2015). A membrane is a permeable barrier that behaves like a filter or sponge to separate one or more gases from a feed mixture. Membrane skids are compact, modular which enables capture systems to be fit into existing plants with little available space and requires little chemical compared to conventional separation processes (Koros, 2004; Kosinov et al., 2016; Rahman et al., 2017). These properties make scaling up easy for membrane-based separation and it is considered attractive for CO_2 capture from emissions of power plant and industrial flue gas streams based on fossil-fuel. Commercially, membrane technology is already being used for removing CO_2 from natural gas at high pressure and having high concentrations of CO_2 (Yeo et al., 2012; Abanades et al., 2015). However, the separation processes using membranes in power generation plants is fundamentally different from the natural gas process. The driving force of a membrane-based separation system is pressure driven. It is a total contribution of both the pressure of the inlet gas stream and the net pressure difference across the membrane. The different gas stream properties i.e. available CO_2 partial pressures, low driving force, low concentration of CO_2 in the flue gas, and the flow rate of flue gas which is 5-10 times more than streams of natural gas and chemical industries that is generally treated (Merkel et al., 2010) makes membrane application not attractive and limited for post-combustion capture. The high-pressure feed from the water gas shift in an IGCC plant and moderate concentration of CO_2 in the feed stream provides a good basis for pre-combustion capture gas separation using a membrane.

CO_2 and H_2 selective membranes can find application for CO_2 separation in a process like IGCC. However, research is focused more on H_2 selective membrane for pre-combustion CCS. This is because the pressure of CO_2 in the retentate stream will remain high, which can conveniently be compressed for transportation and storage at low cost (He and Hägg, 2012). Materials that have been explored in developing H_2 selective membranes include, but not limited to dense metals,

polymers, metal-organic frameworks, microporous amorphous silica, zeolites, carbon molecular sieves, and ceramic, etc. (Lockwood, 2014). Polymeric membranes, which are totally organic, are popular and have received wide research efforts. These membranes have been developed for gas separations on an industrial scale. The techniques for the production of polymeric membranes are very mature and membranes produced thereof have displayed good separation performance (Sanders et al., 2013). However, polymeric membranes suffer from low thermal stability and poor chemical resistance (Bernardo et al., 2009; Kosinov et al., 2014). These inherent limitations faced by the polymeric membranes have led to the development of inorganic membranes such as silica, metallic, ceramics, zeolites, metal oxides, and carbon-based molecular sieves (Ockwig and Nenoff, 2007; Li et al., 2015). The inorganic membranes are known to possess thermal resistance and mechanical strength allowing high temperature and pressure operations (Bernardo et al., 2009; Lin et al., 2002; Huang et al., 2012; Wang et al., 2015b). Among these materials, zeolites which belong to the class of microporous aluminosilicates are considered promising candidates for separation and gas purification (Busca, 2017). This is due to their ordered pore size, molecular sieve properties, potential to achieve high flux, high selectivity, and stability at higher temperatures and corrosive environments (Gu et al., 2008; Shan et al., 2011; Vaezi and Babaluo, 2014).

One of the promising members of zeolites that have received interest for the development of molecular sieve membranes in separation application is sodalite (SOD) (Khajavi et al., 2007a, 2010a; Daramola et al., 2015b, 2017; Kalantari et al., 2015). SOD is a zeolite which has a cage dimension of 0.29 nm. The material has channel apertures formed by six-oxygen ring and forms a cage structure known as β-cage (composite building unit). Properties such as high stability up to 450 °C (Khajavi et al., 2007a, 2010a) with good chemical resistance (Daramola et al., 2015b) makes SOD a promising material for use in the fabrication of molecular sieve membranes for gas separation. SOD membranes have displayed good result for water separation (Khajavi et al., 2007a, 2007b, 2010b). Application of SOD membrane has also been demonstrated for water purification (Lafleur et al., 2017). Daramola and his co-workers have embedded SOD crystals inside polyethersulfone membrane and applied it for acid mine drainage treatment (Daramola et al., 2015a).

Despite the progress made so far, obtaining zeolite membranes displaying appreciable flux, selectivity and reproducibility is still a challenge (Daramola et al., 2012). Several factors such as

the formation of defects (cracks and pinholes), presence of impurities (e.g., the formation of other zeolites), size of particles, synthesis technique etc. could be mitigating factors towards achieving this goal. For separations that rely on molecular sieving or size and shape selectivity, defects in the form of micropores larger than the zeolite pores that form during synthesis are very critical and significantly reduces zeolite performance (Gu et al., 2008; Feng et al., 2015). To minimize or eliminate defect in zeolite membrane, post-synthetic treatments have been attempted to block/repair non-zeolitic pores in membranes to improve selectivity (Li et al., 2007; Simon et al., 2019; Zhu et al., 2019). However, post-synthetic deposition treatment leads to reduced permeance and changes the properties of the membranes (Maghsoudi, 2016). Another approach commonly explored by researchers to increase membrane selectivity is through modification of the membrane surface layer (Hong et al., 2005, Gu et al., 2008; Roy and Das, 2019; Shrestha and Dutta, 2019). Optimized films have shown superior performance for the separation of organic mixtures. However, the end product of this approach is the formation of thin-film zeolite membranes which is compounded when thin-film of zeolite crystals are supported on ceramic or perforated stainless steel or sintered glass (Miachon et al., 2007; Daramola et al., 2009). Because of the huge difference in thermal expansion of these supports in comparison to the zeolite crystals, the formation of cracks and pinholes is promoted. Formation of cracks in membranes is detrimental to the selectivity of the membrane. Further promotion of the formation of cracks due to abrasion during membrane assembly is possible for thin-film membranes prepared by direct hydrothermal synthesis. In other to reduce/control the influence of support over the permeation characteristic of the resulting zeolite membrane prepared by direct hydrothermal synthesis, some researchers have resorted to preparing membranes in two stages. First, by carrying out homogenous synthesis in the absence of the support to yield colloidal zeolite crystals and then using the synthesized zeolite crystals as seeds deposited on the support to coat the support surface (Wang et al., 2015b; Yang et al., 2016). The advantage of this approach is that nucleation and crystal growth process are decoupled, allowing for independent control of each step and greater flexibility in choosing hydrothermal synthesis condition (Tsapatsis and Gavalas, 1999; Bernardo et al., 2009). However, the drawback of this technique is that formation of defects otherwise known as “non-zeolitic pores” are easily formed which promote intercrystalline pathways larger than the zeolite pores, hence lowering the selectivity of the membrane (Bernardo et al., 2009). Moreover, weak adhesion or interaction between the zeolite layer and the support surface may occur therefore lowering its reproducibility.

Membranes synthesized using this approach were found to be relatively thick which provided large transport resistances (Wang et al., 2015b; Yang et al., 2016).

To overcome these problems, Miachon and his co-workers proposed a pore-plugging hydrothermal (PPH) synthesis method (Miachon et al., 2006) in which the zeolite crystals are embedded within the pores of the support by interrupting the synthesis. By so doing, expansion of crystals is limited to the pore size of the support and the effects of abrasion which could promote defects/intercrystalline pores formation during membrane handling is prevented (Alshebani et al., 2008b; Daramola et al., 2010a,b). According to Julbe et al. (2003) and Li et al. (2008), the internal layer of an infiltrated support can contribute to resisting gas transport which may not be positive for obtaining high fluxes. However, the fact that the nanocomposite layer is not susceptible to defects, has higher thermal shock resistance, can provide improved membrane separation performance compared to thin-film or surface layer makes it highly attractive for use in high-temperature environments. MFI membranes prepared via PPH have been demonstrated to exhibit better performance, particularly membrane selectivity when compared to ceramic supported with a thin-film layer of zeolite for xylene separation (Daramola et al., 2009; Daramola et al., 2010a,b), and for N_2/CO_2 separation (Alshebani et al., 2008a).

1.2 Problem Statement

Sodalite (SOD) supported membrane prepared via pore-plugging hydrothermal (PPH) synthesis has been demonstrated for water purification (Lafleur et al., 2017). But as far as could be ascertained, little or no report in the literature appear on the development and application of SOD supported membranes prepared via PPH synthesis for CO_2 capture (especially H_2/CO_2 separation). The first open report, which was a preliminary study, was reported by Daramola et al. (2015b). The authors investigated the mechanism involved in the formation of the SOD crystals and the nanocomposite architecture via the PPH hydrothermal technique. Their findings speculated that primary nucleation occurs at the pre-interruption stage which resulted in the formation of smaller crystals and secondary nucleation occurred at the post-interruption stage which increased the growth rate of the crystals. Daramola et al. (2017) synthesized SOD/ceramic membrane via the PPH synthesis and reported on the synthesis and morphological characterization of SOD membrane supported on α-alumina ceramic tube. The authors further

compared the thermal stability of the as-synthesized nanocomposite membranes to thin-film SOD membrane using similar membrane support. The nanocomposite membrane displayed higher thermal stability compared to its thin-film counterpart. However, no dynamic tests were carried out. By conducting single gas permeation test and H_2/CO_2 separation test, the performance of a membrane for pre-combustion CO_2 application can be evaluated. Oloye et al. (2019) recently reported the procedure developed by Daramola et al. (2017) in preparing nanocomposite SOD/ceramic membrane, but via one-stage and two-stage PPH synthesis. The authors reported SOD fully plugged the 200 nm layer of the α-alumina ceramic support. However, the nanocomposite SOD/ceramic membrane prepared was moderately selective towards hydrogen. Moreover, the authors did not conduct single gas and mixture gas separation test, hence, no information about the real selectivity of the membrane was reported.

It is noteworthy to mention that the formation of high-quality nanocomposite SOD membranes prepared via PPH synthesis is premised on the availability of high purity SOD crystals. Obtaining high purity SOD crystals during PPH synthesis depends on the synthesis conditions which control the interplay between nucleation and growth during the synthesis. Hence, adjusting some synthesis variables could have a significant impact on the SOD zeolite membrane performance produced thereof. Therefore, the development and optimization of the pore-plugging hydrothermal synthesis protocol to synthesize high-purity SOD crystals before synthesizing nanocomposite SOD/ceramic membrane could be instrumental in producing high-quality defect-free SOD/ceramic membrane with reasonable selectivity applicable for pre-combustion application.

1.3 Research Questions

The following questions were addressed in this study:

1. What optimized synthesis protocol via the pore-plugging hydrothermal synthesis technique will yield sodalite crystals having desirable crystallinity and morphology?

2. Will the use of the optimized pore-plugging hydrothermal synthesis protocol in (1) leads to the synthesis of high-quality nanocomposite sodalite/ceramic membrane for CO_2 separation?

3. What is the performance of the nanocomposite sodalite/ceramic membrane obtained via the pore-plugging hydrothermal synthesis in comparison to that of thin-film sodalite/ceramic membrane?

1.4 Research Aim and Objectives

This study aims to investigate the effect of different synthesis variables on the quality and size of sodalite crystals prepared via pore-plugging hydrothermal (PPH) synthesis and to employ the best PPH protocols to develop high-quality defect-free sodalite/ceramic membrane usable in pre-combustion CO_2 capture.

The specific objectives of this research were as follows:

1. To produce and evaluate sodalite crystals prepared via the pore-plugging hydrothermal synthesis protocol by varying interruption time and synthesis temperature.

2. To utilize the best pore-plugging hydrothermal synthesis protocols in objective (1) for the synthesis of high-quality nanocomposite sodalite membrane supported on ceramic tubes.

3. To evaluate the quality of the membranes prepared in objective (2) via single gas permeation test then compare their performance with as-prepared thin-film sodalite membrane.

4. To investigate the mixture gas separation of the best performing membranes in objective (3).

1.5 Dissertation Outline

Chapter 1 presents the background information and motivation for the study.

Chapter 2 provides a short overview of carbon capture and storage (CCS). Also, state-of-the-art on the development of membranes applicable in CCS is provided.

Chapter 3 describes the general methodology used in the study. This chapter also describes the optimization procedure of the pore-plugging hydrothermal synthesis of sodalite crystals.

Synthesis/preparation of sodalite membrane and the characterization techniques used are also described under this chapter. The performance evaluation of the as-synthesized sodalite membranes was described in detail under this chapter.

Chapter 4 discussed the effect of synthesis variables on the quality of sodalite crystals produced via the pore-plugging hydrothermal synthesis technique, and the results obtained were compared with those in the literature. A manuscript from this chapter has been developed and is under review in the journal of *Applied Nanoscience.*

Chapter 5 presents the separation performance of the as-synthesized membranes developed via the optimized pore-plugging hydrothermal synthesis protocol, using single gas of H_2, CO_2, and N_2 and binary mixture of H_2/CO_2 as evaluation criteria. The performance of the as-synthesized nanocomposite membranes was then compared with thin-film sodalite membrane synthesized via direct hydrothermal synthesis technique. A manuscript from this chapter has been prepared and due for submission.

Chapter 6 summarized the general conclusion of the study. This chapter also provided relevant recommendations for future studies.

References to all articles and sources used in this study are provided at the end of this dissertation. Whilst other important information related to this study are presented in the Appendix section.

Chapter 2: Literature Review

In this chapter, a short overview of carbon capture and storage (CCS) is discussed. In addition, state-of-the-art on the development of membranes applicable in CCS is provided.

2.1 Fossil Fuel, Carbon Dioxide Emissions and Global Warming

As global output expands and nations proper, global energy demand will rise (BP, 2019). According to the world energy outlook report (IEA, 2017), global energy demand is projected to double its current level by 2030. As large and growing middle class emerge in the developing world, future energy consumption is expected to grow fast (BP, 2019). In the IEA (2011) new policies scenario, fossil fuels which are considered non-renewable because they are irreplaceable will continue to dominate the energy mix (see Figure 2.1). The international energy outlook (IEO, 2016) reference case projects that fossil fuel will still account for 78 % of the total world energy consumption by the year 2040. As a result, the end-use consumption of electricity will grow fastest globally as it has been for many decades. Fossil fuel is thus envisaged to remain the primary source of energy for a long time especially for developing nations. This is due to the fact there is already reliable technology to produce energy from it, they are low cost, and they possess high energy density.

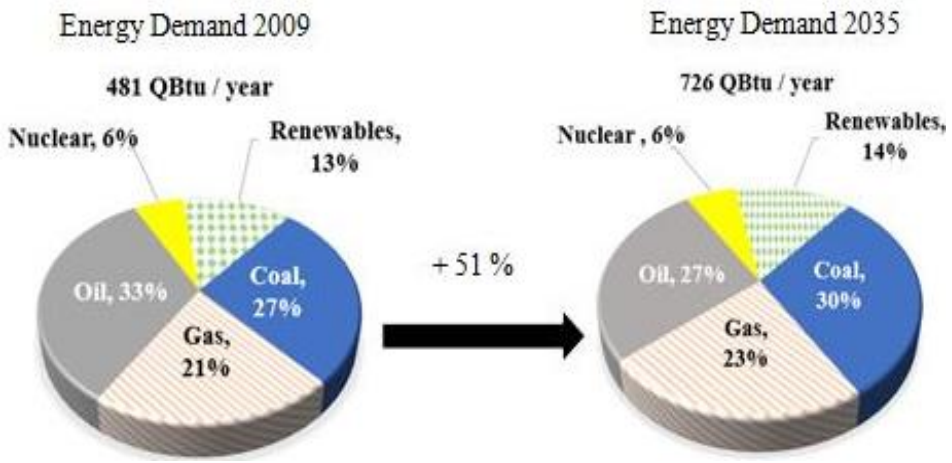

Figure 2. 1 World energy demand projections (Adapted from IEA, 2011)

Of the fossil fuel sources, liquid fuels (mostly petroleum-based) accounts for 32.9 % of total global energy consumption, making it the world's leading fuel (IEA, 2011). Due to the depletion of oil reserve, consumers of energy will need to adopt more energy-efficient technologies and to use less liquid fuels when feasible. Natural gas, the second fuel option is an abundant natural resource, growing in world energy consumption. This is due to its environmental benefit relative to petroleum products or coal particularly for air quality as well as greenhouse gas emissions (IEO, 2016). Because natural gas has high fuel efficiency, it is becoming appealing for new generating plants in the power sector. The third fossil fuel option is coal and it is the world's most widely distributed fossil fuel (IEA, 2013a). Coal is very abundant, has a less volatile price, provides a stable and cheap energy source which makes it very relevant for the future. However, the carbon intensiveness of coal and concerns about its greenhouse gas emissions cloud the future usage of coal. Despite these legitimate concerns, it is anticipated that coal use will play a vital role in the future (IEA, 2013a).

Though fossil fuel accounts for about 50 % of total energy supply by fuel in Africa, electricity remains a scarce commodity for most sub-Sahara Africa countries (IEA, 2011; Deichmann et al., 2011). In Africa, South Africa retains the highest share of coal, producing about 96 % of Africa's coal (IEO 2016). Coal dominates South Africa's energy system meeting about 72.1 % of the country's energy need (www.eskom.co.za). Because the country is dependent on coal, it leads the continent in carbon dioxide emission. South Africa is recognized 14th largest emitter in the world according to BP statistical review of world energy (BP, 2017). Although the South Africa government encourages a diversified generation portfolio with a more renewable energy source, the chronic power shortage added to the economic advantage of coal-fired generation indicate that coal will remain as the primary source of energy supply for South Africa (IEO, 2016). According to Glazewski et al. (2012), coal has driven the nation's energy economy not only in the past but is probably going to do so in the near and anticipated future. Nevertheless, the country is mindful of her responsibilities to mitigate greenhouse gas emissions associated with coal usage.

Human activities like the burning of fossil fuels, the cutting down of trees/forests and various forms of agriculture, etc. have led to an increase in anthropogenic concentrations of greenhouse gases and aerosols since time immemorial. The major greenhouse gases (GHG) are nitrous oxide (N_2O), methane (CH_4), carbon dioxide (CO_2), fluorinated gases (hydrofluorocarbons (HFCs), sulphur hexafluoride (SF6), perfluorocarbons (PFCs), and tropospheric ozone (O_3) (IEA, 2018). Of the listed GHG, CO_2 is the largest contributing gas to the greenhouse effect as shown in Figure 2.2.

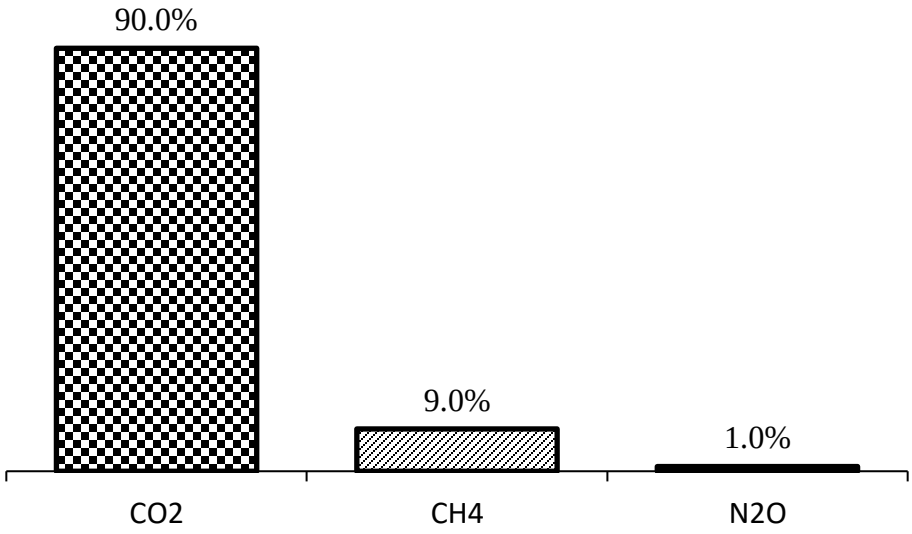

Figure 2. 2 Major greenhouse gases (Adapted from IEA, 2018)

Around 90 % of energy-related emissions are derived from the oxidation of carbon. The energy sector among the human activities produced the largest CO_2 emission (see Figure 2.3). Two sectors combined, electricity and heat, and transport represented almost 67 % of the global emissions in 2013.

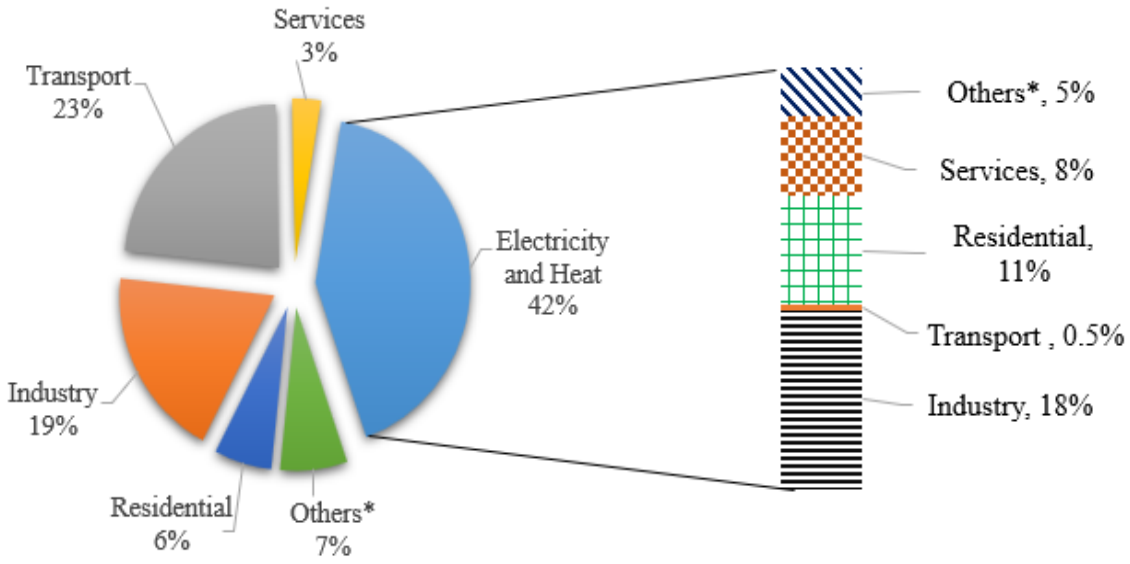

Figure 2. 3 World CO_2 emission by sector in 2013 (Adapted from IEA, 2015)

Carbon dioxide is the principal reason average temperatures are rising, therefore, has shown to have a close link to climate change (IPCC, 2014; Anderson et al., 2016). Due to coal and other fossil fuels projected to remain key as primary fuel consumption, global CO_2 emissions will continue to increase (see Figure 2.4). According to Jiang et al. (2015), atmospheric CO_2 concentrations have slowly increased from 310 to 390 ppm. If we allow CO_2 concentrations to rise and do nothing, the average global temperature would increase to around 6 °C in the future (Jiang et al. 2015). As greenhouse gases (GHGs) emissions increase, such as CO_2, we would experience greater warming and gravity of the associated consequences such as climate change which is one of the most urgent challenges facing the planet.

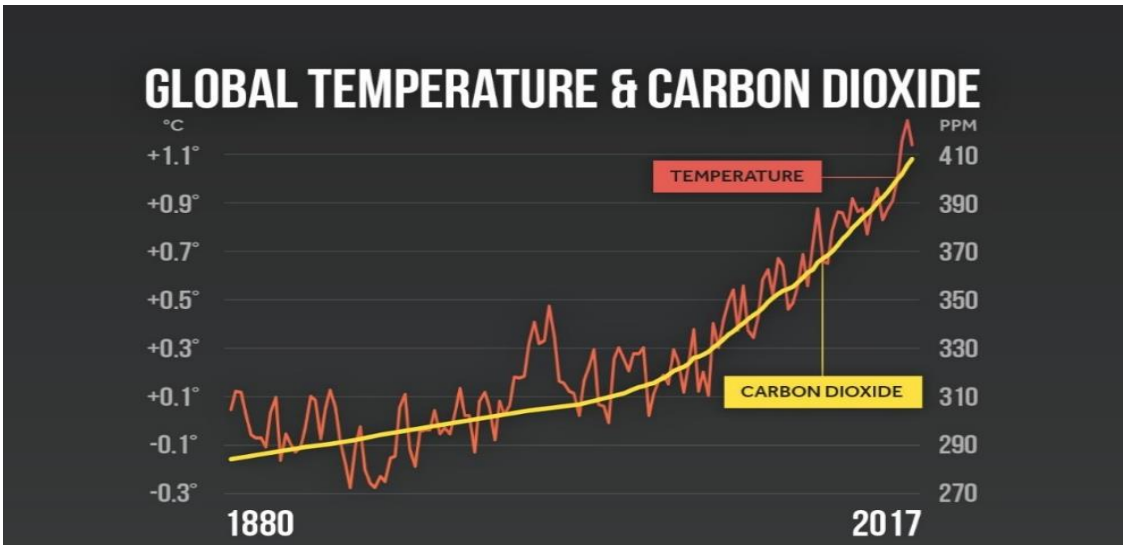

Figure 2. 4 Rising global temperature and CO_2 (Source: https://www.climatecentral.org/gallery/graphics/co2-and-rising-global-temperatures)

According to the IPCC (2014), it is clear that human has an influence on the climate, and anthropogenic emissions of greenhouse gases in recent times have recorded highest in history. The associated consequences include, but not limited to the rise in sea levels which can cause dislocation of human settlements, severe weather events, high incidence of heatwaves, as well as destructive storms. Other effects are changes to rainfall patterns which can result in droughts and floods that could affect food production, ocean acidification, human disease and mortality. To limit future temperature increases and be able to meet the agreement made by the global community in Paris of temperature target "well below 2 °C, CO_2 emissions need to be curtailed significantly. We may need to deploy massively different low-carbon energy technologies in order to achieve the Paris goal.

Several portfolios of technologies to balance the increasing global demand for energy with the recognized need to reduce GHG emissions have emerged. One approach is to reduce the dependence on fossil fuels as the primary energy source by massively replacing them to the extent possible with sources that are less polluting and, in many cases, completely renewable (Perez, 2011; Danaei Kenarsari et al., 2013). Another approach to significantly abate carbon emissions is the use of carbon capture and storage (CCS) technologies (GCI, 2012, Fu and Gundersen, 2012; Cuéllar-Franca and Azapagic, 2015). A third approach is to increase the efficiency of energy usage

through energy conversion and end-use technologies in all sectors (Allwood et al., 2010; Huisingh et al., 2015; Rahman et al., 2017; IEA 2017). However, no single strategy is a win-win. Any of these technologies as discussed in the following section can be used as stand-alone or combined with other technologies. Some of these technologies are discussed in the following section

2.2 Renewable Energy

Increase in world population especially developing countries no doubt would result in an unprecedented demand for energy. To meet this demand, it implies fossil fuel will be consumed increasingly. However, the consumption of fossil fuels leads to environmental degradation and intensifies the rate of climate change. To counter this threat, "environmentally sound technologies" (EST), one of which is the renewable energy sources has been introduced. Renewable sources are termed "cleaner sources" and are often referred to as EST because they protect the environment and are less polluting (Perez, 2011). Renewable sources are continually replenished and potentially inexhaustible. The effects the usage of fossil fuel have on the environment, the concerns about energy security, and high world oil prices that have remained so for a long time has given rise to the use of non-fossil renewable energy sources (IEO, 2016). However, on its own, harnessing renewable energy sources cannot cover world energy demand. Technologies to process renewable resource base are now available and many of them have been well-proven technology. According to IEA (2013a) report, renewables are gradually becoming renowned and it is gradually taking its place in the scheme of the energy mix. Countries and regions that promote the deployment of renewables and have put in place structures to support the use of renewables are experiencing widespread renewable usage, even in the powers sector.

Compared to conventional energy sources, renewables possess fewer disadvantages, hence gaining unprecedented attention as a method to solve the energy problem. The highest potential for electricity generation from renewable energy source has been identified for solar photovoltaic and wind (Zerta et al., 2008; Dinçer, 2011). These sources are unlimited in supply and the output from both these sources is tied to the availability of the resource. Also, the intermittent nature of these renewable sources leads to fluctuations in energy generation (IEA, 2013a). Unlike fossil fuel power plants where electricity generated is dependent on installed capacity, wind and solar energy generation depends on climate and weather which are difficult to predict and are not controllable

(Meulenberg, 2017). Also, energy from renewable sources has associated low density. Other renewables such as hydro and various forms of biomass/biofuels are almost competing with conventional energy sources (Saidur et al., 2011; Popp et al., 2014). Same as wind and solar photovoltaic, renewables such as biofuels can only be produced from specific, limited sources. Apart from the mainstream renewable energy technologies, other renewables like marine energy, enhanced geothermal energy (EGE), concentrated solar photovoltaics (CSP), artificial photosynthesis (AP), cellulosic ethanol, etc. are emerging. A current review of these emerging technologies can be found in a report written by Hussain et al. (2017). Even though methods of storing and converting renewable energies are rapidly improving and evolving, in order to harness the full potential of these energy sources at large scales, huge energy cost is involved. The associated high cost of renewable energy sources in addition to the intermittency of generation relative to conventional energy sources remains a major obstacle to commercialization (Meulenberg, 2017). There is still room for renewable technologies to grow in terms of improvement and cost reduction. Through research and development (R&D), right policy, huge investment and operational maturity, the renewable option can receive a great boost which will eventually turn it into a mainstream technology.

2.3 Carbon Capture and Storage (CCS)

As nations develop, coupled with the demand for a higher standard of living, energy demand will grow rapidly. The foreseeable future will still see coal and gas dominating power generation capacity making them a relevant feature of the electricity mix despite the rapidly increasing share of non-fossil energy sources. According to the international energy agency report (IEA, 2016), there is no other technology solution apart from CCS that is capable of delivering significantly reduced emissions from the use of fossil fuels in power generation and industrial processes. Renewable and energy-efficient sources alone cannot achieve the reduction of CO_2 required to meet the climate goals agreement made in Paris.

In contrast to the power sector that can be partially or totally decarbonized, there is little room for substituting fossil energy use in the industrial (i.e. non-power) sector which accounts for about one-quarter of global CO_2 emission. Renewable technologies cannot mitigate and replace CCS in many industrial sectors (GCI, 2016). The amount of CO_2 this sector produces is likely to grow

over the coming decades (IEA, 2013b). One approach that holds promise for preserving the economic value of fossil fuel reserves in producing low carbon electricity and bridging the transition to low-carbon technology is the application of carbon capture and storage (CCS) technology (Praetorius and Schumacher, 2009; Herzog, 2011). CCS technology is also a crucial solution for decarbonizing the atmosphere (Rubin et al., 2012). Direct/deep emissions reductions from many industrial processes can be reduced significantly with only CCS as the applicable option. By integrating CCS technology with the existing coal power plants and other industrial processes emitting CO_2, a large quantity or volume of CO_2 might be prevented from entering the atmosphere (Figueroa et al., 2008). Figure 2.5 presents the CCS process which would generally consist of single or multiple CO_2 sources with capture, transportation infrastructure (s) and storage location(s).

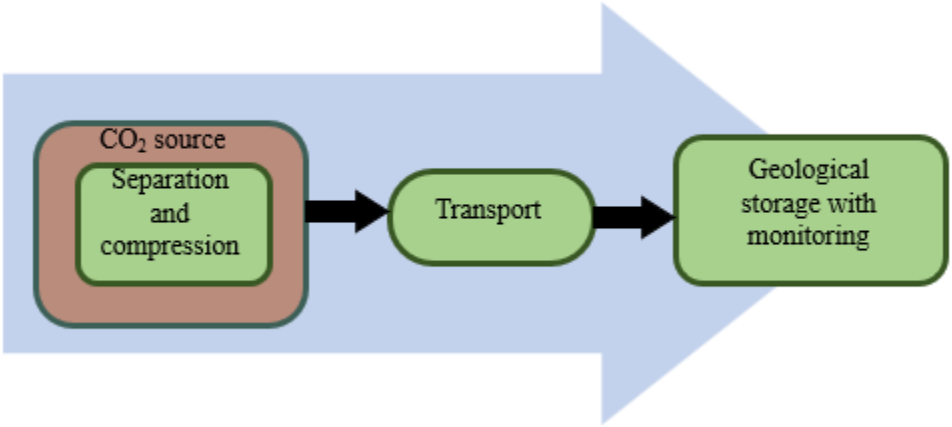

Figure 2. 5 Carbon capture and storage chain

2.3.1 CO_2 transportation and storage

Apart from just capturing CO_2 from large point sources, CCS involves infrastructure for transporting captured CO_2 from source of emission to a storage site. Before captured CO_2 is ready for transport via pipeline for injection or usage, it must first be compressed to a supercritical state where it behaves like a liquid. Technology via pipeline transport is a known and relatively mature technology. Pipelines for CO_2 transport are designed to withstand high pressures. High-pressure pipelines provide steady-state flow from emission source to the final storage site. However, the use of pipelines suffers from pressure drop along the transportation route which could result in

two-phase flow and might lead to operation and/or material problems. For this reason, CO_2 in a stable condition (supercritical/dense) is the preferred condition using pipelines. Transportation using pipeline mode requires CO_2 must be free of water/water vapour to avoid increased transportation cost, pipeline corrosion, clathrate and hydrate formation. The occurrence of these could lead to pipeline plugging (Jiang et al., 2015). CO_2 can also be transported by water carriers e.g. ship, but usually in small quantities (IEA, 2013b). The intergovernmental panel on climate change, IPCC (2005) considers shipping of CO_2 may be cost-effective over long distances (> 2400 km) than transport through pipelines. Ship transportation also provides a more flexible solution regarding quantities transported. Transportation of CO_2 can either be onshore or offshore. While onshore enables storage near emission source, offshore is considered safer based on leakage and believed to be easily supported by the public. The downside for offshore is that it requires a longer route, costly logistic infrastructure, and it is more complex (IPCC, 2005).

Captured and transported CO_2 is then stored intermediately using steel tank technology or permanently underground. For underground storage, CO_2 is injected into natural occurring geologic formations, such as depleted oil and gas fields, deep saline formations, and un-minable coal seams with potential for enhanced coal-bed methane (ECBM) recovery (Herzog, 2011). Storing CO_2 underground in geological sites require high pressure to inject CO_2. Captured CO_2 storage in deep saline formations provides the largest (ranging from 4,000 to 23,000 $GtCO_2$) geological storage option (de Coninck and Benson, 2014). However, their characteristics are less well understood than other potential storage deposits (Sathre et al., 2012). Other methods of storage are deep oceans, mineralization and reuse. Followed storage is the subsequent monitoring of injected CO_2 to ensure no gas escapes. There have been huge advances in the field of measurement, monitoring and verification (MMV) of stored CO_2, along with better techniques that are less interrupting and more precise.

2.3.2 CO_2 utilization

Not all CO_2 captured will be stored in geological formations, some will be utilized. The largest single source for the use of CO_2 is enhanced oil recovery (EOR process, which consumes upwards of 60 million tons CO_2/yr (IEA, 2013b). Due to the cost implication of storing CO_2, underground, there is now interest in the possibilities of improving CCS economies through the valorization of

captured CO_2. CO_2 capture and utilization (CCU) have been put forward as a possible substitute or complement to storing CO_2 underground that could enhance the profitability for captured CO_2 (IEA 2013b). CCU could add as a mitigation strategy in addition to CCS. Some of the roles of CCU in climate change mitigation are that it presents expanded options, reduced cost and can help to accelerate the uptake of CCS by offsetting cost (Qian, 2018). CO_2 is a relatively abundant source of carbon, but its chemical use remains restricted despite carbon forming the basis of most of our goods and fuels. This is because CO_2 is unreactive and large amounts of energy (high temperature, reactive agents and electricity) are usually required to break its chemical bonds to enable a reaction to occur. CO_2 is used as chemical solvents, for the decaffeination of coffee, as refrigerants, for the carbonation of soft drinks, water treatment, and for the manufacture of fertilizer (Hunt et al., 2010). These applications demand small quantities of much less than 1 million tons CO_2 per year. The beverage industry utilizes about 8 million tons of CO_2/yr (IEA, 2013b). Many other emerging areas of applications of CO_2 that provide temporary storage solutions in a small scale and potential high scale applications are biomass e.g. whole algae, inorganic materials e.g. bicarbonates, fuel and organic chemicals e.g. CO_2 syngas and commodity chemicals (https://netl.doe.gov/coal/carbon-utilization/about). However, they are still in small scale and some of them would require time to develop before they reach technical maturity (Aresta et al., 2014; IEA, 2016). Some of the technological pathways for CO_2 utilization are: i) electrochemical conversion to produce syngas, methane, methanol ii) photocatalytic/photothermal catalytic conversion, iii) bioconversion using microbes and enzymes, iv) co-polymerization, and v) mineral carbonation (Qian, 2018).

2.3.3 CO_2 capture

CO_2 capture i.e. the separation of CO_2 from other gases produced at large point sources represents about 70% of the total cost of a CCS project (IEA, 2016) and it is also considered to be technologically challenging (Kosinov et al., 2014). Hence, more research and development effort are required than other components like transportation and storage chain of CCS. To produce an uncontaminated CO_2 stream that can be permanently stored or sequestered, the following sections discuss the three approaches to achieve this goal, namely;

2.3.3.1 Post-combustion CO_2 capture

Post-combustion capture (PCC) which is also termed end-of-pipe capture is the capture of CO_2 at the end of a combustion process. In this approach, CO_2 is captured from the flue gas stream after combustion of carbon-based materials (Figure 2.6). Post-combustion technology can easily be retrofitted and is relevant to most of the existing coal-fired and industrial plants. Another benefit of this capture process is that it does not change the combustion process of the plant. The products of combustion from the exhaust in conventional power plants which typically is a mixture of CO_2, N_2, and O_2 after the removal of SO_X and particulates, are known as flue gas mixture (Olajire, 2010).

The separation of ash/smoke particles is the first process that takes place during the post-combustion capture in a particle removal chamber, thereafter the sulphur removal stage, and then the capture of CO_2. Concerning deploying large-scale CO_2 capture for application in the power generation sector, PCC leads the suite of near-term technologies (IEAGHG, 2017). However, PCC is considered one of the most challenging approach. This is because CO_2 concentration in flue gas is dilute and its pressure in flue gas is low (~12-15 mol % for a coal-fired power plant at 1 bar ambient). Post-combustion capture/separation process mainly involves the capture/separation of CO_2 from CO_2/N_2 mixture (Brunetti et al., 2010). The value of recovered CO_2 captured via post-combustion is usually poor, and it is generally produced at low pressure which does not conform to the sequestration requirements.

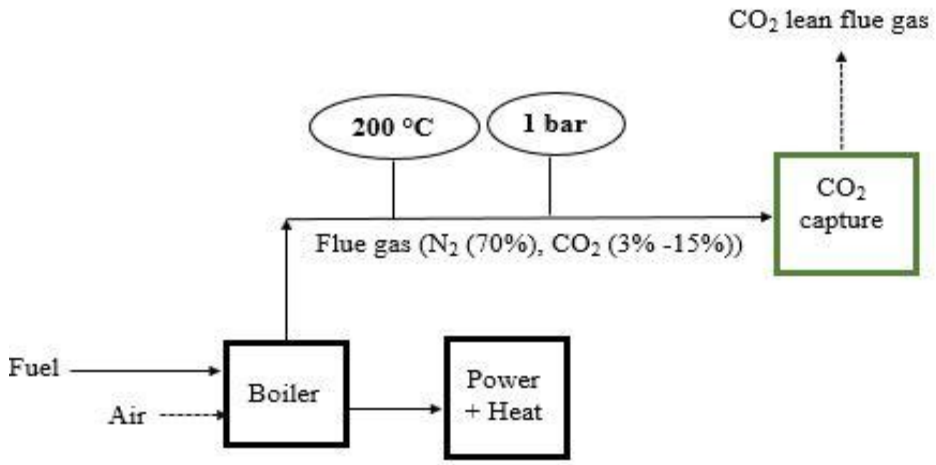

Figure 2. 6 Schematic of post-combustion capture process (Modified from Merkel et al., 2010; Favre, 2011; Rubin et al., 2012)

The main separation technique for capturing CO_2 from flue gas via post-combustion is the absorption technique. Absorption is incorporating a substance in one state into another of a different state. Established chemical solvents (e.g., MDEA and other amines) for example react with acid gases during the capture of CO_2. CO_2 capture using solvent process consumes a large amount of parasitic power, thereby reducing the overall net plant efficiency and significantly increase the net cost of capture and electricity (Ku et al., 2011). Use of chemical solvents is at best when the operating temperature is low, and it is well suitable for selective capture from streams with low CO_2 partial pressure (Ciferno et al, 2011).

2.3.3.2 Oxyfuel Combustion CO_2 capture

Oxy-fuel combustion strategy is almost like post-combustion capture in a way that gases are processed after combustion. This capture approach is considered as an alternative approach to post-combustion capture in a conventional coal plant. The principle of carbon capture by oxy-fuel combustion is to maximize the purity of the CO_2 produced from combustion by replacing the combustion air with pure or nearly pure oxygen. By so doing, the diluting effect of nitrogen from the process is effectively eliminated (Lockwood, 2016). CO_2 flue gases are enriched to prevent unwanted accumulation of substance (a conventional air pollutant) in the recycled flue gas to the boiler. Approximately 75 % less flue gas is produced in oxy-fuel combustion than air-fueled

combustion (McDonald and Rogers, 2014). It also produces exhaust stream consisting chiefly of CO_2 and water (H_2O) ready for capture and sequestration without post-combustion chemical process as illustrated in Figure 2.7. The associated water vapour is easily separated by phase separation (condensation) (Bernardo et al., 2009; Rossi et al., 2014). Oxyfuel technology can be applied to any type of fuel used for power generation. The technology is also suitable for some large-scale industrial cement, steel or oil refining applications (IEA, 2016). The oxy-combustion process does not necessitate CO_2 capture equipment and it is yet to be commercialized (Sreenivasulu et al., 2015)

Apart from the facility needed for flue gas recycle, oxy-fuel combustion process requires several additional pieces of equipment to a standard coal plant. These equipment are an air separation unit (ASU) used for producing oxygen and a compression and purification unit (CPU) utilized for removing impurities still left from CO_2-rich flue gases for compression and transportation (Wall et al., 2011; Porter et al., 2015).

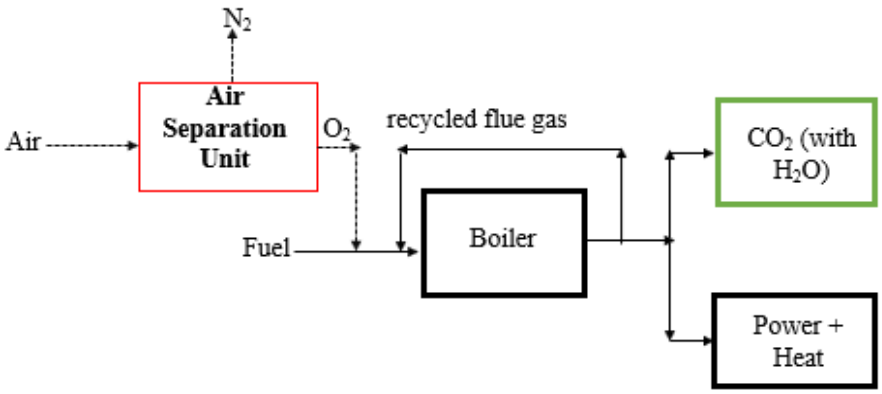

Figure 2. 7 Schematic of oxy-fuel combustion capture process (Modified from Merkel et al., 2010; Favre, 2011; Rubin et al., 2012)

2.3.3.3 Pre-combustion CO_2 capture

Pre-combustion is a process used in decarbonizing fossil fuel by converting the fuel heating value to hydrogen, before being utilized. A schematic of the pre-combustion capture process is shown in Figure 2.8. The pre-combustion technology is inappropriate for application in existing power plant because the fuel conversion steps required for pre-combustion are different and more

complex than the process for post-combustion (Mondal et al., 2012). The technology is already being utilized at large-scale facilities in the chemicals production, oil refining processing and natural gas processing for separating CO_2 from gas streams for decades to meet the requirements of the downstream product (GCI, 2009). In the case of power generation through combustion, the pre-combustion application will require a new plant to be built. This capture approach is mainly associated with an integrated gasification combined cycle (IGCC) (Figueroa et al., 2008; GCI, 2015).

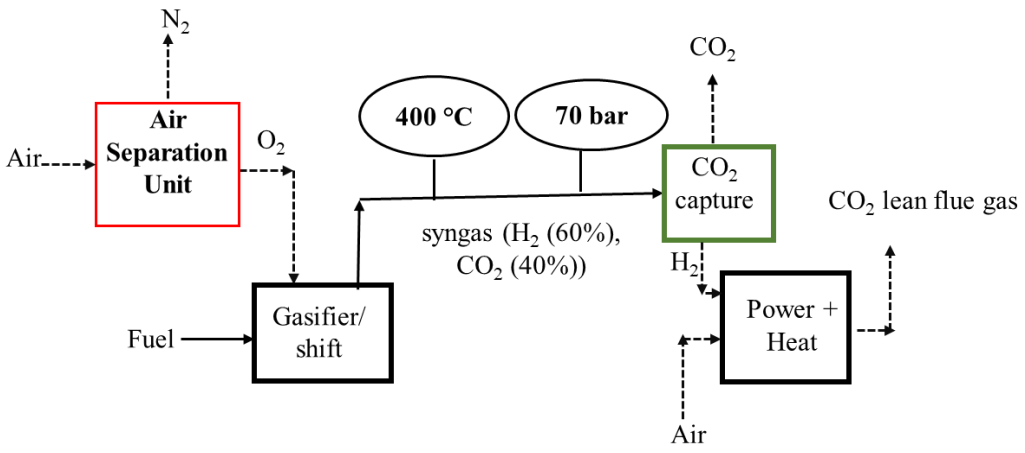

Figure 2. 8 Schematic of pre-combustion capture process (Modified from Merkel et al., 2010; Favre, 2011; Rubin et al., 2012)

One example under pre-combustion CO_2 capture is IGCC. The IGCC is a modern technology power plant that uses high-pressure gasifier to converts fossil-based fuels to synthetic gas (clean fuel gas) by a process of gasification (Jansen et al., 2015), with lower emission of air pollutant. Because of its flexibility, the IGCC plants can also be used to co-produce synthesis gas for industrial applications (fertilizer, hydrogen, chemical products/fuels, methanol production, substitute natural gas, motor fuels) (Smart et al., 2010). Syngas is used in the industry for manufacturing of ammonia, hydrogen, methanol, hydrocarbon (for Fisher-Tropsch process). Processes that produce syngas are shown in Equations 2.1 to 2.4 below:

Coal gasification: $C + H_2O \leftrightarrow CO + H_2 \quad \left({}^{H_2}/_{CO} = 1\right);\ \Delta H = 131.2\ KJ/mol$ (2.1)

Steam reforming: $CH_4 + H_2O \leftrightarrow CO + 3H_2 \quad \left({}^{H_2}/_{CO} = 3\right);\ \Delta H = 206.3\ KJ/mol$ (2.2)

Dry or CO_2 reforming: $CH_4 + CO_2 \leftrightarrow 2CO + 2H_2 \quad \left({}^{H_2}/_{CO} = 1\right);\ \Delta H = 247.4\ KJ/mol$ (2.3)

Partial oxidation: $CH_4 + 0.5O_2 \leftrightarrow CO + 2H_2 \quad \left({}^{H_2}/_{CO} = 2\right);\ \Delta H = -35.6\ KJ/mol$ (2.4)

The IGCC process uses combined cycle to drive combustion and steam turbine to generate electric energy, with a low environmental impact. Excess heat from the gas turbine is then passed to a steam cycle leading to improved thermodynamic efficiency of the plant. The IGCC, which is today the most efficient thermal cycle for power generation plant, though more complex and costlier represents a superior choice over conventional pulverized coal power plants using steam cycle (Kanniche et al., 2010; Merkel et al., 2012; IEAGHG, 2014).

An additional process like a water-gas shift (WGS) reaction can increase gasification efficiency and reduce CO_2 emissions. The main function of WGS is to convert most of the syngas carbon monoxide (CO), a dominant carbon-containing specie downstream the gasifier with steam over a bed of catalyst to enhance H_2 production so that CO_2 by-product can be captured (Scholes et al., 2010). By so doing, hydrogen fuel - a combustible fuel, reducing agent or feedstock for chemical synthesis, for use in IGCC, and fuel cells (Shoko et al., 2006; Ball and Wietschel, 2009) is left behind. The reaction is exothermic as shown in Equation 2.5.

$$CO + H_2O + catalyst \leftrightarrow CO_2 + H_2 \quad \Delta H_{298\,^{\circ}C} = -41.2\ KJ/mol \qquad (2.5)$$

The mixture of H_2/CO_2 coming from WGS converter is known as fuel gas mixture, and the high concentration of CO_2 (about 40 %) in the fuel gas stream must be removed before use. Properties of the WGS stream which makes capture process efficient is that CO_2 partial pressure of fuel gas stream exiting the WGS reactor is high with a stream pressure of between 20 bar to 70 bar (Xu et al., 2015). CO_2 stream at high pressure implies more technology available for separation, increased driving force for separation, and reduction in compression cost/load potential which could lead to

lower cost of sequestration (Kanniche et al., 2010; Jansen et al., 2015). WGS approach can be applied not only to IGCC but also to processes that utilize syngas to produce synthetic fuels.

The major energy losses incurred for pre-combustion capture in IGCC is in processes like the water-gas shift, the air separation unit (ASU), gas cooling unit and CO_2 separation device (GCI, 2012). Thus, research and development are geared towards improving these processes in terms of energy consumption during the separation of H_2 from CO_2. IGCC technology would be more profitable if a cost is placed on CO_2 emissions. This is because removing CO_2 from high-concentration, high-pressure gasification streams of IGCC plant will be way less expensive than CO_2 removal from conventional pulverized coal power plants (Favre, 2007; NETL, 2010).

2.4 Separation Techniques Considered for Pre-combustion CO_2 Capture

According to the international energy agency (IEA, 2016) report, the cost of the capture element of the CCS chain represents a significant portion for the cost of sequestering CO_2. Hence, research and development efforts are focused on reducing cost/energy on CO_2 capture to facilitate its widespread commercial deployment. For example, power generation, deploying large scale CCS facility can cost about 70 % - 90 % of the overall cost, which is driven by the capture and compression process (GCI, 2016). As CO_2 concentration in the atmosphere rises, various CO_2 cost-effective capture techniques are now being developed to improve the efficiency of the capture process. Efficient separation of CO_2 from H_2 (a main mixture of syngas) is of importance for the environment. The following section briefly discusses main separation techniques considered for pre-combustion CO_2 capture are briefly discussed.

2.4.1 Adsorption-based technique for CO_2 capture

The adsorption technique makes use of solid sorbents and it is a promising technology to earn potential energy savings. Also, the low cost of many effective adsorbent materials means capital and operating costs could be low (Yong et al., 2002; García et al., 2011). Besides, sorbent systems generally show faster CO_2 adsorption kinetics than solvents and can be well suited to the production of CO_2 at higher pressures (Lockwood, 2016). Chemisorbents such as metal oxides allow for even higher temperature capture which can be integrated with the water gas shift reactor, improving the efficiency of both processes (Lockwood, 2016). Materials studied as solid sorbents

include but not limited to the use of porous solid materials such as zeolites pellets, activated carbonaceous materials, calcium oxide, hydrotalcite, supported amines, metal-organic frameworks (MOFs), and microporous or mesoporous silica gels (García et al., 2011; Herm et al., 2011). Adsorbing materials owe is adsorptive properties to the internal surface area and pore size distribution. Low capture and selectivity are a major setback with porous inorganic materials as adsorbents (Jiang et al., 2015). For adsorption-based separation technique, the differences in adsorption strength of the various components in the adsorbent are what drives separation. In the case of gasification (pre-combustion capture), the high CO_2 pressure makes physical adsorbents sufficiently effective. Higher partial pressures of CO_2 in pre-combustion capture render the weakly CO_2 binding physiosorbents much more effective than in post-combustion conditions. This allows for efficient pressure swing adsorption (PSA) with high CO_2 loadings (Lockwood, 2016).

Any promising adsorbents for gas separation should have acceptable mechanical property, a reasonable CO_2 working capacity, reasonable CO_2 selectivity, swift adsorption kinetics, optimum enthalpy of adsorption, and regenerability (Merkel et al., 2012). It is not uncommon for H_2S to have high solubility using a specific sorbent, leading to co-capture of CO_2 and H_2S and cost savings (Kenarsari et al., 2013). Solid sorbents are already widely used at a commercial scale for several other gas separation processes such as air drying, air separation, and hydrogen purification. The adsorbent technology was recently demonstrated for the large-scale capture of CO_2 during the production of hydrogen from natural gas (Lockwood, 2016). There are two principal approaches to desorbing CO_2 and regenerating the sorbent material. These are the thermal swing adsorption (TSA) and pressure swing adsorption (PSA). In the former, desorption occurs by warming up the adsorbent with a section of the primary gas product. The latter is accomplished by reducing the partial pressures of the adsorbed components in the gas phase by either passing a section of product gas over the adsorbent without heating by reducing the total pressure or by operating at near ambient temperatures (Herm et al., 2011). Whatever the approach utilized for regenerating the adsorbents, adsorbents application for capture in a gasification set-up requires synthesis gas must be cooled down, heated back up again and re-humidify for firing to turbine making the process not attractive (Lockwood, 2016).

Other techniques considered for pre-combustion CO_2 capture are calcium looping, ionic solutions, the use of hydrates, and the use of hydrophobic polymers. These processes are well defined and elucidated in the report written by Lockwood (2014).

2.4.2 Membrane-based technique for CO_2 capture

A membrane is simply semi-permeable barriers that selectively allow mass transport of certain molecules through them. This technology represents the main technology for water treatment at a lower cost and minimum environmental impact (Bernardo et al., 2009). Membrane-based systems have been developed and employed in the chemical industry to carry out various types of separation over the past three decades (Scholes et al., 2010; Kenarsari et al., 2013). Membrane separation presents energy efficient (no steam load), environmentally friendly alternative to conventional separation techniques like absorption and pressure swing adsorption (Franz et al., 2014). Membrane processes have a conceptually simple structure, environmentally benign, and intrinsically energy-efficient for gas separation (Adhikari and Fernando, 2006; Lindmark and Hedlund, 2010; Huang et al., 2012; Gkanas et al., 2015; Khalilpour et al., 2015; Wang et al., 2015b). Not only that, membrane separation technique lack product waste or emissions, allows continuous operation, and can separate molecules by molecular sieving mechanism (Ilić and Wettstein, 2017).

The modular fashion of membranes permits relatively straight-forward scale-up without significant changes in the process complexity, flexible deployment in space-limited locations, as well as saving on the CO_2 compression energy required downstream (Favre, 2011). These inherent advantages drive research in the field of membrane thus making it a potential replacement to conventional absorption and pressure swing adsorption based-processes (Luis et al., 2012). These attributes have also led to the growing interest in membrane for fuel cell applications, hydrogen production/purification, and application in the catalytic membrane reactor. Membranes are already widely used for a range of liquid and industrial gas separation applications such as air separation and removal of CO_2 from natural gas (Lockwood, 2016). Membranes used for natural gas sweetening cannot be used to treat flue gas as several key differences exist between the two processes hindering its feasibility. The relatively high partial pressures of CO_2 available in

gasification, reforming, and natural gas processing suggest the use of membrane may be more effective than in post-combustion capture applications (Favre, 2011).

A schematic of a gas separation membrane is depicted in Figure 2.9, where a membrane selectively separates gas B from gas A, with the upstream pressure being the side at a higher pressure. Membrane gas separation is pressure-driven and allows continuous separation (Nikolić and Kikkinides, 2015). If the goal is not to obtain a high purity gas stream, membrane technology can be a very cost-effective approach to separating gases. Membranes are suitable for bulk separation, however, if the feed concentration is low, it might not be the best option economically (Khalilpour et al., 2015). Membranes are favourable when the pressure of the feed is high, when the gas mixture contains a minimal amount of contaminants, when there is need for high purity product/permeate, and in situations where the product is accepted at lower pressures (Armor, 1998).

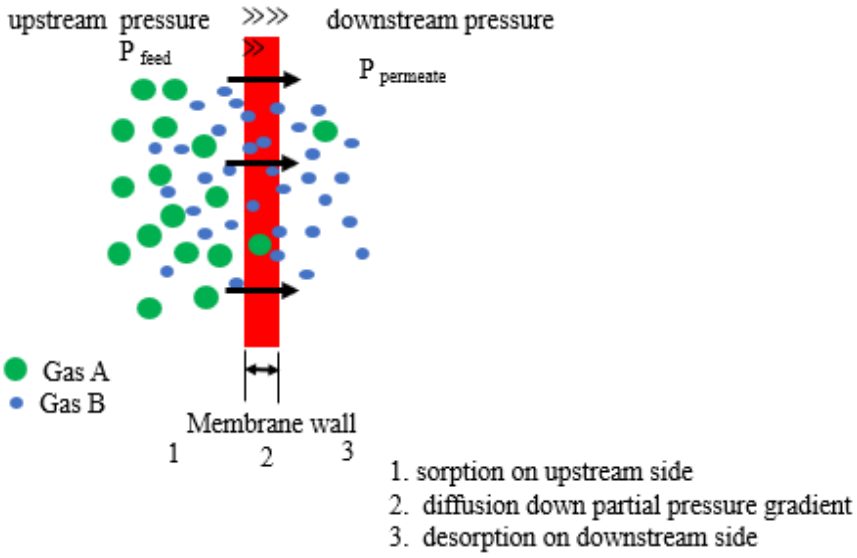

Figure 2. 9 Schematic of a gas separation membrane

The advantage of using membrane in pre-combustion capture is that CO_2 can be retained on the retentate side at high pressure due to the high feed pressure. The concentrated high-pressure feed provides a greater driving force for separation. High-pressure retentate CO_2 is beneficial to avoid the cost of CO_2 compression to meet storage requirement. Based on fundamental engineering and economic advantages associated with the use of membranes, they can compete over other

technologies and are now being surveyed as CO_2 capture technique from power plant emissions. However, membrane material selection, design and scale-up for effective CO_2 capture remain a challenge (Ku et al., 2011).

Gas separation membranes can either be H_2 or CO_2 selective (Scholes et al., 2010). CO_2 selective membranes are not desired and are significantly less advanced than H_2 selective membranes because CO_2 separated is delivered as permeate at low pressure and thus require compression for capture (Davidson, 2011). Because of the wider availability of H_2-permeable materials available for H_2-selective membranes, they are more suitable for pre-combustion conditions (Ku et al., 2011). H_2/CO_2 selectivity and long-term stability under high temperature and pressure are the main requirements for pre-combustion membranes (Luis et al., 2012). Membrane for CO_2 capture can be classified according to pore size and materials they are made of as discussed in the next section.

2.5 Membranes for CO_2 capture

2.5.1 Organic Membrane

Organic membranes are membranes made of polymers or are polymeric in nature. Currently, polymeric membranes dominate the industry are have been applied in food and beverage processing, gas separations, seawater desalination, and for medical devices (Shekhawat et al., 2003; Kenarsari et al., 2013). These membranes (glassy cellulose acetate or rubbery polydimethylsiloxane) are usually dense in nature. Polymeric membranes have shown good separation performance, the technology for processing polymeric membrane is mature, and they have been widely explored for CO_2 separation. Membranes that are polymeric in nature offer the advantages of low-cost fabrication, straight-forward scale-up, and good resistance to sulphur species (Adhikari and Fernando, 2006). Despite these advantages, organic polymer membranes suffer from instability and operational performance issues. At high temperatures, polymeric membranes suffer from degradation and lose selectivity, hence forcing a cooling liability on the process (Scholes et al., 2010).

Even though polymeric membranes have shown high selectivities, their dense nature makes them possess low CO_2 permeance thus requiring large membrane area (Lindmark and Hedlund, 2010). Also, the polymeric selective layer shows low resistance to contaminants when it is in contact with

condensable gases e.g. CO_2 at high pressures, even in low concentration. Hence, the polymeric layer plasticizes leading to loss of selectivity and mechanical strength (Scholes et al., 2010). The polymer in hollow fibre modules is even more problematic when applied in high temperature and aggressive chemical environment (Bernardo et al., 2009; Lindmark and Hedlund, 2010; Zhou et al., 2014; Karimi et al., 2015). When polymeric membranes are operated at high transmembrane pressure, the porous support adjacent to the polymeric selective layers collapse (compaction issues). Physical ageing, fouling issues associated with polymeric membranes leads to mass transfer resistance, and low throughput (Lindmark and Hedlund, 2010; Huang et al., 2012). The permeability of polymeric material determines the effectiveness of gas separation. The permeability of most polymeric membrane materials undergoes a trade-off limitation with selectivity (Bernardo et al., 2009; Wang et al., 2016) limiting its commercial applicability for pre-combustion CO_2 capture. An in-depth review of the polymeric membrane can be found in a report written by Sanders et al. (2013).

2.5.2 Mixed Matrix Membrane

Conventional gas polymeric membranes show a trade-off limitation between selectivity and permeability (Park et al., 2017). To overcome this challenge, researchers are developing membranes that integrate the best attributes of two or more membrane materials to alleviate the unappealing properties of one material (Hashemifard et al., 2010). The membrane formed thereof is a mixed matrix membrane (MMM). Only a few polymeric membranes have been found to exceed the Robeson bound (Robeson, 2008) which best explains the trade-off for binary gas mixtures. Most likely, MMM membranes are composed of blending polymers with inorganic particles/fillers. In this way selectivity compared to a pure polymer can improve. Besides, improved handling can be experienced relative to inorganic membranes (Bryan et al., 2014). The choice of inorganic fillers in developing MMM is usually based on its selectivity towards one specie. By introducing fillers to polymeric membranes, the transport mechanism, pore structure and free volume of the polymer are altered hence altering permeation properties. Other type of novel materials such as metal-organic framework (MOFs), graphene oxide, ionic liquids have been considered and have been incorporated into polymeric substrate to form polymeric MMM showing improved permeation properties for carbon capture (Clippel et al., 2012; Sánchez-Laínez et al., 2016; Sarfraz and Ba-Shammakh, 2016; Sutrisna et al., 2017; Li et al., 2019). Bryan et al. (2014)

investigated different percentage weight loading of 13X zeolite on poly (amide-b-ethylene oxide) (PEBAX MH1657) for post-combustion (CO_2/N_2) separation. Results showed an increase in CO_2 permeability as loading of 13X increased.

Composite polyvinylidene fluoride (PVDF) hollow fibre membranes were developed by incorporating MOF nanofillers Zeolitic Imidazolate Framework-8 (ZIF-8) in the selective layer. PVDF was chosen as the substrate based on its mechanical strength and chemical stability (Li et al., 2019). CO_2 permeance increased dramatically and was stable in the pressurisation and depressurisation process. The MMM developed displayed improved compaction resistance of membrane matrix and swelling resistance of the polymer chain in the polyamide section, thus, improving the membrane plasticization resistance. Musselman et al. (2009) from the University of Texas at Dallas (UTD) developed a bench to a pilot-scale novel, non-precious MMM in flat, hollow fibre and tubular geometrics to separate H_2 from synthesis gas during coal gasification. The MMM was based on polymer composites with nanoparticles of ZIFs. It was found that crosslinking polyamides further improved the H_2/CO_2 selectivity. Also, obtaining the desired gas fluxes was a challenge. In addition, obtaining a defect-free polymer/ZIF interface posed a challenge.

Like other types of membrane material, selectivity and permeability are key in designing MMM. Selecting inorganic fillers or materials that are compatible with the host polymer matrix for MMM preparation is still a challenge. The Maxwell model amongst other models found in the literature has been developed to predict resultant MMM properties (Hashemifard et al., 2010). However, according to Bryan et al. (2014), Maxwell model can only be applied for low filler loading. Though useful, shows a weakness for a wide range of material combinations. Another technical challenge in developing MMM is controlling the inorganic-polymer interface during membrane fabrication process such that the interface between the polymer and organic fillers is devoid of defects such as voids, polymer rigidification and blockage of the filer pores (Li et al., 2019). Several challenges that need to be overcome still exist in the development of MMM. Nevertheless, significant opportunities for improvement abound for mixed matrix membranes.

2.5.3 Metal-Organic Framework Membrane

Metal-organic frameworks (MOFs) are crystalline porous materials constructed of metal-containing nodes linked by organic ligand bridges and assembled through strong coordination bonds (Danaei Kenarsari et al., 2013) to form a one, two-, or three-dimensional coordination network. These materials are attracting attention owing to their potential in areas such as gas storage, heterogeneous catalysis and molecular separation (Sumida et al., 2012). According to Danaei Kenarsari et al. (2013), MOFs have the highest value for hydrogen uptake, surface areas, CO_2 storage, methane among porous materials. The mechanism of selectivity of MOFs can be based on kinetic separation (size-based selectivity) or adsorptive phenomena (Sumida et al., 2012). During H_2/CO_2 separation for example as in the case of pre-combustion CO_2 capture, due to the similar kinetic diameter of these molecules, MOFs need to possess very small pore size to carry out separation based on size selectivity. On the other hand, the selectivity of MOFs based on adsorptive phenomenon can arise as a result of the difference in affinity of the various gas components in the mixture adsorbed on the pore surface of the MOF (Sumida et al., 2012). Its adsorption ability makes MOFs very promising for pre-combustion capture and gas permeation membranes. Due to the very large distribution of MOFs and metals available, a study was done by Avci et al. (2019) to examine the effect of metal centres on CO_2/H_2 mixture adsorption and separation performance of two different MOF series using Grand Canonical Monte Carlo (GCMC) simulations. The authors found out that changing the metal type of MOFs can provide a great avenue to improving the CO_2/H_2 separation performance of materials. Amongst MOFs, the zeolitic imidazolate frameworks (ZIFs) MOFs are very popular and is considered promising for membrane-based gas separation process such as the capture of CO_2. This is as a result of the similar properties they share with zeolites i.e. uniform pore size, high thermal and mechanical stability. According to Li et al. (2010), ZIFs are made of transition metal ions (Zn^{2+}, Co^{2+}) and imidazolate linkers which creates 3D tetrahedral frameworks that look like zeolite topologies and has pore dimensions ranging from 0.2 to 1.5 nm. The difference in topologies among 22 common ZIFs was presented in a report by Phan et al. (2010). Huang et al. (2012) developed ZIF-95 molecular sieve membrane displaying high permeability and selectivity for the separation of H_2 from CO_2. When the membrane was tested with a binary gas mixture of H_2/CO_2 (50:50) at 325 °C and 1 bar, the mixture separation factor obtained, 25.7, far exceeded the corresponding theoretical Knudsen coefficient. ZIF-7 membrane was developed and tested for H_2 separation at elevated temperatures

by Li et al. (2010) and Go et al. (2016). The membranes displayed good thermal and hydrothermal stabilities and were considered promising candidates for developing gas separation membranes.

In summary, despite the good track record of MOF membranes at laboratory scale, the industrial application of MOF membranes is still lacking. This is largely limited by the complex fabrication methods, which are not appropriate for industrial scale-up production. A lot of research is currently in progress using MOF nanoparticles in a standard polymer to form mixed matrix membranes. This could give rise to industrial gas application for MOFs.

2.5.4 Inorganic Membrane

The inherent lack of mechanical and thermal stability, in addition to low permselectivity properties available to polymeric membranes, have increased the momentum in the development and application of inorganic membranes (e.g., silica, metallic, ceramics, zeolites, metal oxides, and carbon-based molecular sieves etc.) (Shekhawat et al., 2003; Scholes et al., 2010). This class of membrane can withstand aggressive chemicals, and very resistant to sulphur (Lin et al., 2002; Bernardo et al., 2009; Huang et al., 2012; Wang et al., 2015c). Membranes that can accommodate high temperature and pressure operations are very promising for use for gas/liquid/vapour separation when used in reactors/separators to improve conversion or product selectivity (Dong et al., 2008; Gallucci et al., 2013; Smart et al., 2013). These properties make the inorganic membrane appealing for CO_2 separation. Inorganic membranes can either be dense or porous in nature. Porous membranes can be subclassified into macroporous (pore diameter > 50 nm), mesoporous (2 nm < pore diameter < 50 nm) and microporous membranes (pore diameter < 2 nm). Inorganic membranes can also either be symmetric or asymmetric. Symmetric membranes have homogeneous structure throughout the membrane while asymmetric membranes are known to display a gradual change in structure throughout the membrane (Shekhawat et al., 2003). Microporous inorganic membranes can either be crystalline (e.g. zeolite material) or amorphous (e.g. silica, oxygen and carbon materials) in structure (Ockwig and Nenoff, 2007; Kayvani Fard et al., 2018).

Dense metallic membranes are quite popular in literature. The development of dense metallic membranes was pioneered by Johnson Matthey in the 1980s. These membranes are purely

designed from metals or alloys (binary alloys, complex alloys, amorphous alloys, coated metals) (Adhikari and Fernando, 2006). Metallic membranes based on palladium alloys have since been widely used for the production of high purity hydrogen for laboratories and electronics applications (Grashoff et al., 1983). Metallic membranes include, but are not limited to niobium, tantalum, and vanadium. The platinum and palladium membranes are typically dense sheets or films through which H_2 permeates. The palladium membranes are extensively studied, and literature has shown that they are highly permeable to H_2 and H_2 selection from other gases (Merkel et al., 2012). The application of "dense palladium-based alloy" as membrane material has shown great potential in high-temperature separation and reaction (Huang et al., 2012). Dense metallic membranes have been found to display infinite selectivity for hydrogen over other gases. This is because the dense structure prevents the passage of large atoms and molecules (Ockwig and Nenoff, 2007; Basile et al., 2011). However, using palladium or its alloys deposited unto the surface of mesoporous supports, achieving a continuous and well-grown surface coverage, leads to the formation of relatively thick palladium layer which limits flux.

The mechanism for the separation of metallic membranes is based on the diatomic dissociation of hydrogen molecules, catalyzing the molecules into hydrogen atoms. These atoms then diffuse through the metal and permeate on the opposite side of the membranes. Despite the high selectivity towards hydrogen which palladium-based membranes possess, they show several limitations in the large-scale separation of syngas. They are easily degraded by contaminants such as hydrogen sulphide, or carbonaceous materials and thus affect their performance. Also, palladium membranes possess low permeability at medium temperatures (Ockwig and Nenoff, 2007; Dong et al., 2008; Huang et al., 2012). Due to the remarkable dissimilarity in lattice constants of Pd and H_2, at ~300 °C, the Pd-H phase transition often leads to membrane embrittlement in the presence of H_2. This is the reason why palladium is alloyed with other materials (silver, gold, copper etc.) to combat H_2 embrittlement and to improve stability. The problem faced due to H_2 embrittlement can also be minimized in Pd membranes through the applied operating conditions, to mitigate a two-phase region (Ockwig and Nenoff, 2007). Commercial palladium-based membranes having silver incorporated into them have shown high selectivity, moderate permeability and thermal stability from 300 °C to 700 °C (Koutsonikolas D. et al., 2013). The highlighted shortcomings of palladium-based membrane hinder the potential of scale up to the size required for pre-combustion capture

applications. For fueling gas turbines, high-purity H_2 selectivity palladium membranes may not be strictly necessary. However, in an application where hydrogen is needed such as chemical synthesis and for the use of fuel cells, the production of high-purity hydrogen could provide valuable flexibility to a pre-combustion capture plant (Lockwood, 2016).

The target range of H_2/CO_2 selectivity of inorganic membrane material applicable at high temperature such as the water-gas shift conditions, within 250 - 380 °C and 20 bars is shown in Figure 2.10.

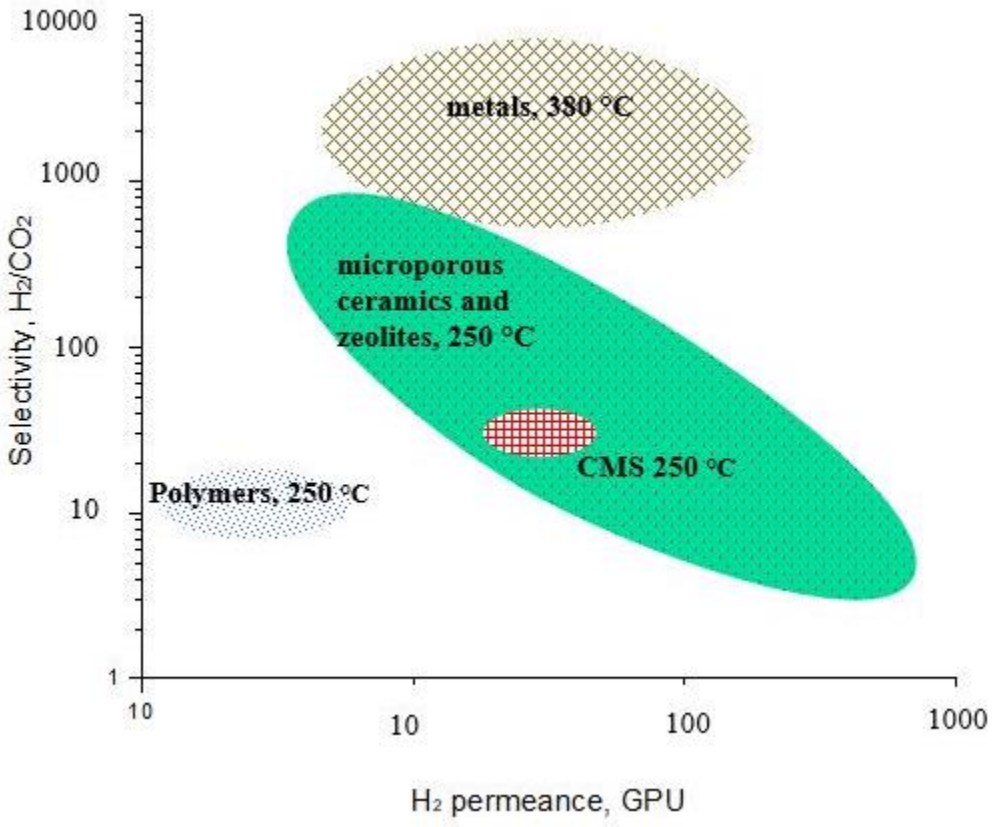

Figure 2. 10 Typical ranges of selectivity and H_2 permeance for the three main types of H_2 separation membrane, including carbon molecular sieves (CMS). 1 gas permeation unit (GPU) = 1×10^{-6} cm^3/cm^2 s cm Hg = $3.3e^{-10}$ mol (STP)/m^2/Pa/s. (Adapted from Ku et al., 2011)

Table 2. 1 Properties of common hydrogen-selective membranes (Adhikari and Fernando, 2006; Ockwig and Nenoff, 2007)

Property/support	Dense polymer	Microporous ceramic	Dense metallic
Temperature range (°C)	< 100	200 – 600	300 – 600
H_2 selectivity	low	5 – 139	> 1000
H_2 flux ($\times 10^{-3} molm^{-2}s^{-1}$) at ΔP=1 bar	low	60 – 300	60 – 300
Mechanical issues	swelling, compaction	Brittle	phase transition
Poisoning issues	HCl, SO_X, CO_2	-	H_2S, HCl, CO
Materials	polymers	silica, alumina, zeolites, titania	palladium, platinum, Pd-Ag
Transport mechanism	solution/diffusion	molecular sieving	solution/diffusion

Some common properties of hydrogen-selective membrane for gas separation are presented in Table 2.1. Despite the superior qualities of inorganic microporous membrane over the polymeric membrane, major drawbacks are preventing it from approaching the intended practical application in the industry. These downsides include costly fabrication methods, and synthesis of continuous defect-free reproducible membranes that will achieve only gas transportation through the zeolite pores (Li et al., 2015).

2.5.4.1 Zeolite membrane

Zeolites are a class of microporous aluminosilicates, open 3-dimensional framework structures composed of corner-sharing TO_4 tetrahedra, where T is Al or Si (Cundy and Cox, 2003; Zhang et al., 2013). They are inorganic crystalline solid having well-defined channels running through them that intersect at cavities. They are developed from different T atoms connected by O_2 atoms resulting in zeolites with different pore size, structure and physicochemical properties (Feng et al., 2015). Zeolites are generally expressed as $M_{x/n}[(AlO_2)_x (SiO_2)_y] mH_2O$ (see Figure 2.11). The cations of zeolites are loosely associated with the framework oxygens. The water molecules are removable and the non-framework cations can be exchanged. x, y is the total number of tetrahedral per unit cell, y/x ranges from 1-5 and 10-100 for silica sodalites (Georgiev et al., 2009).

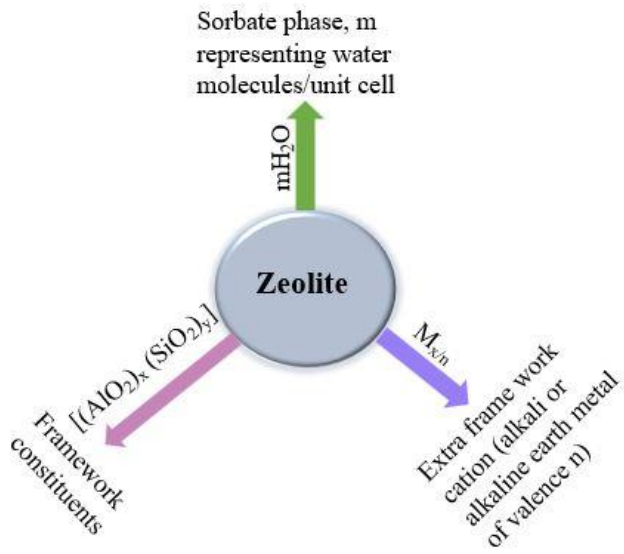

Figure 2. 11 Representation of each term of the general zeolite expression (Georgiev et al., 2009)

The primary building blocks (single TO_4 tetrahedra) of zeolites can be linked by 2, 3, or 4 corners (see Figure 2.12) to form a wide variety of structure called secondary building units (SBU) (Maghsoudi, 2016; Ilić and Wettstein, 2017).

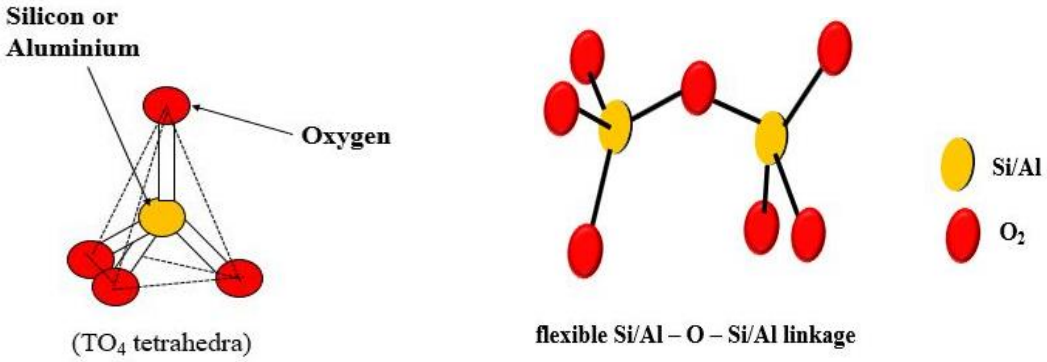

Figure 2. 12 Primary building unit of zeolite (left), corner-shared primary building blocks of zeolite (right)

The International Zeolite Association, (IZA) (http://www.iza-structure.org/databases) classifies zeolites according to their SBU framework symmetry with an identification code of three capital letters (in boldface type) e.g., SOD for the sodalite topology, MFI for the ZSM-5 and silicalite

topologies, FAU type molecular sieves with a faujasite topology (e.g., zeolites X, Y), etc. They can also be classified according to pore structure or according to the number of O_2 atom making up the ring in their framework as shown in Table 2.2.

Table 2. 2 Typical pore sizes of zeolites (Petrov and Michalev, 2012; Mohammadi and Maghsoodloorad, 2013)

Pore	O_2 rings	Zeolite	Pore size (nm)
Small	6-, 8-, 9- member	HSOD, Zeolite A	0.2 – 0.4
Medium	10- member	ZSM-5	0.5 – 0.6
Large	12- member	Zeolite X, Y	0.7 – 0.8
Ultra-large	14-, 18-, or 20- member	VPI-5	0.9 – 1.0

Currently, there are about 260 fully ordered type materials of zeolite frameworks approved by the Structure Commission of the International Zeolite Association (IZASC) (http://www.iza-structure.org/databases). Due to their high external specific surface areas and reduced diffusion path lengths, zeolites are used for clean-up applications and have found applications as catalyst in hydrocarbon processing, as sensors for detection and/or controlling, as ion-exchangers in detergents to soften water. They have also found applications as liquid separation devices, as well as corrosion protective coatings (Walton et al., 2001; Bowen et al., 2004; Zaarour et al., 2014; Maghsoudi, 2016). Its potential as gas membrane is dealt with great enthusiasm due to their molecular sieving ability to sort, and selectively separate certain molecules primarily on size exclusion difference. Zeolites can be applied as powders, pellets and can be grown on/in an inert support to form a membrane.

Molecular sieve zeolite membranes are promising as selective membranes for molecular separation and membrane reactors. This is due to their remarkable hydrothermal stability combined with the ability to display high permeance and selectivity towards H_2 (Dong et al., 2008). Zeolite membranes have been applied for pervaporation both at the laboratory and industrial scale (Bowen et al., 2004). Zeolite materials have been used to prepare membranes and have exhibited different separation properties. 8-member ring LTA (0.3 – 0.5 nm), 10-member ring MFI (0.55 nm), and 12-member ring FAU (~ 0.78 nm) type zeolites are among the most studied/synthesized zeolite

membranes (Huang et al., 2010c; Mohammadi and Maghsoodloorad, 2013). Zeolite-A (Linde Type A) was the first synthetic zeolite to be prepared and membranes synthesized thereof have found widespread application in both laboratories and industries. They are currently used in large scale application in dehydrating alcohols, other organic compounds, and for solvent recovery by pervaporation as well as vapour permeation (Kita et al., 1995; Masuda et al., 1995; Kondo et al., 1997). However, the presence of residual intercrystalline pores limits its application for gas separation (Czyperek et al., 2010). There has also been an accumulated knowledge in the synthesis of MFI structure (silicalite-1 and ZSM-5). The relative ease of preparation and relatively excellent thermal and chemical stability (high Si/Al ratio) makes MFI membranes interesting for industrial use (Caro et al., 2000; Bowen et al., 2004). But due to their large pore size larger than both H_2 (0.289nm) and CO_2 (0.33nm), MFI (0.55 nm) membranes usually do undergo pore modification to be able to separate H_2/CO_2 mixture. However, with the difference in diffusivities between these two gas molecules, hydrogen separation at elevated temperature using MFI membranes may be possible (Caro et al., 2000).

Despite extensive research work and the potential of zeolite membrane, their application in the industry for gas separation is lacking (Feng et al., 2015). According to Dong et al. (2008) and Feng et al. (2015), economic feasibility (low flux membranes) and poor membrane reproducibility is a challenge. The high synthesis cost and difficulty in reducing defects that arise during membrane synthesis are also contributing factors (Caro et al., 2000; Feng et al., 2015). These problems make zeolite membrane display inadequate H_2/CO_2 selectivity and/or permeance. For practical application, pure zeolite membranes having a closed structure other than the pores of the zeolite structure are desirable. The development of higher flux zeolite membrane free of interzeolitic pore can reduce both the cost of membrane and module which is a drawback to their application.

An interesting zeolite material is a sodalite (SOD) zeolite. Sodalites are crystalline aluminosilicate 6–ring zeolites with three-dimensional channel network. They belong to the clathrasils group and formed by a network of alternating and corner-sharing SiO_4 and AlO_4 tetrahedrons (Julbe et al., 2003). The channel apertures of sodalite are formed by 6-rings only. Hydroxy sodalite (HSOD) is a member of the sodalite family with structure is made of a cubic array of sodalite unit (sod, β-cages or composite building unit) (Khajavi et al., 2007b). Hydroxy sodalite (sodalite hydrate, hydroxo sodalite) is the hydrated form of sodalite and it is expressed as $Na_6(SiAlO_4)_6(OH)_x\ nH_2O$

(Naskar et al., 2011a; Pan et al., 2016). The six-member O_2 aperture pore window of the SOD structure has a kinetic diameter of 0.265 nm which falls between the kinetic diameters of CO_2 (0.33 nm) and H_2 (0.265 nm). This diameter is large enough to enable H_2 to pass and to exclude CO_2 and other larger molecules, thus allowing separation based on geometry/size exclusion to be possible. The pore window can provide access to smaller molecules like helium (0.26 nm), water (0.27 nm), ammonia (0.25 nm), etc. (Xu et al., 2004; Kalantari et al., 2015, Daramola et al., 2015b, 2017). Due to its small pore size and its reasonable ion exchange capacity, SOD crystals have found applications in hydrogen storage, optical materials, catalysts, and pigment occlusion (Naskar et al., 2011b, Esaifan et al., 2017). Sodalite crystals have been developed into a membrane and applied as water selective material for the separation of water from different organic mixtures (Kazemimoghadam and Rigi, 2018). Gas separation performance of SOD membrane has been mainly reported for helium (Kalantari et al., 2015). The small window opening of the SOD structure and its high thermal stability up to 450 °C (Khajavi et al., 2007b; Czyperek et al., 2009) makes SOD a potential material to develop membrane utilize in pre-combustion CO_2 capture.

2.6 Transport Mechanisms in Zeolite Membranes

How a membrane performs is a function of the gas permeation mechanism that play host in the membrane. One or more transport mechanism can plays host to a zeolite membrane depending on the concentration of defects in the membrane (Gkanas et al., 2015). A well synthesized and defect-free membrane usually has zeolitic pores as the only available pathways for gas or reactive molecules transport. As such the membrane becomes highly selective to certain gases or group of gases (Wang et al., 2009). On the other hand, a defective membrane possesses trans-membrane pathways larger than the intercrystalline zeolite pores. Permeation flux through both pathways contributes to the total permeate flux and dictates the dominant transport mechanism (Jareman et al., 2004; Hosseinzadeh Hejazi et al., 2011). According to the International Union of Pure and Applied Chemistry (IUPAC) definitions and corresponding size, zeolite defects can be classified into macro-defects (size > 50 nm). Cracks and pinholes fall into this group. They can also be classified into meso-defect (size > 2 nm and < 50 nm) and micro-defects (size < 2 nm) (Čejka, J. 2007; Ockwig and Nenoff, 2007). Micro- and meso- defects are intercrystalline grain boundaries formed by non-perfect intergrowth between zeolite crystals in hydrothermal synthesis. Also,

intracrystalline defects resulting from broken Si-O-Si bond may exist in the zeolite crystals. These defects fall under micropore defects (Cundy and Cox, 2005; Maghsoudi, 2016).

Gas transport mechanisms in porous membranes may depend on number of properties such as the membrane pore size, the interactions between the permeating molecules and the membrane pore surface, difference in chemical affinity between zeolite and permeating molecules, the feed gas composition, and the operating temperature and pressure (Dong et al., 2008). Besides, properties such as structure, crystal orientation, film thickness, Si/Al ratio, counterions, chemical composition as well as the kinetic diameter of the permeating species could also determine gas transport in zeolite membranes (Gkanas et al., 2015). Some common gas permeation mechanisms that occur in zeolite membrane are discussed in the following section.

2.6.1 Molecular sieving mechanism

A defect-free synthesized zeolite membrane possesses molecular sieving and can separate gas components based on size selectivity/size exclusion principle. If this happens, the pore size of the membrane is large enough for the smaller molecule to transport through but small enough to prevent the larger molecules from entering the pores (Gilron and Soffer, 2002). When separation is based on molecular sieving, the extent of separation (separation factor) is determined by the membrane pores size. That is the pore size of the membrane fall in between the molecular size of the two targeted gas components to be separated (Pandey and Chauhan, 2001). Size exclusion selectivity mechanism results in an extremely high membrane selectivity. Faster diffusion rates of small molecules transporting through zeolite membrane based on size selectivity enhance the molecular sieving ability of the membrane (Li et al., 2015). More often than not, in the small molecule mixtures, using microporous zeolite membranes, separation will occur based on size selectivity (Zhong et al., 2016). However, for the size selectivity principle to be fully relied upon, it is required zeolite membranes are free of pinholes and cracks and the membrane pore size should be within the molecular sizes of the two targeted components to be separated.

2.6.2 Adsorption mechanism

In addition to molecular sieving, gas transport in some zeolite membranes can also follow mechanism based on preferential adsorption (competitive adsorption). The transport of gases

through zeolite membrane by adsorption mechanism depends on the adsorption strength of the gases in the zeolite membrane pore surface. Adsorption is an exothermic, a competitive phenomenon, and a non-activated process which is driven by fugacity (Gkanas et al., 2015). Competitive adsorption occurs in microporous membranes if one of the gas pair is absorbing and the other is non-adsorbing or weakly adsorbing. During separation, the adsorbing gas(es) are preferentially adsorbed into the internal zeolite pore surfaces and permeate through the membrane via surface diffusion. As a result, the free spaces of the membrane pores are blocked and is dramatically reduced by the adsorbing molecules. Thus, the entry and passage of non-adsorbing molecules are limited (Dong et al., 2008).

2.6.3 Diffusion mechanism

Diffusion is an activated process which depends on the heat of adsorption, on the molecular size of the adsorbate and the fractional coverage. Key parameters for gas transport in zeolites for both surface and micropore (molecular) diffusion include pressure, the heat of gas adsorption, temperature, molecular weight, pore diameter, kinetic molecular diameter, thermal activation energies (Gkanas et al., 2015). Gas transport by surface diffusion takes place when adsorbed molecules jump from one adsorption site to another on the pore walls and migrate along the surface of zeolite membrane (Jareman et al., 2004; Li et al., 2015). When this is the case, zeolite membrane selectivity is dependent on both adsorption and diffusion properties of the gases on the pore walls (Dong et al., 2008; Li et al., 2015). Molecular diffusion occurs when the collision between the molecules are primary, and it is dominant when the mean free path of the molecules is smaller than the pore size (Fan et al., 2013). Diffusion through microporous membranes whether for multi-component mixtures or single component species is described by the generalized Maxwell-Stefan model for diffusion (Kapteijn et al., 2000; Grahn and Hedlund, 2014; Nikolić and Kikkinides, 2015; Gkanas et al., 2015). The more simplistic phenomenological Fick law equation could also be used to describe diffusion through membranes, particularly for small gases at elevated temperatures.

2.6.4 Knudsen diffusion mechanism

Knudsen diffusion (KD) flow occurs when the mean free path of the permeating molecule is comparable to or greater than the pore size of the barrier. According to Jareman et al. (2004), Knudsen diffusion mechanism/separation relies upon pores in the barrier that are smaller in diameter compared to the distance a molecule would travel in gas phase between collisions. Gas molecules thus experience more collision with the pore walls than collisions with other gas molecules (Ruthven et al., 2009). When the mechanism of separation for a given gas pair is based on Knudsen diffusion, it is as a result of the difference in molecular masses arising from frequent collision with the pore walls (Armor, 1998). Knudsen diffusion selectivity for binary gas pair is calculated using Equation 2.6 as the inverse square ratio of the molecular weight of gas A and gas B and represents the ideal separation factor.

$$\mathrm{KD}_{\mathrm{A}/\mathrm{B}} = \sqrt{\frac{\mathrm{MW_B}}{\mathrm{MW_A}}} \tag{2.6}$$

Where KD is Knudsen Diffusion, $\mathrm{MW_B}$ is the molecular weight of gas B , and $\mathrm{MW_A}$ is the molecular weight of gas A This ratio gives the relative permeation rate and thus provides a theoretical value of Knudsen selectivity. The theoretical value predicted by Knudsen diffusion mechanism for a mixture of H_2/CO_2 is 4.67 (Pandey and Chauhan, 2001; Khalilpour et al., 2015). Knudsen selectivity of H_2 over other small gases is generally low, not attractive and ineffective for high purity hydrogen separation. The implication of which is that a large amount of hydrogen is lost in the permeate.

In summary, the separation of gases in zeolite membranes may follow mechanisms based on molecular sieving, Knudsen diffusion, preferential adsorption and/or diffusion effects. Either one or a combination of the mechanisms can govern or dominate selective transport and could occur in parallel. Any particular mechanism dominant will depend on the pore size of the membrane, the size of the molecules and the trans-membrane pressure difference (Lindmark and Hedlund, 2010). Figure 2.13 shows the schematic representation of the different gas transport mechanisms in an inorganic microporous membrane and their effect on the gas separation efficiency.

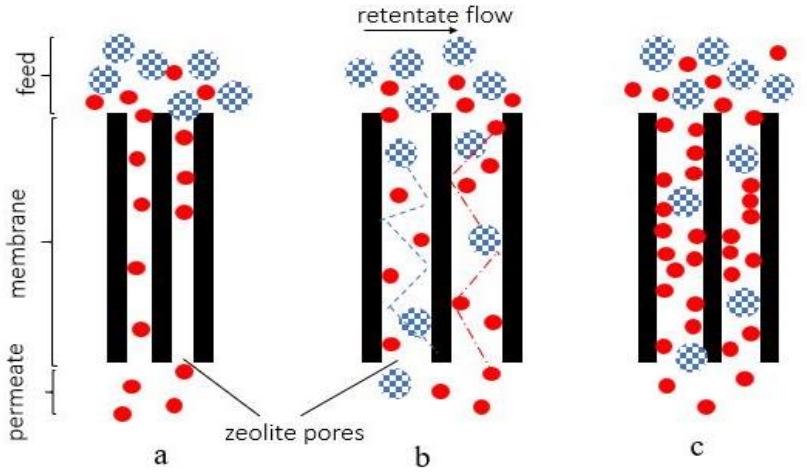

Figure 2. 13 (a) molecular sieving (b) Knudsen diffusion (c) convective flow (Adapted from Shao et al., 2009; Al-Mufachi et al., 2015)

2.7 Synthesis Strategies for Zeolite Membranes

Zeolite can occur as natural minerals (Hosseinzadeh Hejazi et al., 2011) and can be synthesized into a uniform and pure state phase (synthetic). The crystalline product of synthetic sodalite is pure and the particles are uniform. Hence, they are of more commercial value and are more utilized than natural zeolite (Cundy and Cox, 2003). Also, synthetic zeolite possesses greater stabilities and can be engineered to display several chemical properties and pore sizes (Petrov and Michalev, 2012; Esaifan et al., 2017). Various strategies of synthesizing zeolite membranes have emerged in the literature. Synthetic zeolites can be prepared by treating natural zeolites (natural clay minerals) which preserves their initial crystalline structure and by conventional hydrothermal synthesis (Georgiev et al., 2009). However, the hydrothermal technique as discussed in the following section is the commonly used method for the synthesis of a variety of zeolites crystals/membranes (Caro et al., 2000; Esaifan et al., 2017). Depending on synthesis conditions such as pH, temperature, time, etc., the amorphous phase at the point of mixing is converted into crystalline zeolites. Literature over the years has described three different hydrothermal synthesis method for fabricating zeolite membranes. They are;

2.7.1 Direct hydrothermal synthesis method

In this method, a thin selective zeolite layer is crystallized from the gel solution under hydrothermal conditions in one or more step in the presence of the support under autogenous pressure (Cundy and Cox, 2003). The gel for the surface crystallization forms a surface layer and eventually grows a zeolite membrane on top of the support (Khajavi et al., 2010a). According to Daramola et al. (2010b), zeolite synthesis via this approach results in nucleation and crystal growth occurring simultaneously, thus leading to competitive and less homogenous growth. As a result, a low-density film of zeolite crystals is formed on the surface of the support (Miachon et al., 2006). In addition, the synthesis approach provides little flexibility for control over the microporous structure of the final film (Tsapatsis and Gavalas, 1999). Often, membranes prepared by the direct hydrothermal synthesis in one cycle usually possess defects because of lack of connectivity or continuity between the individual zeolite crystals (lack of enough intergrowth) (Kalantari et al., 2015). Therefore, to prepare zeolite membranes with continuous film, more than one hydrothermal cycle is done. The eventual outcome is a membrane that becomes too thick such that membrane fluxes are dramatically reduced. Not only that, the inherent presence of high intercrystalline porosity on the film surface leads to loss of selectivity of the membrane (Daramola et al., 2010b). This synthesis approach is has been well reported in the literature (Sebastián et al., 2007; Van Niekerk et al., 2007; Khajavi et al., 2007a, 2010b; Vaezi and Babaluo, 2014; Fasolin et al., 2019; Guan et al., 2019).

2.7.2 Secondary seeded growth (SSG) hydrothermal synthesis method

The seeding technique for zeolite membrane preparation was proposed after it was observed that competition between nucleation and crystal growth from direct hydrothermal synthesis technique limit nuclei density on the support surface. In other to reduce or control the influence of support and to improve heterogeneous nucleation on support surface over the characteristic/permeation properties of resulting zeolite membrane prepared by direct hydrothermal synthesis, some researchers have resorted to preparing membranes in two stages (Kalantari et al., 2015; Wang et al., 2015c; Yang et al., 2016; Kazemimoghadam and Rigi, 2018). In the SSG approach, homogenous synthesis in the absence of the support to yield colloidal zeolite crystals is first carried out. Secondly, the synthesized zeolite crystals are then used as seeds deposited on the support to coat the support which provides the needed nucleation site (Kalantari et al., 2015). The coating of

the support is commonly achieved by methods such as dip coating, vacuum suction or mechanically scrubbing the surface with zeolite crystals (Liu et al., 2011). The seeded support is then brought in contact with a solution containing the necessary dilute nutrients and then hydrothermally grown to eliminate intercrystalline porosity. Because low precursor concentration is needed for secondary growth, zeolite nucleation is strongly decreased further and almost all the crystal growth takes place over the existing crystal seeds during subsequent hydrothermal synthesis. Since the composition and concentration of the secondary growth solution can be controlled, crystallization of undesired zeolite phases (parasitic phase) and leaching of the support can be avoided. Since both nucleation step and crystal growth process are decoupled, this approach allows independent control of each step and for greater flexibility in choosing hydrothermal synthesis condition to achieve desired nutrient (Tsapatsis and Gavalas, 1999; Bernardo et al., 2009).

However, a drawback of this technique is difficulty in dispersing high purity seed homogenously on the support surface (Fan et al., 2013), difficult control of the amount of seed deposited on the support surface (Kazemimoghadam and Rigi, 2018), and the ease of formation of defects or non-zeolitic pores on the film. The presence of defect which forms intercrystalline pathways, larger than the zeolite pores lower the selectivity of the membrane (Bernardo et al., 2009). Not only that, since the support surface is coated with zeolite seed, the pore size of the support is decreased. As a result, thick or dense zeolite layer is formed which lowers flux and leads to loss of significant permeance. Moreover, weak adhesion or interaction between the zeolite layer and the support surface may occur therefore reducing the chances of reproducibility (Kalantari et al., 2015). Membranes prepared with this method have been well reported (Huang et al., 2010c; Kalantari et al., 2015; Wang et al., 2015; Yang et al., 2016). The membranes were found to be relatively thick, provided large transport resistances and exhibited crack development due to seeding.

In summary, membrane prepared via direct hydrothermal synthesis technique and secondary seeded growth technique form a continuous thin layer of zeolite crystals on top of the porous support. Resultant membrane is referred to as a thin-film architecture membrane and is well documented in the literature (Li et al., 2013; Kalantari et al., 2015; Kazemimoghadam and Rigi, 2018). To crystallize a continuous and well-grown zeolite film without cracks while trying to maintain a very thin microporous zeolite layer for optimal flux is quite challenging. Thus, to reduce

interparticle void between adjoining crystals, the zeolite layer is often grown thick. Thick membrane limits flux i.e. slow down the transport of permeating species (Bedard and Liu, 2018). Equally important to note is, when thin-film like membranes are operated at high temperature, > 400 °C, crystalline opening (the gap between two well contact crystallites) are formed or existing gaps are enlarged which could govern mass transfer (Yang et al., 2016). This is due to thermal expansion mismatch between the support and the zeolite layer leading to crack formation/grain boundary opening (Yang et al., 2016). From a practical perspective, this effect translates to low reproducibility making scale-up of a film like zeolite membranes difficult (Alshebani et al., 2008b; Daramola et al., 2010b).

2.7.3 Pore-plugging hydrothermal synthesis method

To overcome the challenges of a film like zeolite membranes while maintaining selectivity, the pore-plugging hydrothermal (PPH) synthesis was developed by Miachon et al. (2006). In this technique, zeolite nanoparticles are crystallized hydrothermally inside the porous matrix of the support to form a nanocomposite membrane rather than forming a thin-film on top of the support. During synthesis, an interruption time is introduced by decreasing the temperature. During the interruption, nucleation and crystal growth process is inhibited, thus allowing an increase in precursor concentration to diffuse into the pores of the support. Zeolite nucleation and growth process are therefore enhanced when hydrothermal synthesis begins again without the formation of a continuous film on top of the support (Giroir-Fendler et al., 1996; Miachon et al., 2006; Daramola et al., 2010b). No literature has ever reported interruption time using the SSG and direct hydrothermal synthesis techniques. Recently, Lafleur et al. (2017) reported a new pore-plugging technique for developing a water-selective zeolite composite membrane. The resultant pore-plugged membranes performed fairly well using single-component gas permeation experiments and displayed considerable thermal stability at 250 °C even in the presence of water for long hours. Guillou et al. (2009) developed a faujasite membrane using the PPH synthesis technique. The scanning electron microscopy analysis test conducted shows that the interparticle porosity membrane was closed by the FAU crystals after two hydrothermal treatments.

The difference between nanocomposite and thin-film architecture is shown in Figure 2.14. Plugged zeolite membranes have exhibited different separation behaviour and improved mechanical

stability over their film-like counterpart membrane (Miachon et al., 2006; Daramola et al., 2010b, Lafleur et al., 2017). Nanocomposite membranes have been well studied for different applications also (Ciavarella et al., 2001; Dyk et al., 2005; Camus et al., 2006; Daramola et al., 2010b). Membranes having nanocomposite architecture offer the following advantages: (i) Reduced or minimal thermal expansion mismatch between support and zeolite that may appear in film-like configuration, (ii) easy scale-up, and (iii) easy module assembly/handling, (iv) reduced abrasion and thermal shocks which could promote defects/intercrystalline pores formation, (v) mass transfer governed by the zeolite pores of the membranes, (vi) enhanced gas separation, (vii) preferred architecture when large membranes areas are required, and (viii) high potential in several separation applications like xylene isomer separation, ammonia recovery, isobutane dehydration, and xylene isomerization (Miachon et al. 2006; Alshebani et al., 2008a). However, synthesizing defect-free, reproducible, and high permeance nanocomposite zeolite membranes such that gas transport through zeolite pores only is still a challenge (Caro et al., 2000; Kosinov et al., 2016).

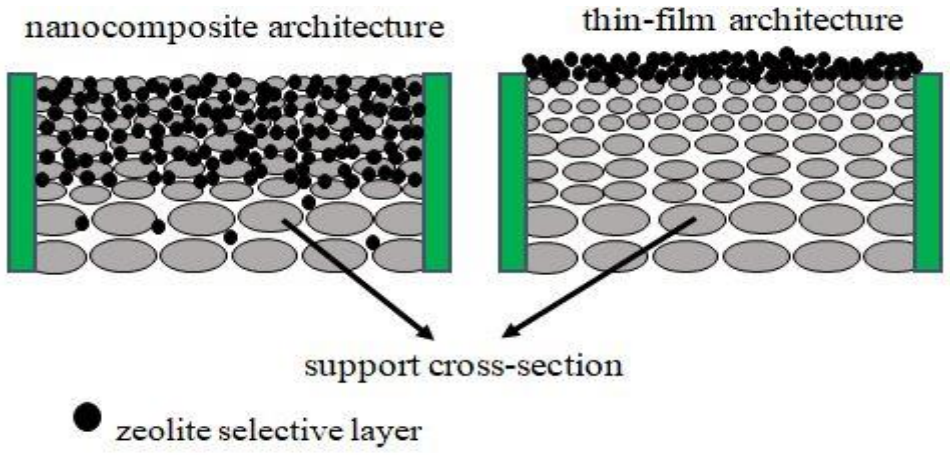

Figure 2. 14 Nanocomposite architecture versus thin-film architecture membrane

2.8 Reported Zeolite Membranes for H_2/CO_2 Separation

Zeolite membranes have been synthesized for different purposes under different condition using different techniques. However, most results for H_2 permeance have been commonly achieved by thin or thick membranes as discussed in the previous section. Sodalite membranes for CO_2 separation have focused on the separation of the CO_2/N_2 gas pair (Lafleur et al., 2017) or CO_2/CH_4

gas pair (Nabavi et al., 2014). Scanty literature exists for H_2/CO_2 gas pair using sodalite zeolite. Table 2.3 presents a literature survey of selected zeolite membranes for H_2/CO_2 separation.

Table 2. 3 Selected results of some inorganic zeolite membrane

Zeolite	Support	Preparation Technique	Temp (°C)	TMP (KPa)	Permeance (10^{-7} mol.s^{-1}.m^{-2}.Pa^{-1})		IS	Ref.
					H_2	CO_2		
Silicalite	γ-Al_2O_3 tube	DH	25/170	-	34/36	-	-	Bai et al. (1995)
ZSM-5	TiO_2 disk	DH	27/187	138	18/24	-	-	Coronas et al. (1997)
DDR	Clay Al_2O_3 tube	SSG	30	-	4.04	1.10	3.7	Bose et al. (2014)
DDR	α-Al_2O_3 disk	DH	25	207	22.8	-	2.4	Zheng et al. (2008)
DDR	α-Al_2O_3 disk	SSG	500	50	0.22	0.04	-	Kanezashi et al. (2008)
HSOD	α-Al_2O_3 tube	DH	-	0.38	0.02	-	19	Vaezi and Babaluo (2014)
SSZ-13	Mullite tube	DH	20	200	-	2.9	-	Wang et al. (2019)
$AlPO_4$-18	α-Al_2O_3 tube	SSG	25	200	1.5	6.2	-	Wang et al. (2015c)
NaX-Ga	Clay Al_2O_3 tube	SSG	25	300	36.1	5.4	6.69	Roy and Das (2019)
SAPO-34	α-Al_2O_3 tube	SSG	25	200	17	39	-	Mei et al. (2018)
HSOD	Porous Al_2O_3	DH	20	150	2.4	0.75	-	Fasolin et al. (2019)
HSOD	α-Al_2O_3 tube	PPH	25		0.74	0.11	6.46	Oloye et al. (2019)

SG: secondary seeded growth; PPH: pore-plugging hydrothermal; DHS: direct hydrothermal synthesis; IS: ideal selectivity

Concluding Remarks

A short overview of carbon capture and storage (CCS) has been presented. The state-of-the-art on the development of membranes applicable in CCS has also been provided. Only a handful of researchers have reported on sodalite zeolite membrane for H_2/CO_2 gas pair. Optimizing the pore-plugging hydrothermal synthesis protocol to produce pure zeolite crystals could be instrumental in developing high-quality zeolite membrane applicable for pre-combustion CO_2 capture. Based on this insight, the remaining chapters of this dissertation will demonstrate, provide results and discuss;

1. The optimization of the pore-plugging hydrothermal synthesis protocol for the production of high purity sodalites.
2. Synthesis of high-quality nanocomposite sodalite membrane supported on ceramic tube using the optimized protocol(s) obtained in (1).
3. The evaluation of the as-synthesized nanocomposites sodalite membranes developed in (2) using single gas permeation of H_2, CO_2, and N_2 in comparison to thin-film as-synthesized membranes.
4. The investigation of the best performing sodalite membranes in (3) using a binary mixture of H_2/CO_2.

Chapter 3: Experimental Procedures and Analysis

3.1 Experimental

The materials and equipment used in this study are briefly described in this chapter. A detailed description of the sodalite precursor preparation, sodalite crystal optimization, sodalite membrane synthesis, and the various characterization techniques applied are discussed in this chapter. Figure 3.1 shows a summary of the experimental procedure employed in this study.

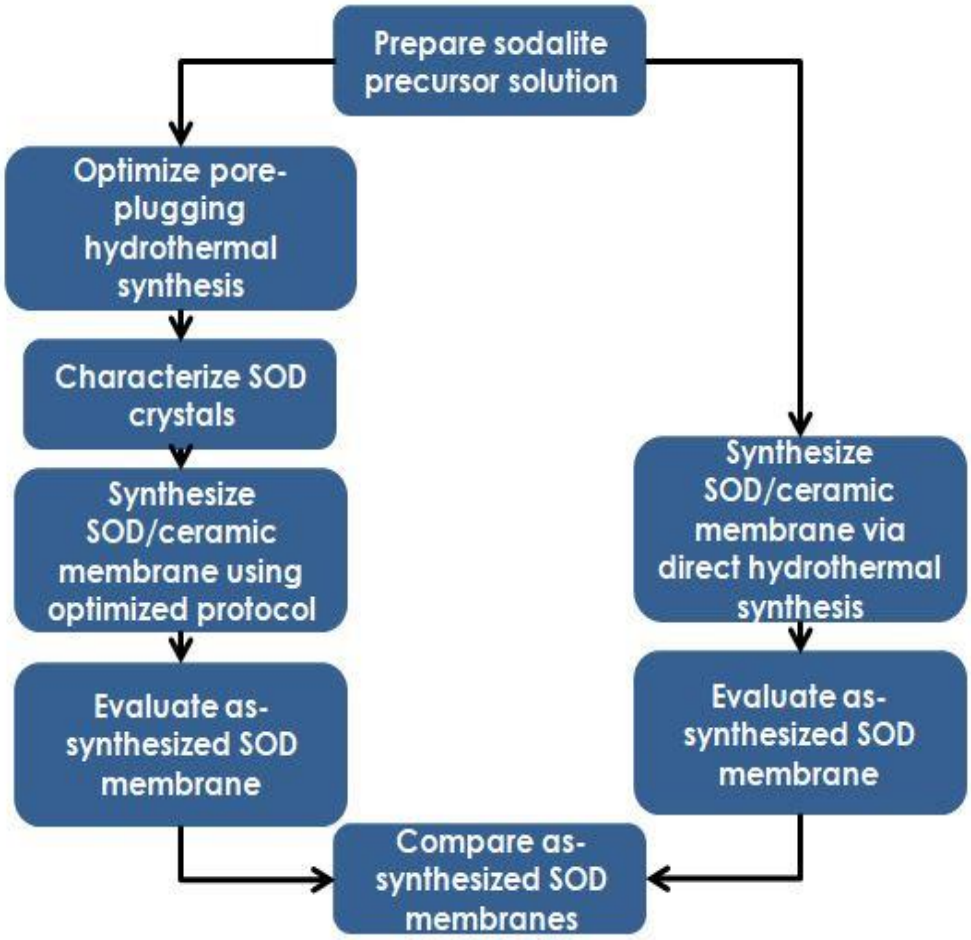

Figure 3. 1 Summary of experimental procedure

3.1.1 Chemicals and materials

The chemicals used in the synthesis of sodalite (SOD) crystals and SOD membranes are anhydrous sodium aluminate ($NaAl_2O_3$), sodium metasilicate (Na_2SiO_3), and anhydrous sodium hydroxide (NaOH). The chemicals were purchased from Sigma-Aldrich (Pty), South Africa and used without further purification. Deionized water used in the synthesis was prepared in-house. The gases used for this study were hydrogen (baseline, 99.999 %), nitrogen (baseline, 99.999 %), carbon dioxide (technical), and binary mixture of H_2/CO_2 (60/40) supplied by African Oxygen Limited, South Africa (AFROX). The α-alumina (Al_2O_3) tubular support (Figure 3.2) for membrane synthesis were purchased from Pall-Exekia, Germany, with no modifications done on the tube before synthesis. The support consists of three layers (see Figure 3.3) of different average pore size (0.2 μm microporous top layer, 0.8 μm mesoporous middle layer, 12 μm macroporous bottom layer). The tube (o.d. 10 mm, i.d. 7 mm) have both ends of the support coated with 1 mm non-porous surface for sealing in the module, making the total permeating length 13 cm. See Table 3.1 for other properties of the support.

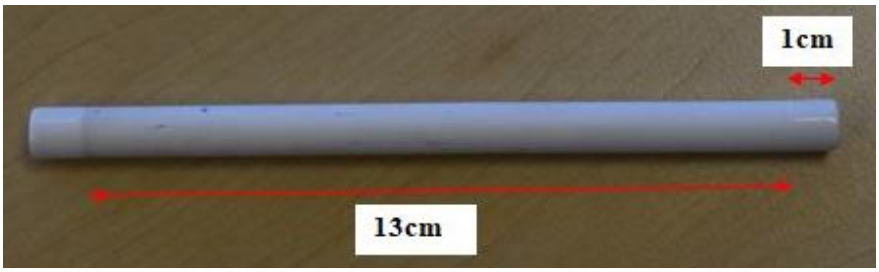

Figure 3. 2 Picture of typical tubular support (pictures not to scale)

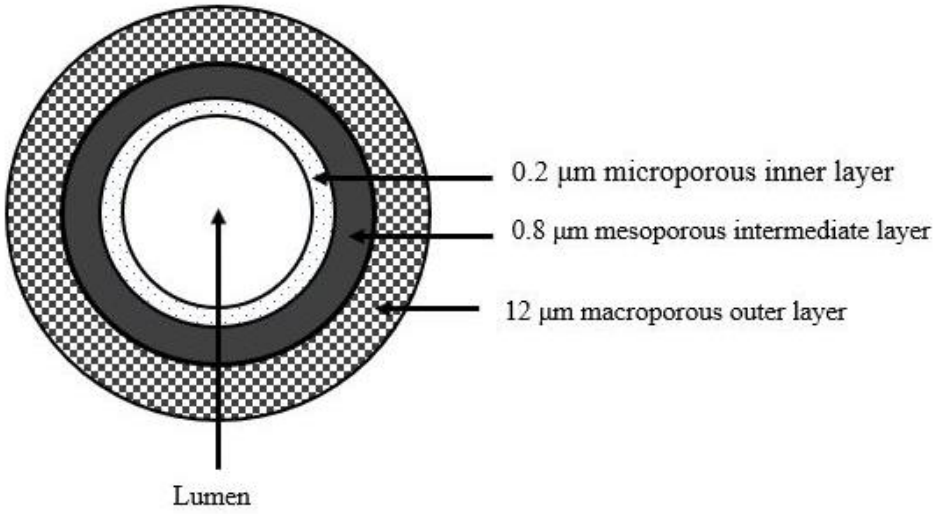

Figure 3. 3 Cross-section of the tubular support

Table 3. 1 Property of raw support

Property	α-Al_2O_3 tube
O.D (mm)	10
I.D (mm)	7
Sealing (mm)	10 (both ends)
Permeable length (mm)	130
Active internal surface area (mm^2)	2859
Porosity (%)	32
Thickness (mm)	1.50
Core volume (mm^3) using permeable length	5207
Surface to volume ratio (m^2/m^3)	200
Weight (g)	16.293

O.D: Outside diameter; I.D; Internal diameter

3.1.2 Experimental equipment

The following equipment were used in this study: magnetic stirrer, hydrothermal synthesis reactor/autoclave, LABOTEC EcoTherm® oven, filtration set-up, heating plate, membrane module, and membrane gas separation set-up. Hydrothermal synthesis of SOD crystals and SOD membrane was done in an autoclave. A 45mL capacity Teflon® lined stainless-steel vessel (model 4744) manufactured by Parr Instrument Company, U.S.A, with a maximum temperature rating and working pressure of 250 °C and 12.4 MPa, respectively (Figure A.1 in the Appendix section) was used in the synthesizing of SOD crystals. This vessel has an inner PTFE (Teflon) liner which helps

prevent corrosion and a stirrer to mix the precursor solution to obtain a homogenous solution. A 3284-model large-capacity vessel (Figure A.2) fabricated by Amar Equipment Pvt. Ltd was also used in the synthesizing of SOD/ceramic membrane. The vessel has a 250 mL removable PTFE cup in a stainless-steel body with six cap screws to seal the flanged PTFE cup. It has a working temperature and pressure of 250 °C and 110 bar, respectively. The pre-treatment of the support was done in boiling de-ionized water to remove dirt, loose particles and oily matters, over a heating plate. A membrane gas separation system designed by CHEMVAK cc South Africa, Pty was used for the evaluation of as-synthesized membrane (Figure A.3 in the Appendix section).

3.1.3 Description of the membrane module

The as-synthesized SOD/ceramic membrane was gently placed inside the membrane module (Figure 3.4a) and held firm in the module using graphite O-rings seals (Figure 3.4b), which also sealed the non-porous ends of the ceramic tube membrane to the membrane module. After setting laboratory gas supplies from the cylinder to the desired pressure, forward pressure regulators were adjusted to tune individual gas inlet pressure into the module. Thereafter, feed gas was fed inside of the membrane in the module at a specific pressure (0.1 MPa – 0.5 MPa) and temperature (25 °C – 200 °C). The temperature was increased in small increments to avoid sudden overheating of the furnace and module. A schematic of the membrane module is shown in Figure 3.5.

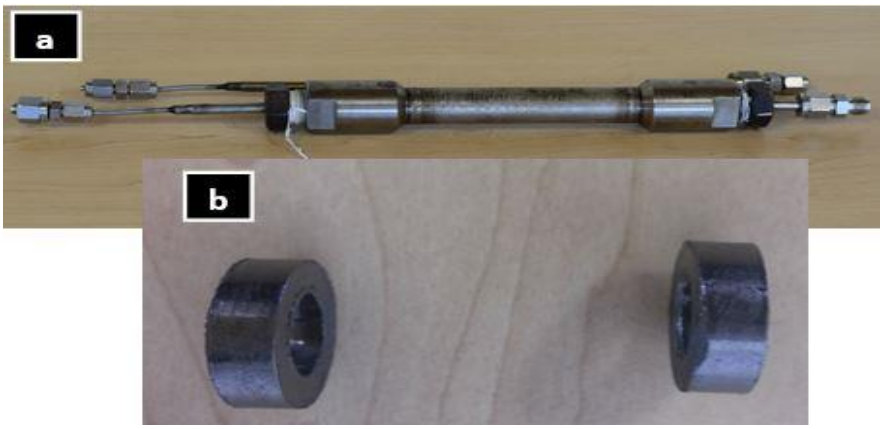

Figure 3. 4 Picture of the membrane module used in this study showing graphite seals below (picture not to scale)

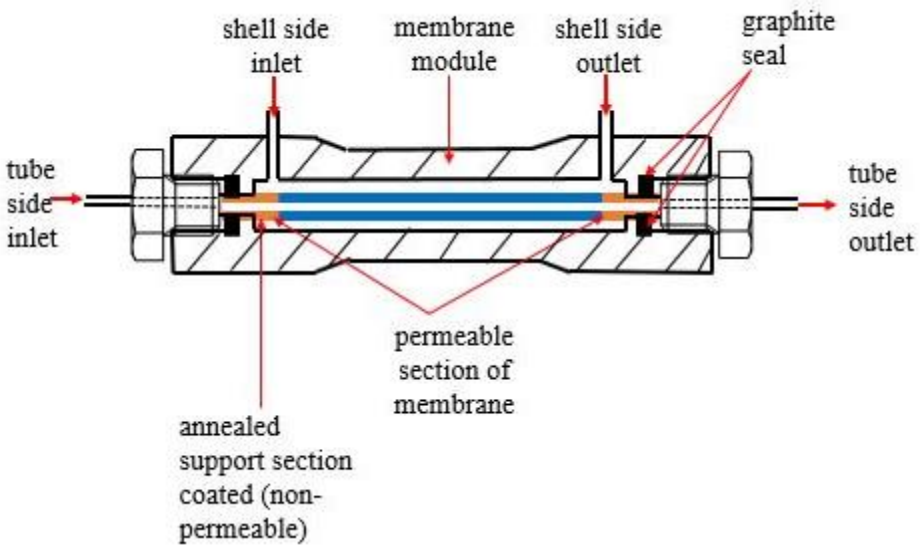

Figure 3. 5 Schematic of membrane module inside which the synthesized tubular membrane sits in (Modified from Miachon et al., 2007)

3.1.4 Membrane gas separation equipment

The membrane gas separation system used in the study is a laboratory-scale research instrument designed for the separation of CO_2 from different gas mixtures. The unit houses a furnace with temperature ranging from ambient to 500 °C. Attached to the furnace is a temperature control unit with a built-in thermocouple connected to the heated elements for setting the temperature of the furnace. Another thermocouple was also connected to the membrane module furnace for measuring the feed gas temperature after passing through the heat exchanger coils. The pressure range of the unit is from atmospheric to 500 KPa (5 bar), operating at a flow rate range between 0 ml/min – 500 ml/min for each gas. The omega mass flow meter (MFM), with a 0 – 5 VDC output signal was used to adjust the gas flow rate. Flow rates of the permeate gas were measured using soap bubble flow meters. When the unit was not activated, connected ASCO 3-way electro-pneumatic valves were used to exhaust the feed/retentate and permeate line to the atmosphere. The front and side view of the membrane gas separation system is depicted in Figure A.3. Figure A.4 show feeding cylinders to the membrane gas separation testing rig. The detailed process flow diagram with the component list for this set-up is presented in Appendix B.

3.2 Synthesis of SOD Crystals

The synthesis of SOD crystals followed a modified method of Miachon et al. (2006) as reported by Daramola et al. (2017). A precursor solution with a molar composition of $5SiO_2$:$0.5Al_2O_3$:$50Na_2O$:$1005H_2O$ and a pH of 14, was subjected to PPH synthesis in a pre-heated conventional oven. Parallel experiments were carried out by ageing under stirring continuously 45 mL of the precursor solution for 4 hours at ambient temperature before PPH synthesis. At the end of SOD crystal synthesis, the hot autoclave was cooled under flowing tap water to obtain the as-prepared SOD crystals. Then, the crystals were washed and centrifuged at 4000 rpm for 4 times using deionized water until the pH of the filtrate is approximately 7. Afterwards, SOD crystals were dried at 100 °C overnight in an oven. The illustration of the synthesis of SOD crystals with ageing is depicted in Figure 3.6

3.3 Synthesis of SOD/Ceramic Membrane

Nanocomposite sodalite/ceramic tubular membrane was prepared following a modified method by Miachon et al. (2006) as reported by Daramola et al. (2017). Before the membrane was synthesized, raw support was pre-treated thermally in boiling DIW in a 2 L volumetric flask for about 1 hour until no more bubbles emerged from the support surface. This cleaning process was done to degas any trapped air inside the support and to remove any loose particles, dust, the oily matter that might have formed on/in the porous structure of the support. Support was dried for 1 hour in an oven at a temperature of 100 °C, cooled to ambient temperature and inserted vertically into a Teflon liner containing SOD precursor solution. The Teflon liner with its content was left for about 15 mins to allow the displacement of air from the pores of the support. After which it was covered with its lid and placed in a stainless-steel autoclave where it was properly sealed with 6 bolts and nuts. The autoclave with the tube in it was then transferred to a pre-heated conventional oven for pore-plugging hydrothermal synthesis. The illustration of the synthesis of SOD/ceramic membrane is depicted in Figure 3.6.

Because of the small pore size of SOD which are too small to let void-filling guests pass, structure-directing agent (SDA), was not required and therefore no SDA was used in this study. The removal of SDA requires burning off the template to activate zeolite microporosity. This is detrimental to the SOD material (Fan et al., 2008). SOD membrane prepared with SDA lead to loss of

crystallinity, crack formation, and finally the destruction of sodalite layer (Dong et al., 2000; Czyperek et al., 2010). After PPH synthesis, membrane and SOD crystals formed on the base of the Teflon liner were recovered and washed with deionised water until the pH of the water was neutral. Afterwards, washed membrane and SOD crystals were dried overnight in an oven at 100 °C. The membrane was then ready for testing as no activation was needed.

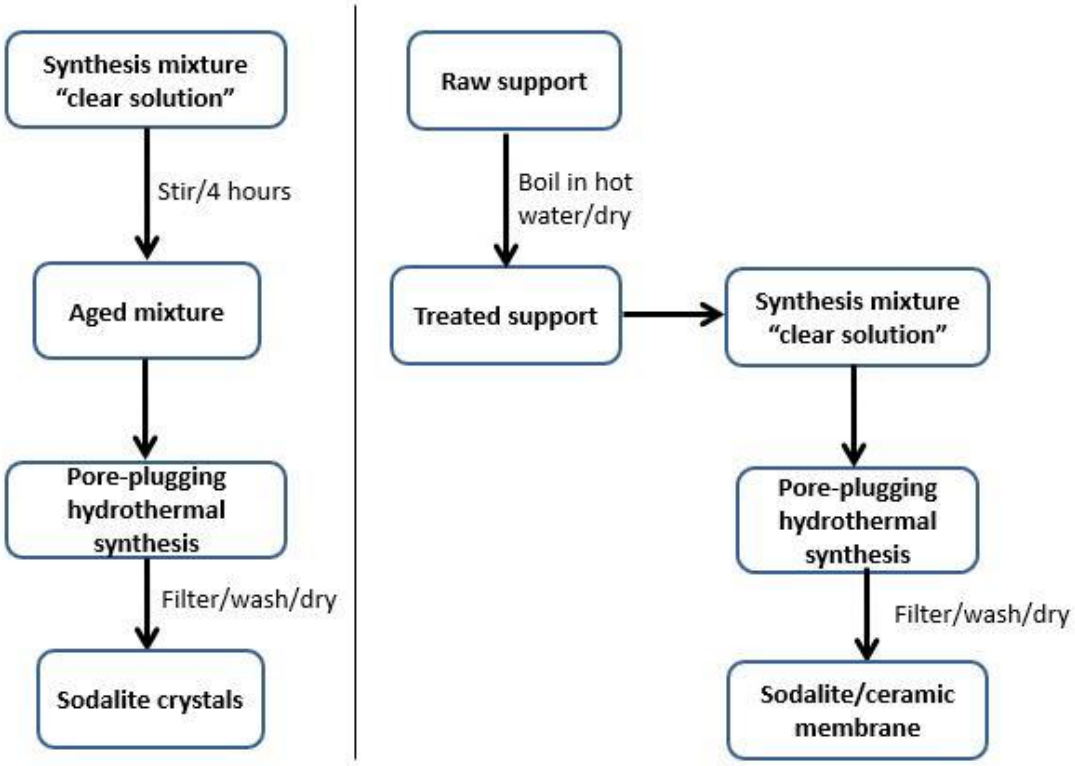

Figure 3. 6 Illustration of sodalite crystal synthesis with ageing (left) and sodalite/ceramic membrane synthesis

3.4 Membrane Characterization Techniques

Several techniques for characterizing zeolite crystals and membrane have emerged in the literature (Bonilla et al., 2001; Bernal et al., 2002; Kumakiri et al., 2008; Korelskiy et al., 2012). The scanning electron microscope (SEM) coupled with electron dispersion x-ray spectroscopy (EDX), and x-ray diffractometer (XRD) were used as physico-chemical techniques to characterize SOD crystals and SOD/ceramic membrane qualitatively. The performance of zeolite membrane depends on the quality and intergrowth of the zeolite crystals. In zeolite membranes, permeating molecules

can pass through both zeolite pores and defects (non-zeolite pores plus intercrystalline pores e.g. open grain boundaries and intercrystalline pathways e.g. broken Si-O-Si bonds), (Maghsoudi, 2016). Hence, it is vital to characterize the microstructure of membranes. To evaluate the transport or dynamic properties of the as-synthesized membrane, single gas (H_2, N_2, and CO_2) permeation measurement was employed as a dynamic characterization technique for this study.

3.4.1 X-ray diffraction (XRD)

X-ray diffraction technique is a very useful tool and the most common technique used to characterize zeolite crystals and membrane. In this study, the crystallinity and purity of SOD nanoparticles were checked using an X-ray diffractometer (Bruker D2 phaser diffractometer) equipped with Cu Kα radiation [λ = 1.54184 Å] in the 2-theta range of 10 to 50 °C, at 0.02° with a counting time of 31.4 s per step. XRD patterns were generated and compared to the reference SOD XRD pattern from the International Zeolite Association (IZA) database (Treacy and Higgins, 2007). If the XRD diffraction peaks matched with the reference SOD crystals, it thus indicates the successful formation of pure SOD.

The generated XRD pattern is also useful in calculating the percentage of SOD crystallinity. SOD crystallinity estimation was done using sodalite peaks at d_{110}=13.89°, d_{112}=24.30°, d_{310}=31.74°, d_{222}=34.38° and d_{411}=43.06° of the as-synthesized SOD crystals and reference SOD from IZA following Equation (3.1) (Liu et al., 2018):

$$\%\, crystallinity = \frac{\Sigma\, peak\ intensities\ of\ sample}{\Sigma\, peak\ intensities\ of\ reference} \times 100\% \qquad (3.1)$$

Particles size of the crystals was obtained via the Scherrer formula Equation (3.2) (Bayati et al., 2008)

$$d = {}^{k\lambda}/_{\beta \cos\theta} \qquad (3.2)$$

Where K represents the geometrical coefficient and denoted to be 0.9, D is the crystallite size (nm), λ is the radiation wavelength, θ is the angle of the diffraction peak in radian and β is the full-width at half minimum (FWHM).

3.4.2 Scanning electron microscopy (SEM) coupled with energy-dispersive x-ray spectroscopy (EDS)

The scanning electron microscope (SEM) is an instrument that uses a focused beam of high-energy electrons to generate a variety of signals at the surface of solid specimens. SEM instrument was used in this study to check the morphology of the as-synthesized crystals. To obtain high-resolution electron imaging, the samples were coated with Gold Palladium (AuPd) metal. An FEI Nova NanoLab 600 SEM machine operated at an acceleration voltage of 30.0 kV and 0.63 nA housed at the microscopy and microanalysis unit (MMU), University of the Witwatersrand, Johannesburg was used for SEM analysis of all samples. SEM was also used, semi-quantitatively in determining the elemental compositions (e.g., Si/Al and Na/Al ratios) of the SOD crystals using energy-dispersive X-ray spectroscopy (EDS).

3.4.3 Fourier transform infrared (FT-IR)

Fourier transform infrared (FT-IR) analysis was used to investigate the surface nature of the as-synthesized SOD crystals. Perkin Elmer Spectrum Two FT-IR spectrometer (Perkin Elmer, USA) equipped with attenuated total reflectance (ATR) accessory was used in identifying the surface functional groups of SOD crystals. All spectra were obtained in the range of 4000 - 450 cm^{-1}.

3.4.4 Thermogravimetric analysis (TGA)

The thermal stability of SOD crystals produced was characterized using TGA 701 Leco thermal analyzer with a nitrogen flow rate of 60 mL/min from room temperature to 900 °C at a ramping rate of 5 °C/min.

3.5 Membrane Performance Evaluation

3.5.1 Single gas permeation

Single gas permeation was conducted to evaluate membrane quality. Pure gases of N_2, H_2 or CO_2 was fed to the inner surface of the membrane. Table 3.2 presents the properties of the gases utilized.

Table 3. 2 Properties of gases used in this study (Shao et al., 2009; Ghadimi et al., 2014; Kosinov et al., 2016)

Properties	H_2	CO_2	N_2
Molecular weight (g/mol)	2.02	44.01	28.01
Kinetic diameter (nm)	0.289	0.330	3.64
Critical temperature (K)	33.2	304.1	126.2
Condensability (K)	60	195	-

Single gas permeation was measured as a function of pressure ranging from 0.1 MPa to 0.5 MPa and at a temperature ranging from 25 °C to 200 °C in dead-end mode (retentate stream blocked). Permeate gas flowed through the gap between the membrane and module. The test was conducted without sweep and permeate side pressure was kept at atmospheric pressure all through. It was ensured that the system reached steady-state under a set of experimental variables before any measurements were taken. Also, the experimental test for each membrane was done at least twice to ensure reliable statistical average. A schematic process flow diagram (PFD) of the permeation set-up employed for single gas permeation is presented in Figure 3.7.

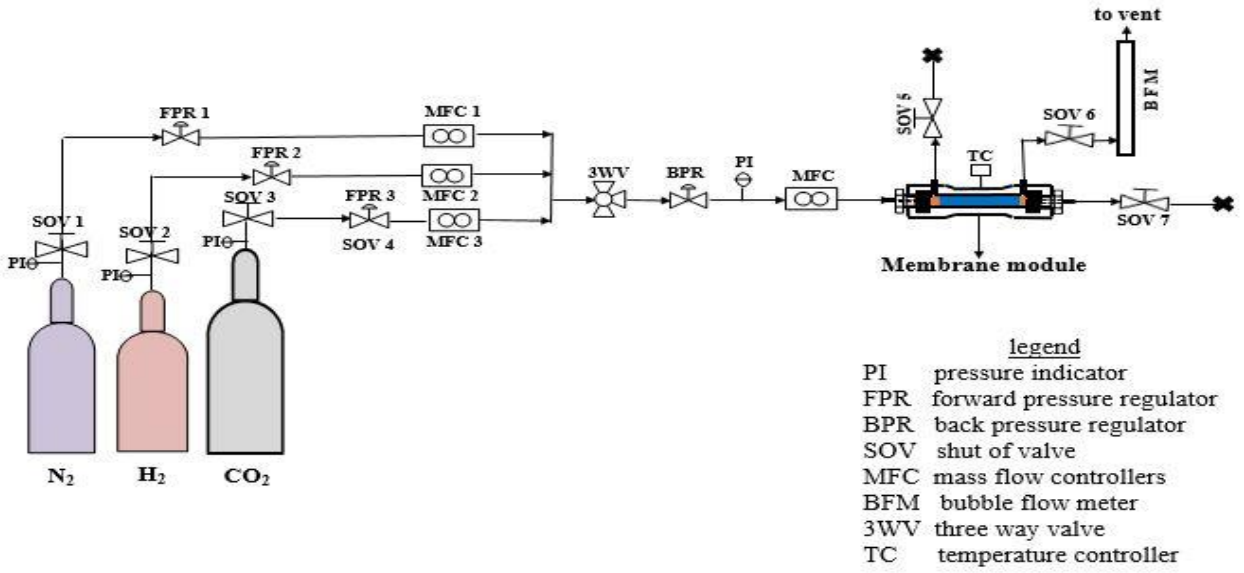

Figure 3. 7 Process Flow Diagram (PFD) of the permeation set-up employed for single gas permeation

Transport properties and performance for microporous inorganic gas separation membranes are commonly reported in flux, permeance and/or selectivity. Flux can be defined as the total transport of material through the membrane. The flux, F of specie i, through the membrane was calculated by dividing molar flow rate, f_i of the gas by membrane area. Flux was obtained using Equation 3.3.

$$F_i = \frac{f_i}{A} = \frac{n}{A\,t} \qquad [\text{mol.s}^{-1}.\text{m}^{-2}] \tag{3.3}$$

Where n is the amount of gas in mol of each pure gas permeated through the membrane area A, in permeation period t (s). Calculation of molar flow rate $f_{i.}$ was according to Equation 3.4.

$$f_i = \frac{y_{i \times} Q_{stp}}{22400} \qquad [\text{mol.s}^{-1}] \tag{3.4}$$

Single gas permeance, Π_i was obtained by dividing pure component gas flux, F_i through the membrane by transmembrane (TMP) partial pressure difference between upstream (feed) and downstream (permeate side) as shown in Equation 3.5.

$$\Pi_i = \frac{F_i}{\Delta P_i} = \frac{f_i}{A \times \Delta P_i} \qquad [\text{mol.s}^{-1}.\text{m}^2.\text{Pa}^{-1}] \tag{3.5}$$

TMP, ΔP_i across the membrane of a gas component i, was calculated using Equation 3.7.

$$\Delta P_i = P_{i,f} - P_{i,p} \qquad [\text{Pa}] \tag{3.6}$$

Where $P_{i,f}$, and $P_{i,p}$ are pressures of component i in the feed, and permeate sides, respectively.

Selectivity of a membrane is the ability of the membrane to accomplish a given separation. Membrane selectivity provides useful information that can be used to compare the quality of two membranes and provides understanding into zeolite flexibility.

Ideal selectivity ($S_{i/j}$) for a component i over j describes single gas selectivity of a membrane. Ideal selectivity also known as permselectivity of a membrane is permeance based and was computed as the ratio of pure gas permeances for i over j shown in Equation 3.7.

$$S_{i/j} = \frac{\Pi_i}{\Pi_j} \quad [-] \tag{3.7}$$

Where Π_i and Π_j are the permeances of pure gas feed i and feed j respectively.

3.5.2 Mixture gas separation

The true quality of a membrane is reflected using a mixture gas permeance measurement (Wang et al., 2002). In zeolite membrane using single gas permeance measurement, the permeating species can transport through non-zeolitic pathways and can offer a preferential route that could

lead to high fluxes (Bernal et al., 2002). As-synthesized membranes based on high-quality single gas performance were investigated for H_2/CO_2 binary mixtures (H_2:CO_2 = 60:40). This mixture/ratio was chosen because it represents the hydrogen concentration expected in coal gasification after the water-gas-shift reaction. During separation of H_2 from H_2/CO_2 mixture, some H_2 permeated from the feed gas through the gap between the membrane and the module. Gas mixture exiting the module from the outside of the membrane contained rich H_2 and it was called the permeate. Gas mixture exiting the module from the inside of the membrane contains non permeated CO_2 and was called the retentate. A mass flow controller was used to control the flow rate of the feed. No sweep was used in the experiment. The permeate pressure was kept at atmospheric all through the experiment. The pressure of the mixture gas was varied from 0.1 MPa to 0.5 MPa. The process flow diagram (PFD) for permeation set-up employed for mixture gas separation is similar to the PFD for single gas (Figure 3.7). The difference is that the retentate stream (SOV 7) was left opened and controlled by a valve, the permeate stream was vented to the atmosphere while SOV 5 remained locked. A gas syringe was used to collect the permeated gas for analysis. A detailed process flow diagram of the set-up for a mixture experiment is shown in Figure B.1 in the Appendix section. For each measuring point, temperature, feed pressure, and retentate flow were kept fixed. The permeate flux for a given temperature was calculated based on the flow rate readings obtained from the flow meter attached to the equipment after it has stabilized. The gas composition in the retentate stream was not known, however, a mass balance was used to get retentate composition. Obtained results were used to further quantify membrane permeance under a given set of conditions. The gas compositions of the feed and permeate streams were analyzed offline using a Bruker 430-GC gas chromatography (Figure A.5) equipped with a thermal conductivity detector (TCD) and coupled with stainless-steel column (2 m, OD:3.175 mm, ID;2 mm). The oven, detector, and injector temperatures are 220 °C, 150 °C, 140 °C respectively. The GC was calibrated with a standard gas H_2/CO_2 mixture before use. At least two sample loop injections for each analysis was done to ensure reliable statistically repeatable results.

The hydrogen permeance for mixture gas separation experiment was calculated according to Equation 3.8.

$$\Pi_{H_2} = \frac{F_{H_2}}{\Delta P_i} = \frac{f_p \times y_{H_2}}{A \times \Delta P_{In,H2}} \tag{3.8}$$

Where F_{H_2} is the steady-state flux of H_2 component, f_p is the molar flow rate of the permeate, y_{H_2} is the mole fraction of the H_2 component in the permeate stream, A is the membrane area. The difference in partial pressure between the feed and permeate sides is denoted by ΔP_i and was calculated using the logarithmic mean method of Equation 3.9 since the module has a cross-flow design.

$$\Delta P_{In,i} = \frac{\left(P_{f,i-P_{p,i}}\right) - \left(P_{r,i-P_{p,i}}\right)}{In\left[\left(P_{f,i}-P_{p,i}\right)/\left(P_{r,i-P_{p,i}}\right)\right]} \quad \text{(Salim et al., 2019)} \tag{3.9}$$

Where $P_{f,i}$, $P_{p,i}$, $P_{r,i}$ are the partial pressures of component i in feed, permeate, and retentate side respectively.

Separation factor (SF) sometimes referred to as the separation selectivity of the membrane describes the real selectivity of the membrane. The membrane ($SF_{i/j}$) of component i over j of binary mixture permeation was computed as the quotient of the molar ratios of the components (i/j) in the permeate, divided by the quotient of the molar ratio of the components (i/j) in the feed, as shown in Equation 3.10.

$$SF_{i/j} = \frac{\left(y_i/y_j\right)_{permate}}{\left(x_i/x_j\right)_{feed}} \quad [-] \tag{3.10}$$

i denote the gas component H_2 and *j* denotes gas component CO_2; y and x are the mole fractions of gas components on the permeate and feed side of the membrane.

Concluding Remarks

A short overview of the procedure used in the preparation and characterization of sodalite crystals and membrane have been presented in this chapter. Also, the optimization of sodalite crystals conducted in this study is described in detail. Also, the techniques for evaluating the quality of

sodalite crystal and membrane have been emphasized. Results obtained from the experimental procedures as described in this chapter are reported and discussed in later chapters.

Chapter 4: Development of Pore-Plugging Hydrothermal Synthesis Protocol for the Synthesis of Hydroxy Sodalite Nanoparticles: Effect of Synthesis Parameters on Crystallinity, Seed Size and Morphology of Sodalite Crystals

In this chapter, the effect of synthesis variables such as ageing and synthesis time on the synthesis of sodalite crystals via the pore-plugging hydrothermal synthesis technique are reported and discussed.

4.1 Introduction

Polymeric membranes, which are organic, are some of the earliest commercial membranes developed for gas separations commercially. The techniques for the production of polymeric membranes are very mature and membranes produced thereof have displayed good separation performance (Sanders et al., 2013). However, polymeric membranes suffer from low thermal stability and poor chemical resistance (Bernardo et al., 2009; Kosinov et al., 2014). These inherent limitations faced by the polymeric membranes have led to the development of inorganic membranes such as silica, metallic, ceramics, zeolites, metal oxides, and carbon-based molecular sieves (Ockwig and Nenoff, 2007; Li et al., 2015).

Zeolites are a class of microporous aluminosilicates, open 3-dimensional framework structures composed of corner-sharing TO_4 tetrahedra, where T can be either Al or Si, Ga, Be etc. (Georgiev et al., 2009; Colella and Wise, 2014). They can occur naturally and can also be synthesized from pure chemicals (Cundy and Cox, 2003; Hosseinzadeh Hejazi et al., 2011). Single TO_4 tetrahedral forms the primary building block of zeolites which can be linked by 2, 3, 4 or more corners via a common oxygen atom to form a wide variety of structure called secondary building units (SBU) (Maghsoudi, 2016; Ilić and Wettstein, 2017). Zeolites are largely used in the industry for catalytic cracking, as adsorbents for gas purification and can be developed into membranes for gas separations (Busca, 2017). Properties which render zeolites attractive for these applications are their large internal surface area, ion-exchange capacity, good shape selectivity, a regular array of micropores with well-defined dimensions, high thermal resistance, chemical inertness and high mechanical strength (Bayati et al., 2008; Shan et al., 2011).

Sodalite, a promising member of zeolites, have been explored in separation application (Van Niekerk et al., 2007). Sodalite (SOD) is a zeolite which has channel apertures formed by six-oxygen ring and forms a cage structure known as β-cage (polyhedral cage) (Khajavi et al., 2007b). Its framework is very flexible; hence, different types of sodalite which are suited for different applications can be made. Under the sodalite family is an interesting member known as hydroxy sodalite (SOD) formed by connecting sodalite cages through common 4- and 6- ring (Felsche et al., 1986; Pan et al., 2016). The cage dimension of the SOD material is around 0.29 nm and the material is remarkably thermally stable (up to 450 °C) with high chemical resistance (Khajavi et al., 2010b). These properties of SOD make it a promising separation material for small molecules like water (0.27 nm), helium (0.26 nm) and hydrogen (0.27 nm) under certain conditions (Khajavi et al., 2007a; Daramola et al., 2015b, 2017).

Numerous researchers have reported on the successful transformation of SOD crystals into membranes for separation applications (Khajavi et al., 2007b, 2010b; Kalantari et al., 2015; Daramola et al., 2017; Lafleur et al., 2017). For instance, supported SOD membranes have been prepared via direct hydrothermal synthesis and applied in pervaporation and desalination of saltwater (Khajavi et al., 2007a, 2010b). Recently, Daramola and his co-workers have embedded SOD crystals inside polyethersulfone (PES) membrane and applied it for acid mine drainage (AMD) treatment (Daramola et al., 2015a). According to Fan et al. (2008), the phase of the formed sodalite crystals, as well as the size, critically depends on the synthesis conditions. In spite of the progress made in the field, obtaining inorganic membranes displaying appreciable flux, selectivity and reproducibility is still a challenge (Daramola et al., 2012). Several factors such as the formation of defects (cracks and pinholes), presence of impurities (e.g., the formation of other zeolites), size of particles, synthesis technique etc. could be mitigating factors towards achieving this goal. This problem is compounded when thin-film of zeolite crystals are supported on ceramic or perforated stainless steel or sintered glass (Miachon et al., 2007; Daramola et al., 2009). Because of the huge difference in thermal expansion of these supports in comparison to the zeolite crystals, the formation of cracks and pinholes is promoted. Formation of cracks in membranes is detrimental to the selectivity of the membrane. Further promotion of the formation of cracks due to abrasion during membrane assembly is possible for thin-film membranes prepared by direct hydrothermal synthesis.

To overcome this problem, Miachon and his co-workers proposed a pore-plugging hydrothermal synthesis method (Miachon et al., 2006). By so doing, expansion of crystals is limited to the pore size of the support. MFI membranes prepared via PPH have been demonstrated to exhibit better performance, particularly membrane selectivity, when compared to ceramic supported with a thin-film layer of zeolite for xylene separation (Daramola et al., 2009; Daramola et al., 2010b), for N_2/CO_2 separation (Alshebani et al., 2008a). For SOD supported membrane prepared via PPH synthesis, an application has been demonstrated for water purification (Lafleur et al., 2017). But as far as could be ascertained, scanty literature appears on development and application of SOD supported membranes prepared via PPH synthesis for CO_2 capture (especially H_2/CO_2 separation). First open report, which is preliminary in nature was reported by Daramola et al. (2015b).

It is noteworthy to mention that the formation of high-quality nanocomposite SOD membranes prepared via PPH synthesis is premised on the availability of high purity SOD crystals. Obtaining high purity crystals during PPH synthesis depends on the synthesis conditions which control the interplay between nucleation and growth during the synthesis. Therefore, in this chapter, the effect of synthesis variables such as interruption time, ageing and synthesis temperature on the morphology and crystallinity of SOD crystals is reported.

4.2 Experimental

The materials for the preparation of SOD crystals, characterization techniques used, and detailed description of experimental procedures employed in this chapter are provided in Chapter 3 (Section 3.1.1, 3.1.2, 3.2, and 3.4) of this dissertation. Equations 3.1 and Equation 3.2 were used to calculate percentage crystallinity and particle size of as-synthesized SOD crystals. The SOD crystals synthesis conditions are represented in Figure 4.1 and Figure 4.5.

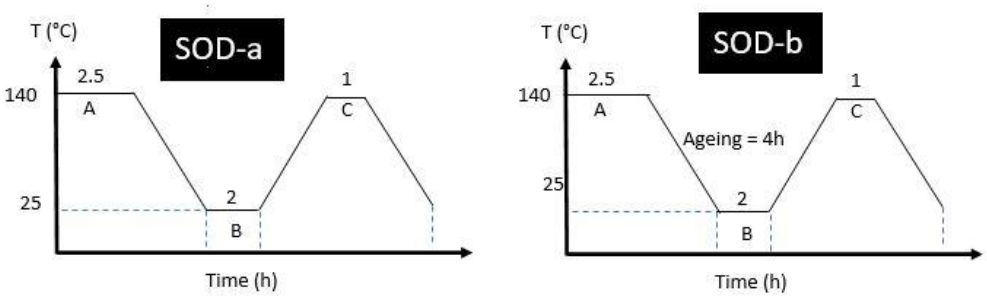

Figure 4. 1 Pore-plugging protocol to produce SOD-a and SOD-b

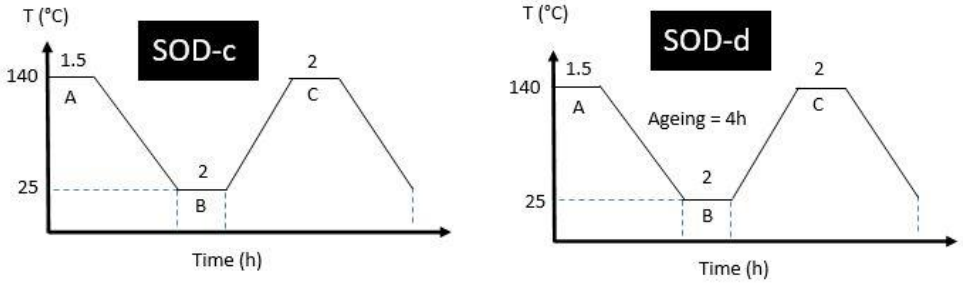

Figure 4. 2 Pore-plugging protocol to produce SOD-c and SOD-d

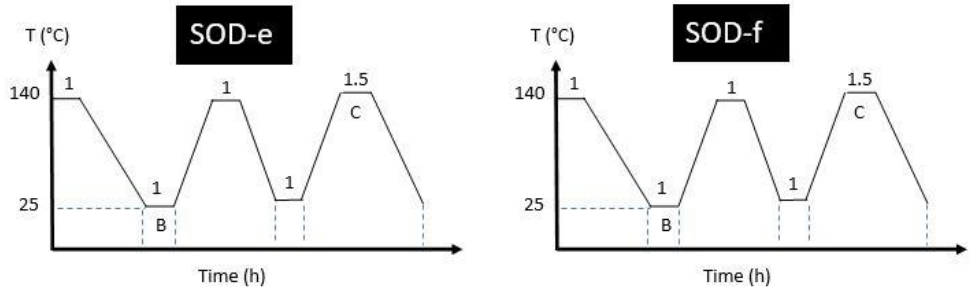

Figure 4. 3 Pore-plugging protocol to produce SOD-e and SOD-f

A - pre-interruption time, B - interruption time, C post-interruption time

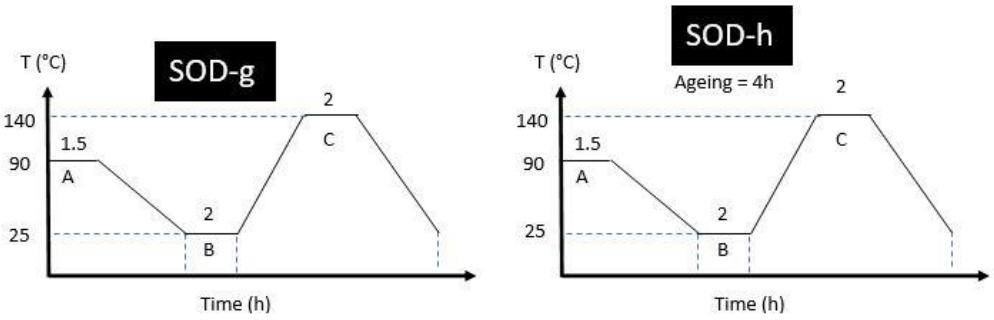

Figure 4. 4 Pore-plugging protocol to produce SOD-g and SOD-h

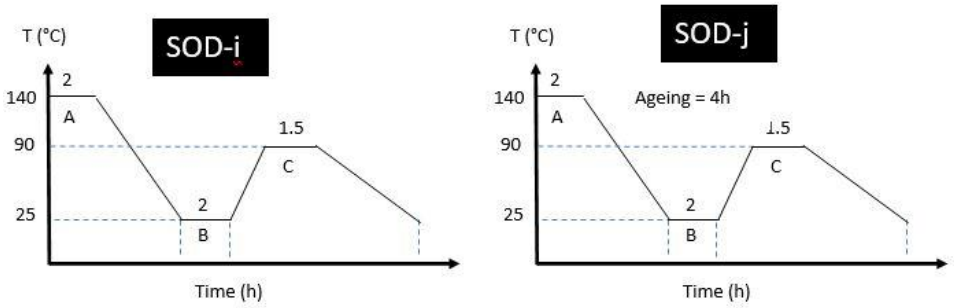

Figure 4. 5 Pore-plugging protocol to produce SOD-i and SOD-j

A - pre-interruption time, B - interruption time, C post-interruption time

4.3 Results and Discussion

4.3.1 Crystallinity

Pore-plugging hydrothermal (PPH) synthesis conditions yielding high crystallinity SOD crystals is necessary to improve the synthesis of SOD membranes towards high reproducibility and membrane performance. X-ray diffraction patterns (Figure 4.6 and Figure 4.7) of the as-prepared SOD zeolites (SOD-a to SOD-j) obtained after PPH synthesis show the particles are crystalline in nature. By comparing the diffraction patterns of the as-synthesized SOD crystals to that of the reference SOD from the International Zeolite Association (IZA) database (Treacy and Higgins, 2007), there is a great match. This indicates that SOD crystals were produced. However, judging by the intensity and position of the as-prepared SOD crystals peaks compared to the reference SOD, there exist significant variations in crystallinity and purity of the as-synthesized SOD crystals.

XRD patterns of SOD-a (Figure 4.6) and SOD-e (Figure 4.7) produced the best match when compared to the XRD pattern of the reference SOD zeolite and a few others from the literature (Van Niekerk et al., 2007; Naskar et al., 2011a). This indicates qualitatively, high purity SOD crystals were obtained at these synthesis conditions. The SOD peak positions of SOD-i matched close to the reference SOD. However, a very weak intensity single Linde Type A (LTA) phase was found present around the d_{110}=13.89° peak. External factors may have introduced the LTA phase. Careful control of external influence may lead to the formation of high purity SOD crystals and subsequently high-quality sodalite/ceramic membrane at this synthesis condition.

SOD-b, SOD-d, SOD-f, SOD-h, and SOD-j were obtained by stirring the precursor solution for 4 hours at ambient temperature before PPH synthesis. Diffraction patterns of these SOD crystals (Figure 4.6 and Figure 4.7) reveal the presence of crystalline contaminant phases, characterized by a decrease in SOD peak intensity. These observations suggest sodalite phase was consumed in favour of contaminant phases and hence, a change in the size distribution of SOD crystals. The contaminant phases were matched with other zeolites from IZA database and have been attributed to be faujasite (FAU), Linde type N (LTN), zeolite P (NaP), cancrinite (CAN), Linde type A (LTA), mordenite (MOR), etc. type zeolite. The CAN and NaP phase found present in the diffraction patterns of SOD-f and SOD-h were also found present in a study by Pourali and Samadi-Maybodi (2015) when the SOD precursor solution was aged for 2.5 hours. The cancrinite phases commonly do occur as a secondary phase in the synthesis of SOD (Fan et al., 2008). Other zeolite phases like the LTA, FAU type zeolites have SOD cage in their framework structure. These zeolites could be synthesized under similar reaction conditions and may have formed at low temperature alongside sodalite (Ming Leung et al., 2015).

Diffraction peaks of SOD-c (Figure 4.6) and SOD-g (Figure 4.7) show a few broad SOD peaks which illustrate very small SOD crystallites were formed. The synthesis conditions used in obtaining these sodalites are similar; a short pre-interruption time of 1.5 hours and a 2-hour post-interruption time. At these synthesis conditions, SOD crystals do not grow. According to a study by Reyes et al. (2013), in the mechanism of nucleation and crystal growth of SOD zeolite, metastable zeolite A can form at low temperature (SOD-g) and at short synthesis time (SOD-c). This suggests a short pre-interruption hour before interrupting the synthesis would, therefore, impede the effective dissolution of the early metastable phases of LTA. This, in turn, will prevent

the nucleation and growth of the more stable SOD phase after interruption. Bear in mind that at the break of synthesis, nucleation and crystal growth slows down.

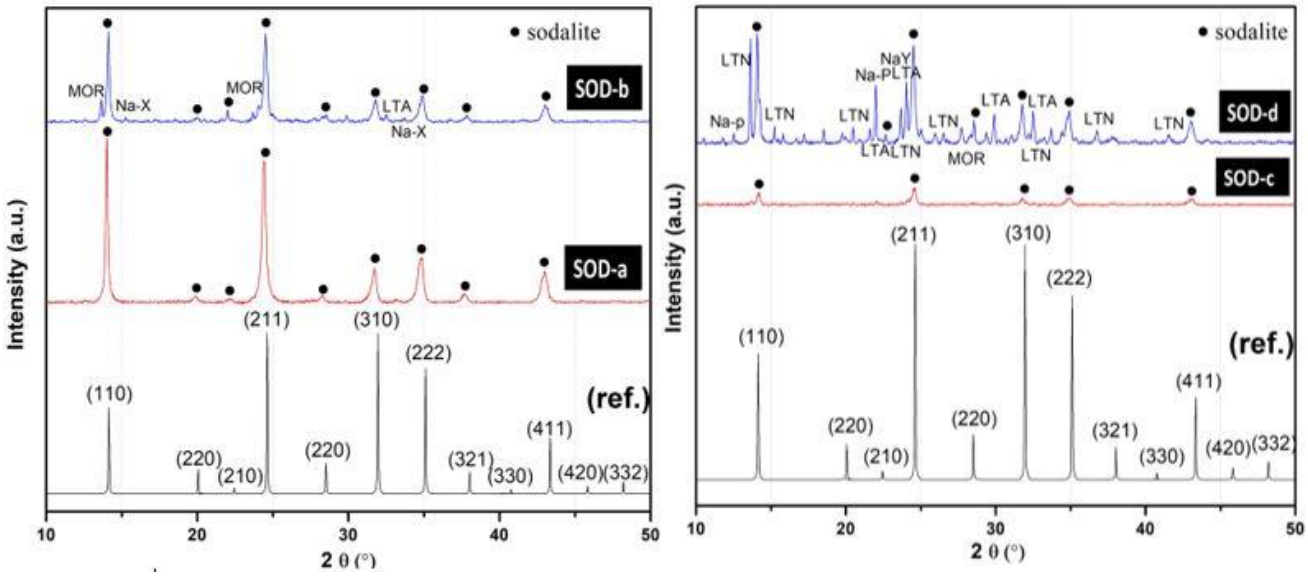

Figure 4. 6 X-ray diffraction patterns of as-synthesized SOD-a to SOD-d

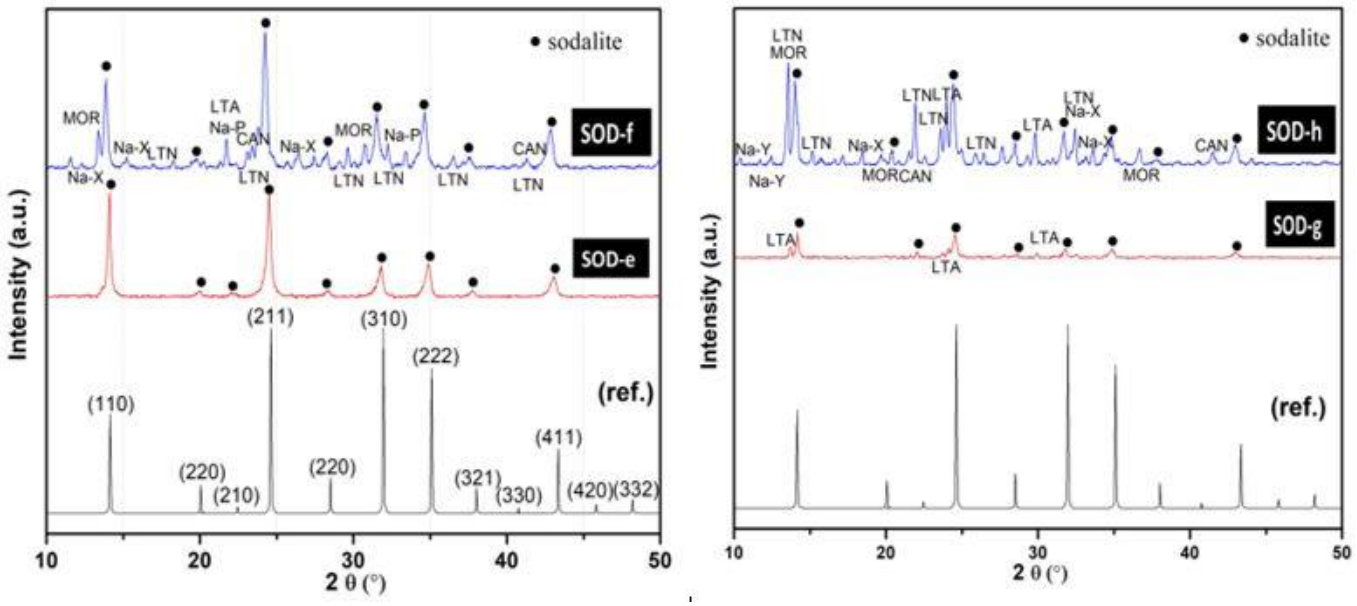

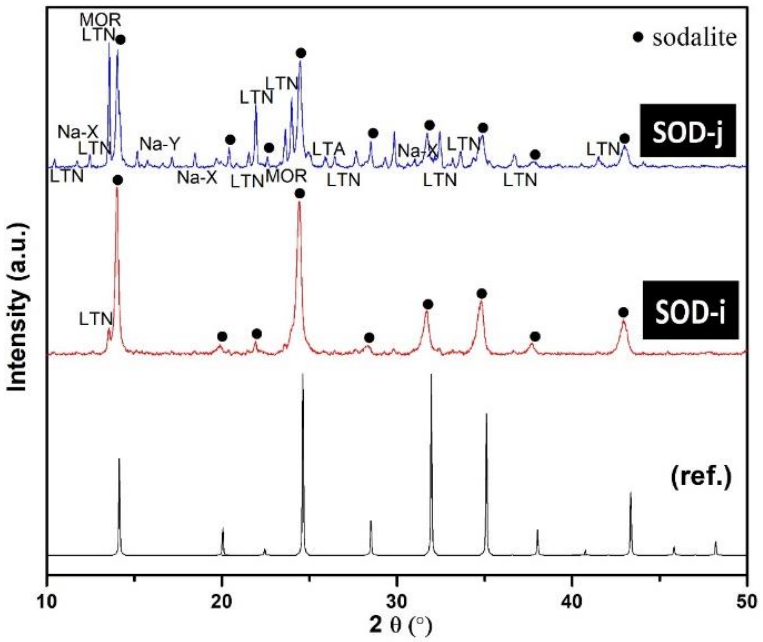

Figure 4. 7 X-ray diffraction patterns of as-synthesized SOD-e to SOD-j

Based on the good quality XRD patterns obtained for SOD-a, SOD-e, and SOD-i and optimum crystallinity of 75%, 71% and 67% respectively, the PPH synthesis conditions used to obtain these sodalites could be used to develop high-quality sodalite membrane. The reduced percentage crystallinity of SOD-i was due to the single LTA phase found present in its XRD pattern. The XRD results demonstrated ageing the precursor under stirring before PPH synthesis led to very poor-quality SOD nanoparticles.

4.3.2 Crystal particle size

The crystal size of SOD seed is an important factor in various applications, especially in the synthesis of zeolite membrane (Bayati et al.,2008). The smallest particle size (see Table 4.1) was obtained for SOD-c and SOD-g as evident by the broad SOD diffraction peaks of these sodalites (Figure 4.6 and Figure 4.7). During the synthesis of zeolite membrane via the PPH technique, the zeolite seed is formed in-situ before the interruption of the synthesis. Consequently, heterogeneous nucleation and growth are promoted after interruption which eventually enhances growth into bigger crystals (Miachon et al., 2006; Daramola et al.,2017). To develop quality, defect-free nanocomposite SOD membrane, it is expected that pores of the support be plugged fully with SOD

crystals. Synthesis conditions to produce SOD-c and SOD-g, apart from being plagued with impurities would reflect incomplete pore-plugging. The averagely large particle size of SOD-a, SOD-e, and SOD-i suggest the synthesis conditions used to obtain these sodalite crystals could be used to achieve a fully plugged SOD membrane.

Table 4. 1 Estimated SOD crystal sizes

SOD	A	B	C	D	E	F	G	H	I	J
Estimated crystal size (nm)	419.37	378.28	227.56	473.47	347.88	336.52	289.18	493.91	347.45	469.38

4.3.3 Morphology of as-synthesized SOD crystals

The micrographs of the as-synthesized SOD crystals produced in this study are presented in Figure 4.8 and Figure 4.9. A quality SOD membrane should preferably be made of pure zeolite crystals with uniform crystal size embedded within the pores of the support. SOD-a formed agglomerate of thread balls of uniform size. Spherical agglomerates of quality SOD crystals was recently reported by Liu et al. (2018). Cubic crystals attributed to A-type zeolites was present in SOD-c which increased when the solution was aged (SOD-d). The micrographs obtained for SOD-e and SOD-i resemble SOD-a except with a low degree of uniformity of the SOD crystals. Micrograph of SOD-g shows spherical aggregates of SOD growing out unto the surface of pseudo-cubic agglomerates of A-type zeolites. This image reflects the ineffective dissolution of the metastable LTA phase is more severe in the instance of short pre-interruption time and at a lower temperature. Cubic shaped zeolite-A seeds and pseudo-cubic grains of A-type zeolite have been reported by Bayati et al. (2008) and Liu et al. (2018).

The shape observed when the solution was aged (SOD-h) showed disoriented octahedral faced cubes and imperfect spherical thread balls coexisted. SEM morphology of all the SOD samples substantiates the obtained XRD patterns. The most common shapes of SOD reported in the literature is thread ball-like and urchin shaped (Khajavi et al., 2007a, 2010b; Kundu et al., 2010; Daramola et al., 2015b; Das et al., 2017; Liu et al., 2018). However, according to Naskar et al. (2011b), more than one morphology for SOD crystal may be present depending on the synthesis

time and precursor solution concentration. Cabbage-like SOD structures obtained by the direct hydrothermal synthesis technique was reported by Pourali and Samadi-Maybodi (2015) under prolong stirring ageing of the precursor solution for 72 hrs.

The desired SOD crystal shape is of importance in developing quality sodalite membrane via PPH synthesis technique. Intergrowth between different type of zeolite crystals is usually poor compared to that between the same type of zeolite crystals. The existence of different shape zeolite crystals alongside SOD crystals in the pores of the support would result in many intercrystalline defects. For this reason, membrane quality could be impacted and may make reproducibility difficult to achieve.

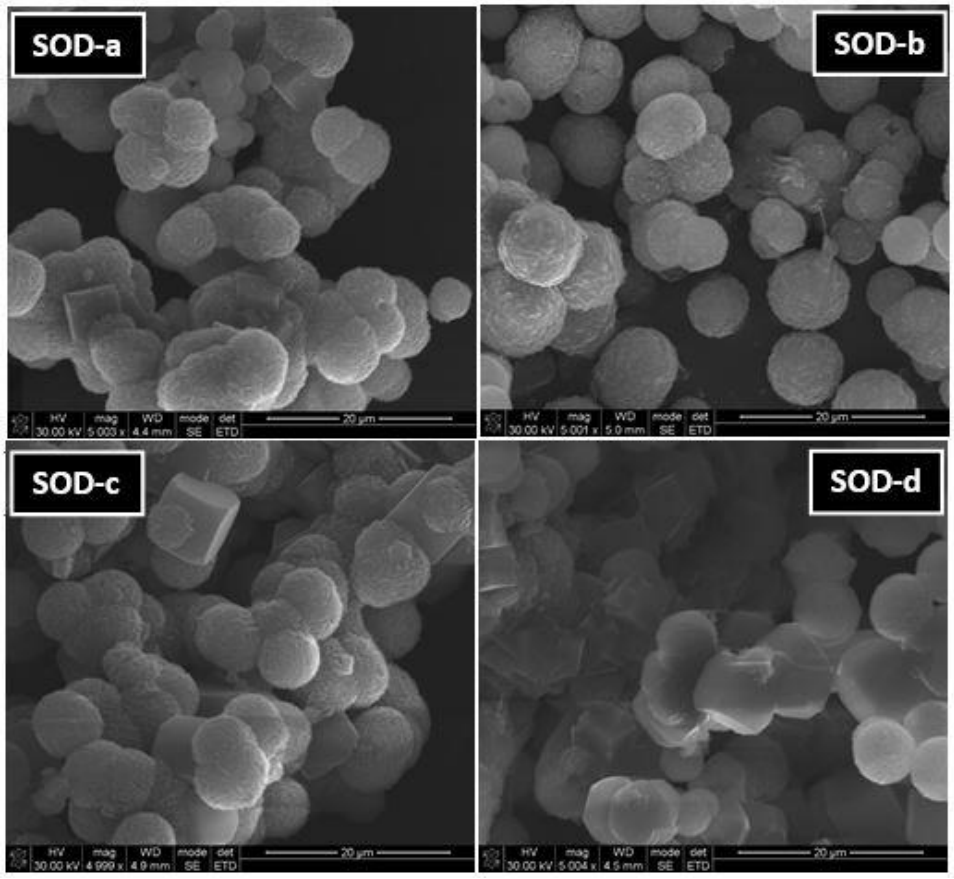

Figure 4. 8 SEM images of the as-synthesized SOD-a to SOD-d

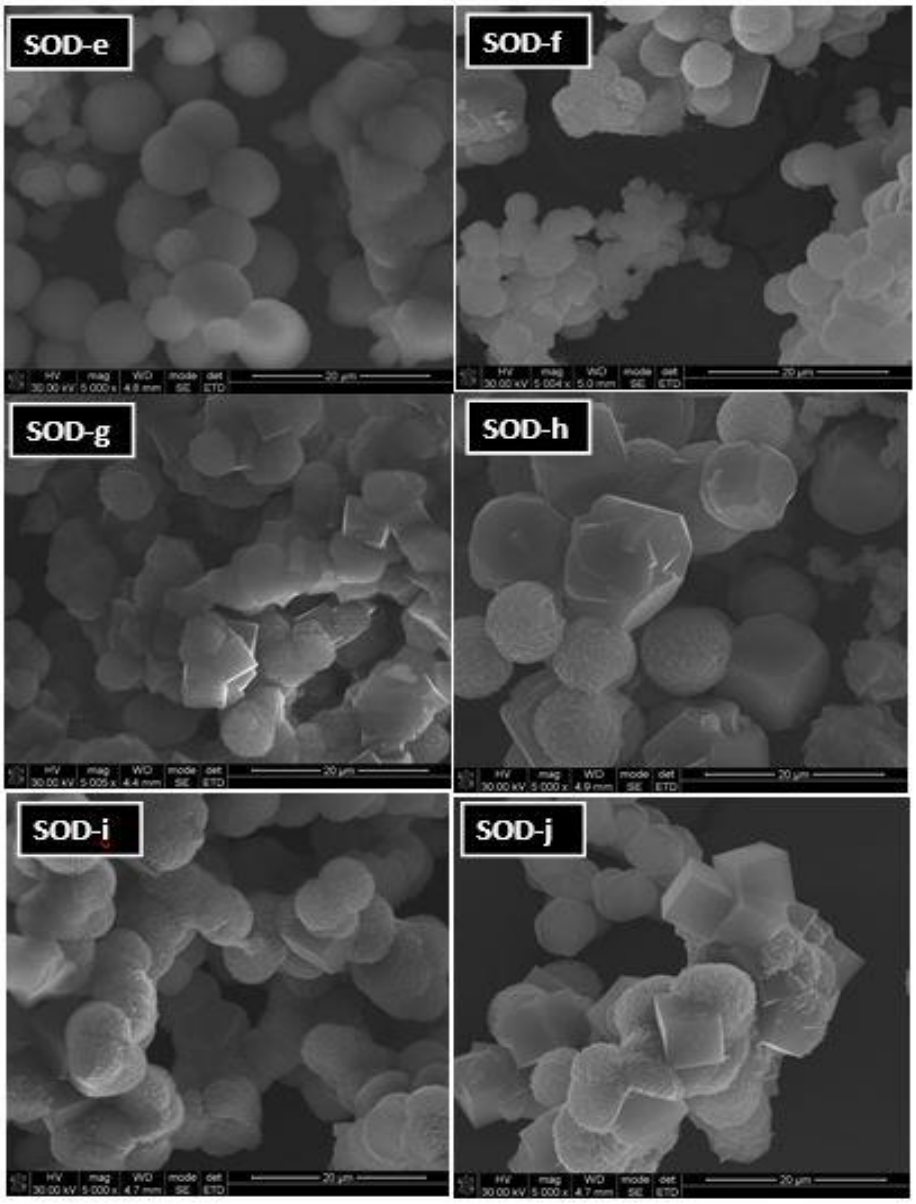

Figure 4. 9 SEM images of the as-synthesized SOD-e to SOD-j

For further confirmation that high-quality SOD was produced for sample reference SOD-a, SOD-e, SOD-i, the elemental analysis revealed a Si/Al ratio of 1 for the three samples. This value agrees with literature (Khajavi et al., 2010a; Daramola et al., 2015b). However, Na/Al ratio of 1.6, 1.3, and 1.4 was obtained for SOD-a, SOD-e, SOD-i respectively. This variation may have an implication on the performance of SOD membranes prepared by the respective synthesis conditions thereof.

4.3.4 FTIR characterization

To confirm fingerprint adsorption bands of SOD and to ensure consistency with literature, FTIR spectra of the structural region of the as-synthesized SOD are presented in Figure (4.10). All the SOD samples (SOD-a to SOD-j) show fingerprints adsorption bands of SOD at 429, 459, 660, 697, 722, 992 cm^{-1} (Tobia, 2007; Musyoka et al., 2011; Naskar et al., 2011a; Das et al., 2017). These bands represent different adsorption band within the SOD structure (Yamaura and Fungaro, 2013). On the other hand, the difference in number and frequency of absorptions (Figure 4.10) can be observed, reflecting the variation in the purity of SOD crystals produced. Despite this, framework vibrations that are more intense and less broad are desired, which indicates the level of crystallinity of SOD zeolite. SOD-a, SOD-e, SOD-i possess higher percentage absorbance, reflecting higher quality SOD was successfully synthesized at these conditions.

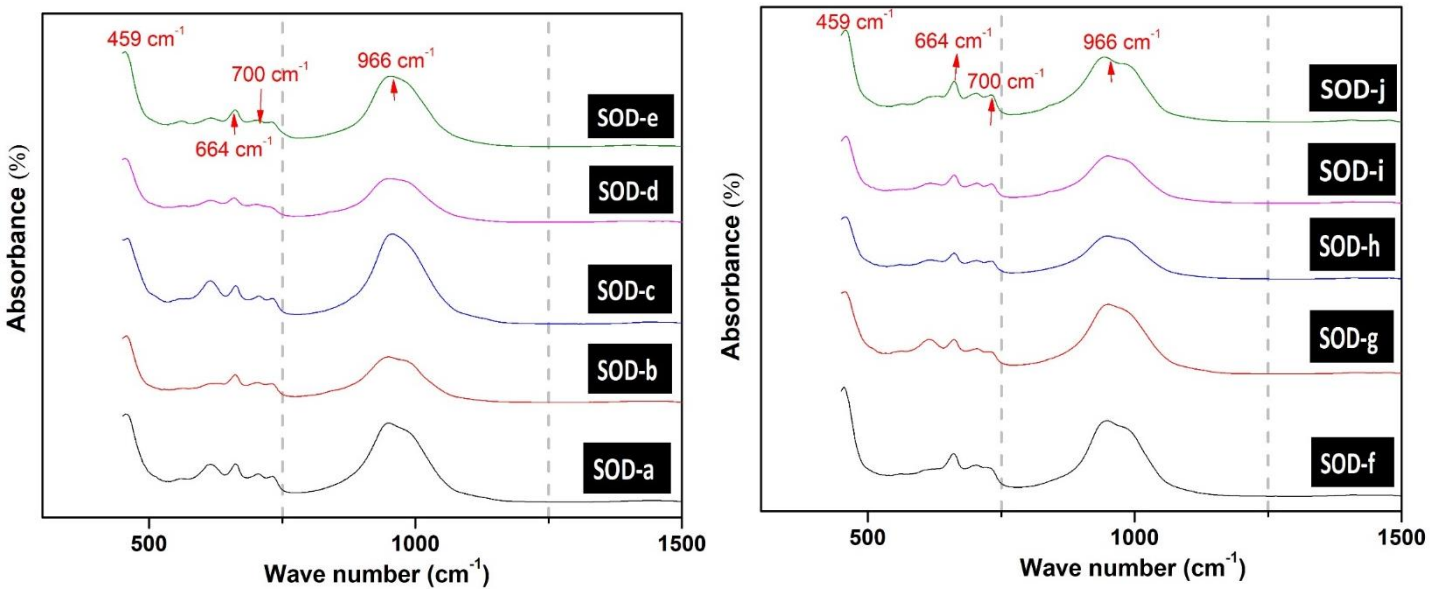

Figure 4. 10 FT-IR spectra of the as-synthesized SOD-a to SOD-j

In a study by Das et al. (2017) and Daramola et al. (2017), the broadband centred around 3600 cm^{-1} was assigned to the presence of OH- group. However, in this study, the OH-broad band did not appear. OH-broad band mode was also absent in the spectrum of microcrystalline sodalite sample prepared by Buhl et al. (2011). According to Engelhardt et al. (1992), the synthetic sodalite with the formula $Na_{6+y}Al_6Si_6O_{24}(OH)_y.nH_2O$ can be differentiated due to the content of water and

hydroxyl ions. When y = 2, it is regarded as the basic form of SOD. When y = 0, it is non-basic. The absent of the OH-band in sodalite prepared in this study suggest it is a "non-basic" hydroxy sodalite with less than two water molecule (Günther et al., 2015). This is as a result of $NaOH/H_2O$ exchange which occurs during the washing of the crystals with water that is generally applied to remove NaOH impurities from the outer surface of the crystallites (Engelhardt et al., 1992). The difference in FTIR spectra obtained for SOD nanoparticles in this study to other studies could also have been due to the different molar composition ratio used in synthesizing sodalite in this study.

4.3.5 Thermal stability

The thermogravimetric analysis for SOD-a, SOD-e, and SOD-i was investigated to check the variation in thermal stability of sodalites produced by each of these protocols. TGA curve of the samples is shown in Figure 4.11. Rate of mass loss from room temperature to about 450 °C for SOD-e and SOD-i was faster than SOD-a. SOD-e and SOD-i showed a weaker almost continuous weight loss in the range between 150 °C and 400 °C. Also, these SODs (SOD-e and SOD-i) showed significant mass loss with increasing temperature - A total mass loss of 14.62 % for SOD-e and 14.16 % for SOD-i was observed owing to the release of hydrate water (Yao et al., 2006; Liu et al., 2018). SOD-a produced using one interruption had the smallest mass loss with SOD crystals containing 86.8 % of the original mass at 850 °C and therefore produced the most stable SOD crystals. Khajavi et al. (2010a) reported a 12 % mass loss for SOD crystals (helium flow of 50 ml/min at a rate of 1 K/min from room temperature to 1273 K). 10 % weight loss for low-silica sodalite from 50 to 1200 °C prepared by direct hydrothermal synthesis has been reported by Zheng et al. (2009). Liu et al. (2018) reported a 11.79 % mass loss for reaction conditions of 12 hours, 90 °C, Na/Si=12, Si/Al=1. 13.91 % was also reported by Buhl et al. (2011) for the synthesis of microcrystalline NaCl-sodalite. The difference in the mass loss as observed in this study compared to the previous study might be due to the higher water content in the SOD crystal structure (Günther et al., 2015). The difference in the synthesis techniques, starting materials used in producing SOD crystals and/or the conditions at which TGA measurement was taken could also be factors that contributed to the different weight loss observed in this study and those in the literature.

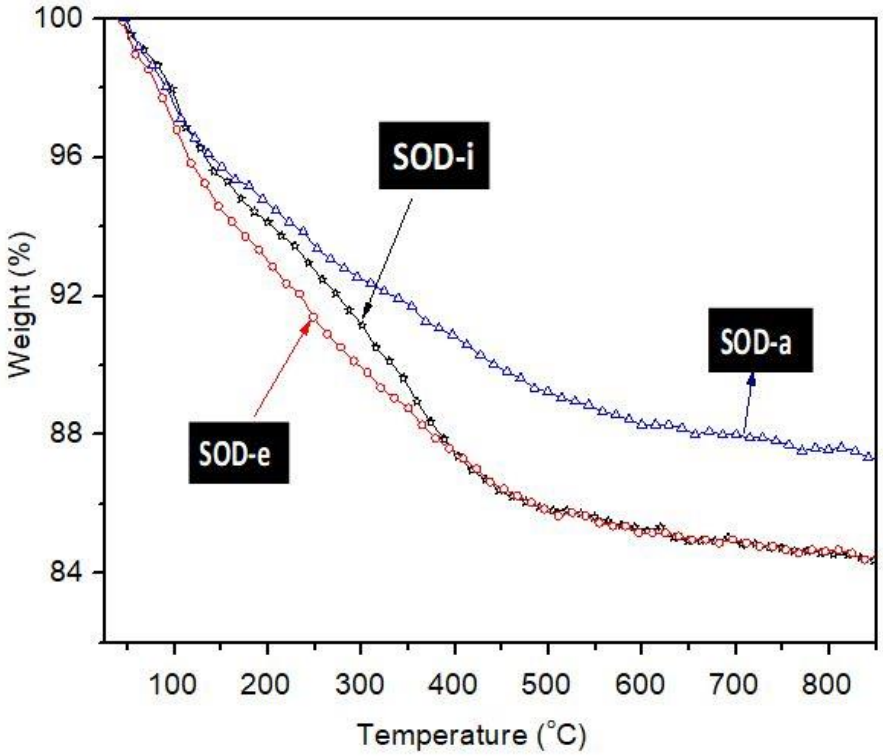

Figure 4. 11 TGA curves of SOD nanoparticles of SOD-a, SOD-e, and SOD-i.

Concluding Remarks

In conclusion, SOD crystals of different quality via the pore-plugging hydrothermal synthesis protocol at different synthesis conditions have been successfully produced. As far as it can be ascertained, no study has investigated the effect of synthesis variables on sodalite crystals prepared via the pore-plugging hydrothermal technique. The results demonstrate that ageing time before PPH synthesis can lead to the formation of impurities with SOD crystals. The results from this study further confirm that playing with conditions of the PPH synthesis can positively or negatively impact the quality of the as-produced SOD crystals. The results show that SOD crystals produced at synthesis conditions referred to as ‘a’, ‘e’, and ‘i’ are of high-quality SOD with high purity (100%), suggesting that these synthesis conditions, when used in synthesizing membranes, could yield high-quality nanocomposite SOD/ceramic membranes applicable in pre-combustion CO_2 capture. For quick dissemination of the results of the investigation described in this chapter to the scientific community, one manuscript has been developed and is under review in the journal of *Applied Nanoscience* (see Appendix D).

Chapter 5: Preparation and Performance Evaluation of Nanocomposite Sodalite/Ceramic Membranes

In this chapter, the preparation and performance evaluation of sodalite/ceramic membranes are reported. These membranes were obtained using the pore-plugging hydrothermal protocol developed to obtain pure sodalite crystals presented in Chapter 4.

5.1 Introduction

The application of inorganic membranes for liquid separation and evaporation have proven to be energy-efficient (Kita et al., 1995; Masuda et al., 1995; Kondo et al., 1997). These class of membranes can invade territories currently occupied by existing technology like absorption technology (Li et al., 2015). Successes experienced so far have led to the exploration and development of inorganic membranes as molecular sieves membranes for gas separation. Inorganic membranes are well adapted and promising to perform intrinsic difficult separation such as pre-combustion CO_2 capture (H_2/CO_2) (Dong et al., 2008; Gallucci et al., 2013; Smart et al., 2013). Ultimately this would help fast track the goal of process intensification for membrane-based separation.

The common approach of preparing zeolite membrane is to grow a thin selective layer referred to as “thin-film” on top of a substrate via direct hydrothermal synthesis method (Van Niekerk et al., 2007; Vaezi and Babaluo, 2014) or secondary-seeded growth method (Huang et al., 2010c; Kalantari et al., 2015). These approaches have produced good membranes. However, when the as-synthesized membranes are subjected to large temperature changes, thermal expansion mismatch between the membrane layer and support often lead to grain boundary opening and build-up of long-range stresses. Such effect creates non-selective transport pathways for permeating molecules (Miachon et al., 2006; Akhtar et al., 2015; Farjoo and Kuznicki, 2016). The performance of the membrane is thus impacted negatively. To overcome this shortcoming, the pore-plugging hydrothermal (PPH) synthesis was proposed as a better alternative to synthesizing zeolite membranes (Miachon et al., 2006; Li et al., 2008). In this technique, zeolite particles are embedded within the pores of the support by temporarily withdrawing the autoclave from the oven during synthesis. However, the challenge with this technique is to reproducibly synthesize high-quality,

defect-free supported membrane with high permeance while maintaining high H_2/CO_2 selectivity (Daramola et al., 2012). The number of reports on supported sodalite membranes prepared via PPH technique focusing on gas separation especially H_2/CO_2 separation is still very limited. Daramola et al. (2015b, 2017) have synthesized nanocomposite HSOD ceramic membrane via PPH technique. Unfortunately, the gas permeation measurement and capability of the membrane for molecular sieving was not validated or investigated. Therefore, in this chapter, the molecular sieving capability of SOD membrane prepared via the PPH protocol used to obtain pure sodalite crystals (SOD-a (one interruption step) and SOD-e (two interruption steps) of Figure 4.3 in Section 4.2 was investigated. Pure gas of H_2, CO_2 and N_2 and mixture gas of H_2/CO_2 was used as evaluation criteria. For comparison, thin-film membrane synthesized via direct hydrothermal synthesis method (Teflon around the outer surface of the support) was also synthesized. The membranes produced in this study and their performance were compared with other zeolite membranes in the literature.

5.2 Membrane preparation, characterization and performance evaluation

Nanocomposite sodalite/ceramic membrane used in this study was prepared by the established best pore-plugging hydrothermal (PPH) synthesis protocol used to produce high-quality sodalite crystals obtained in Chapter 4. The support used is an asymmetrical pall-Exekia α-alumina tubular support (i.d. 7 mm, o.d. 10 mm, active permeation area 28.59 cm^2). The support consists of three layers of different average pore size (0.2 μm microporous top layer, 0.8 μm mesoporous middle layer, 12 μm macroporous bottom layer). A detailed description of the PPH technique is provided in Chapter 3, Section 3.3. Parallel synthesis of SOD/ceramic membrane via the direct hydrothermal synthesis technique was also conducted. However, the outer surface of the support was covered with Teflon tape to prevent the growth of sodalite on the outer surface. The conditions of the synthesis of the membranes in this chapter are summarized in Table 5.1.

Table 5. 1 Conditions for synthesis of SOD/ceramic membrane

Synthesis	Membrane	Temperature (°C)	Synthesis time (hours)
A	M1, M2	140	2.5-2-1
B	M3, M4	140	1-1-1-1-1.5
C	B1, B2	140	3.5

*Number in red indicate interruption time in hours

The membranes were characterized using an X-ray diffractometer (Bruker D2 phaser diffractometer) and FEI Nova NanoLab 600 scanning electron microscopy (30.0 kV and 0.63 nA). This has been described in detail in Chapter 3 of this dissertation. Single gas N_2, H_2 or CO_2 permeation and binary mixture separation H_2/CO_2 was used to evaluate the performance of the as-synthesized membranes. The gases used for this study were hydrogen (baseline, 99.999%), nitrogen (baseline, 99.999%), carbon dioxide (technical), and binary mixture of H_2/CO_2 (60/40) purchased from African Oxygen Limited, South Africa (AFROX). The set-up for single gas permeation and mixture separation test has been described in Chapter 3, Section 3.5. Before permeation test, the membranes were thermally treated at a temperature of 100 °C to remove absorbed moisture and other contaminants. The test was conducted without sweep gas and permeate side pressure was kept at atmospheric pressure throughout the experiment. To obtain consistency in data reporting under a set of experimental variables, at least 1-hour stabilization/equilibrium time was necessary for the system to reach steady-state. A Bruker 430-GC gas chromatography (Figure A.5) equipped with a thermal conductivity detector (TCD) was used offline to analyze the composition of the permeate stream. The membrane performance was evaluated in terms of H_2 permeance, H_2/CO_2 ideal selectivity and H_2/CO_2 mixture separation factor following Equation 3.3 to Equation 3.10 presented in Chapter 3.

5.3 Results and Discussion

5.3.1 Membrane synthesis and characterization

The SOD crystals recovered from the bottom of the autoclave after each membrane synthesis was examined to confirm their phase purity. XRD patterns of SOD crystals and membranes M1, M2, M3, M4, B1, and B2 are shown in Figure 5.1 (a and b). Membrane M1, M2 confirmed the

successful formation of a large amount of SOD in the pores of the support judging by the strong SOD peak intensities observed. Membrane M3, M4, and B1 revealed extra peaks were formed which coincided with the peaks from the alumina support and new crystalline zeolite phases that are not SOD. SOD crystals of membrane B2 show high purity SOD seeds were synthesized. XRD patterns of all membranes showed SOD peaks matched with reference SOD from IZA (Treacy and Higgins, 2007), and those that have been reported in literature (Julbe et al., 2003; Van Niekerk et al., 2007; Fan et al., 2008; Naskar et al., 2011; Nabavi et al., 2014).

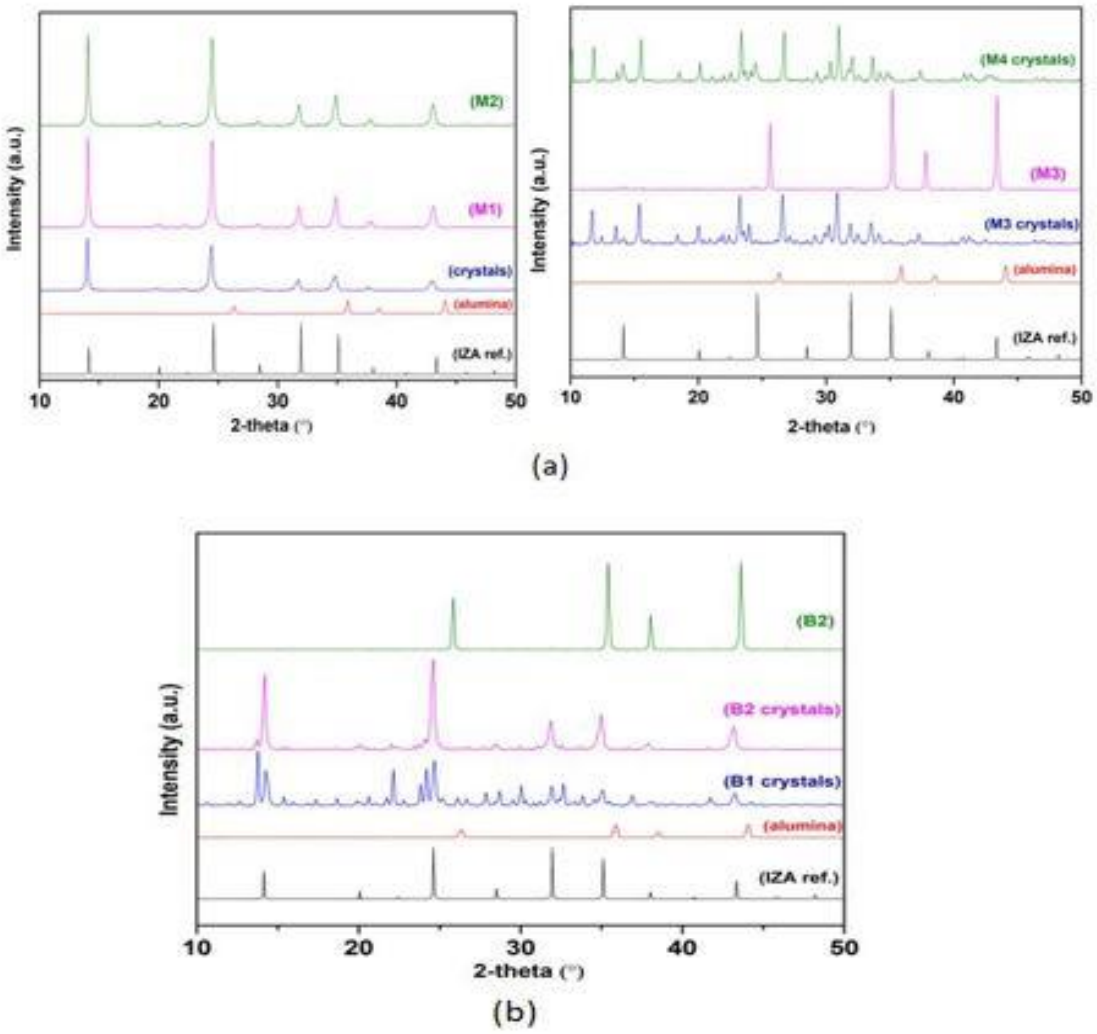

Figure 5. 1 (a) XRD patterns of membrane M1, M2, M3, M4 (b) XRD patterns of membrane B1, B2

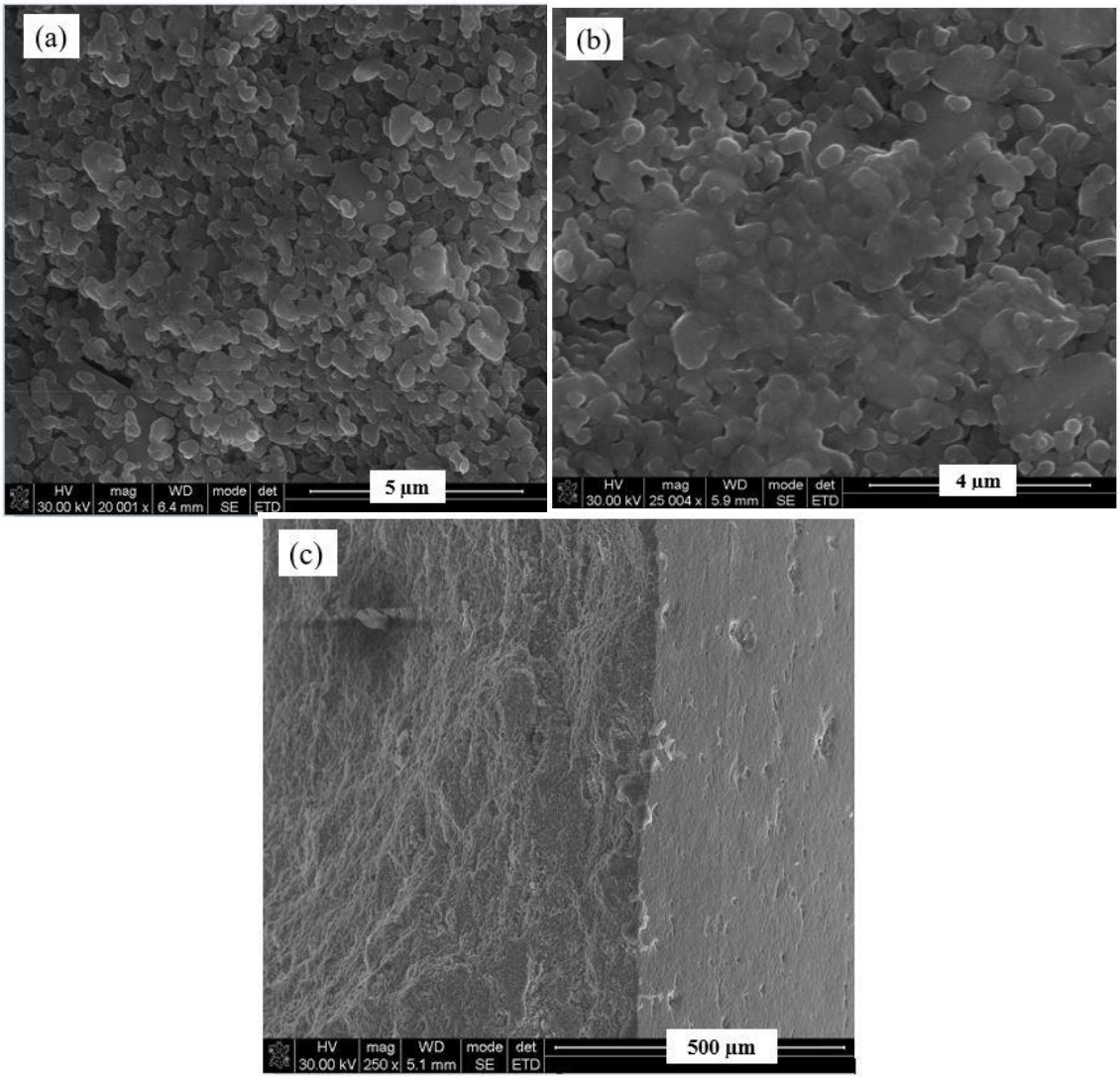

Figure 5. 2 SEM micrographs of (a) support top view, (b) support inner layer, (c) support cross-section

SEM images of raw support (top layer, inner layer and cross-section) are shown in Figure 5.2. Micrographs of SOD crystals (Figure 5.3a) collected after via pore-plugging hydrothermal synthesis and SEM images of as-synthesized nanocomposite membrane M1 (Figure 5.3b) are presented. The thread ball shape of SOD crystals formed is alike with those reported in the literature (Julbe et al., 2003; Fan et al., 2008; Kalantari et al., 2015; Lafleur et al., 2017), indicating pure SOD was formed. From the micrograph (Figure 5.3b), it can be seen that SOD crystals were indeed deposited within the inner surface pores of the support. However, one cannot rule out the

formation of incomplete pore-plugging within the larger surface pores which was difficult to capture using SEM microscopy. Figure 5.3c displays the cross-section of as-synthesized nanocomposite SOD/ceramic membrane M1.

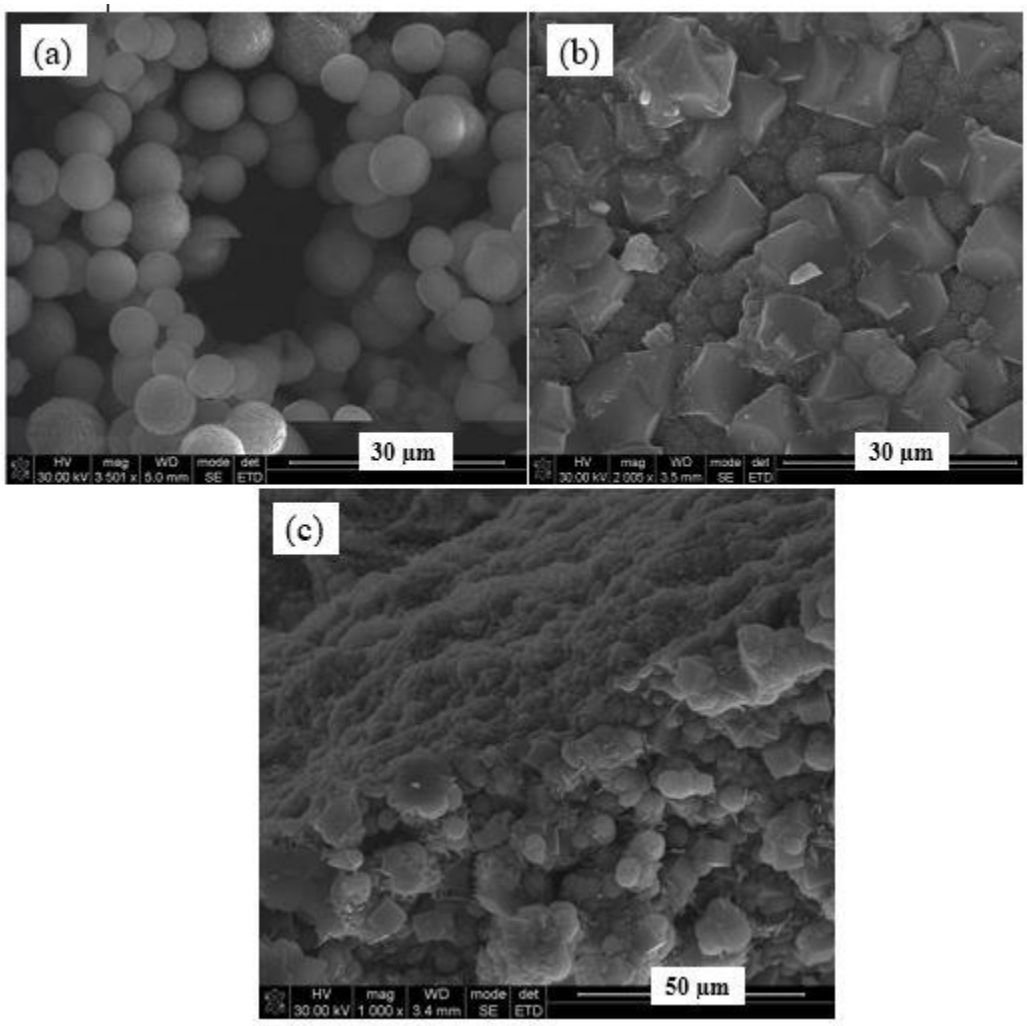

Figure 5. 3 SEM micrographs of (a) SOD crystals collected from the bottom of the autoclave, (b) membrane surface (M1), (c) membrane cross-section (M1)

Membrane B1 prepared via direct hydrothermal synthesis technique showed SOD crystals well intergrown (Figure 5.4b), forming a continuous membrane layer on the inner surface of the support tube for membrane. From the image (Figure 5.4c), a clear interface between membrane and support could be identified with limited penetration of the zeolitic phase into the underlying pores of the

support. These observations confirm a thin-film membrane was formed and agrees well with similar studies conducted by Fan et al. (2008); Lafleur et al. (2017). Micrograph of SOD crystals (Figure 5.4a) collected after the hydrothermal synthesis is also presented. The thread ball shape of SOD crystals formed is similar with those reported in the literature (Julbe et al., 2003; Fan et al., 2008; Kalantari et al., 2015; Lafleur et al., 2017), confirming SOD was indeed formed.

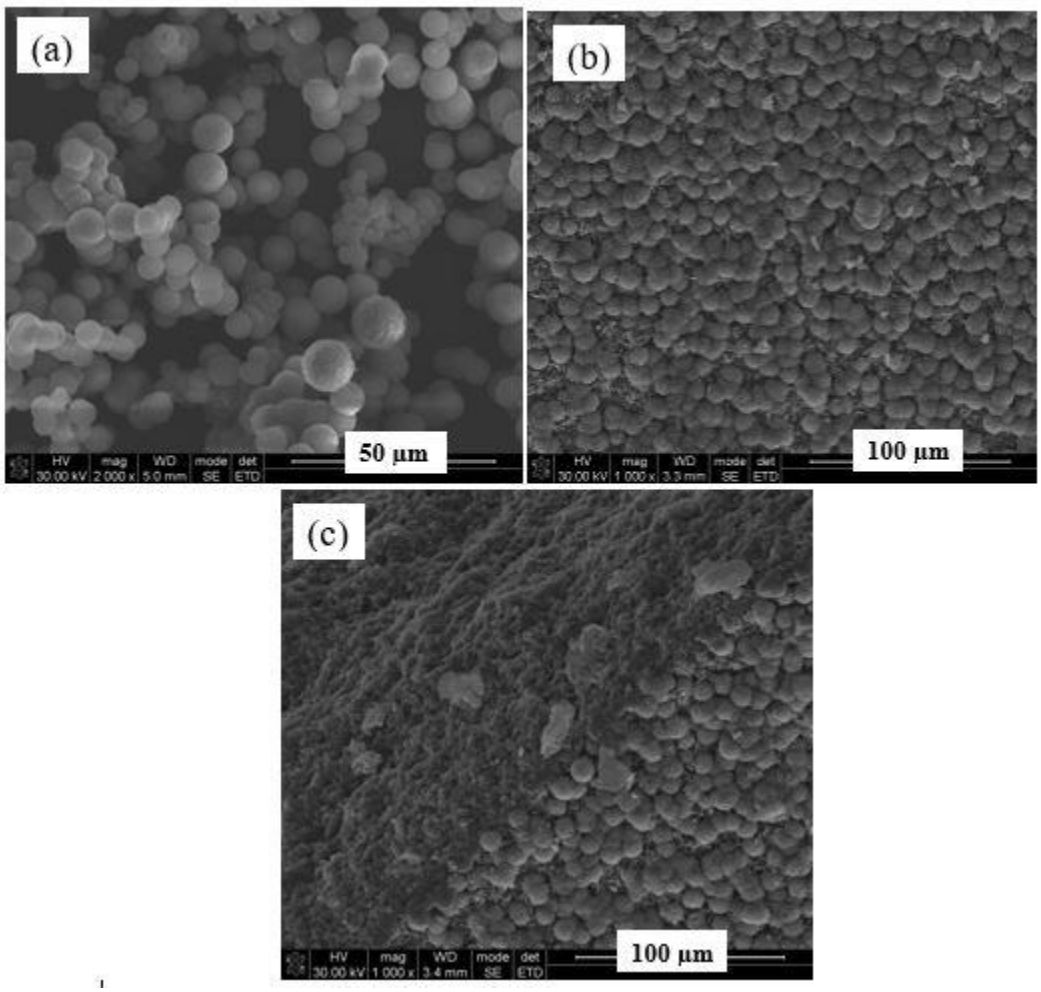

Figure 5. 4 SEM micrographs of (a) SOD crystals collected from the bottom of the autoclave, (b) membrane surface (B1), (c) membrane cross-section (B1)

5.3.2 Single gas permeation

Previous studies have shown that XRD and SEM can reveal if a continuous membrane was formed in/on the support or not. Yet, they cannot confirm whether a defect-free zeolite membrane was

formed (Lee et al., 2006; Kalantari et al., 2015). Comparison of single gas permeance provided information about the reproducibility of each technique, permeation/transport mechanism through the membrane, and H_2/CO_2 ideal selectivity of the membranes. The quality of membranes in this study was evaluated using H_2, CO_2 and N_2 pure gases at different total feed pressures and temperatures. A summary of permeation results taken at room temperature (25 °C) and 0.18 MPa feed pressure are presented in Table 5.2.

Table 5. 2 Permeation results at 25 °C and 0.18 MPa

Membrane Ref.	Synthesis technique	H_2 permeance	CO_2 permeance	N_2 permeance
			(10^{-7} mol.s^{-1}.m^{-2}.Pa^{-1})	
M1	PPH (one-interruption)	7.99	2.58	2.21
M2	PPH (one-interruption)	8.00	7.78	2.91
M3	PPH (two-interruptions)	7.95	9.63	2.71
M4	PPH (two-interruptions)	8.03	4.01	2.68
B1	Direct hydrothermal	7.97	1.04	2.63
B2	Direct hydrothermal	7.97	2.60	2.65

The permeation data of the membranes are presented in Table 5.2. It was observed H_2 permeance of membrane M1, M4, B1, and B2 was highest compared to N_2 and CO_2. This was expected as H_2 possesses the smallest kinetic diameter of 0.289 nm. Membrane M2 and M3 displayed similar H_2 and CO_2 permeance. This is not normal considering the size of CO_2 molecule (0.33 nm) compared to the pore dimension of SOD (0.29 nm). These observations confirmed the presence of some large defects in membrane M2 and M3 and have been discarded in the discussions going forward. The permeance trend for membrane B1 and B2, i.e. membranes prepared via direct hydrothermal synthesis was in the order of $H_2 > N_2 > CO_2$. This is following a decreasing trend of molecular weight. A study on MFI zeolite membranes prepared on porous α-alumina support also showed a decrease in permeance with increasing molecular weight and not molecular size (Kanezashi and Lin, 2009). However, membranes prepared via PPH synthesis (M1, M4) show a reverse trend i.e. permeance reduced as molecular kinetic diameter increased ($H_2 > CO_2 > N_2$). This trend reflects that gas permeation through pore-plugged membranes was controlled by the molecular sieving

through zeolite channels rather than surface diffusion through grain boundaries (Poshusta et al., 1998; Xu et al., 2001a; Xu et al., 2001b). Regardless of the synthesis technique that was used for SOD membrane synthesis, H_2, and N_2 permeances were reproducible and produced almost similar values as seen in Table 5.2. However, the permeances of CO_2 were not reproducible.

Permeance as a function of kinetic diameter (KD) of the molecules is presented in Figure 5.5 and Figure 5.6. The crystalline pore of SOD (0.29 nm) closely near the KD of H_2 (0.289 nm), it was therefore expected that H_2 would permeate through SOD pores. Notwithstanding the technique used in SOD zeolite membrane synthesis in this study, the pore size of a quality SOD/ceramic membrane should allow for a near-total exclusion of gases whose KD is more than 0.3 nm such as N_2 and CO_2. The CO_2 permeance for membrane M2 and M3 (figures not displayed) was very close to H_2 permeance and did not follow the normal trend of decrease in permeance with KD. These observations confirm again the pore quality of these membranes. Single gas permeance of membrane M1, M4 (Figure 5.5); B1, B2 (Figure 5.6) decreased dramatically as KD increased at high temperature. The drop in permeance with respect to KD of the gases was remarkably noticeable at high temperature (200 °C). As temperature reduced, the effect of a dramatic reduction in permeance became less severe. This can be attributed to activation of the gas diffusion mechanism within the pores of SOD at high temperature (Coronas and Santamaría, 1999).

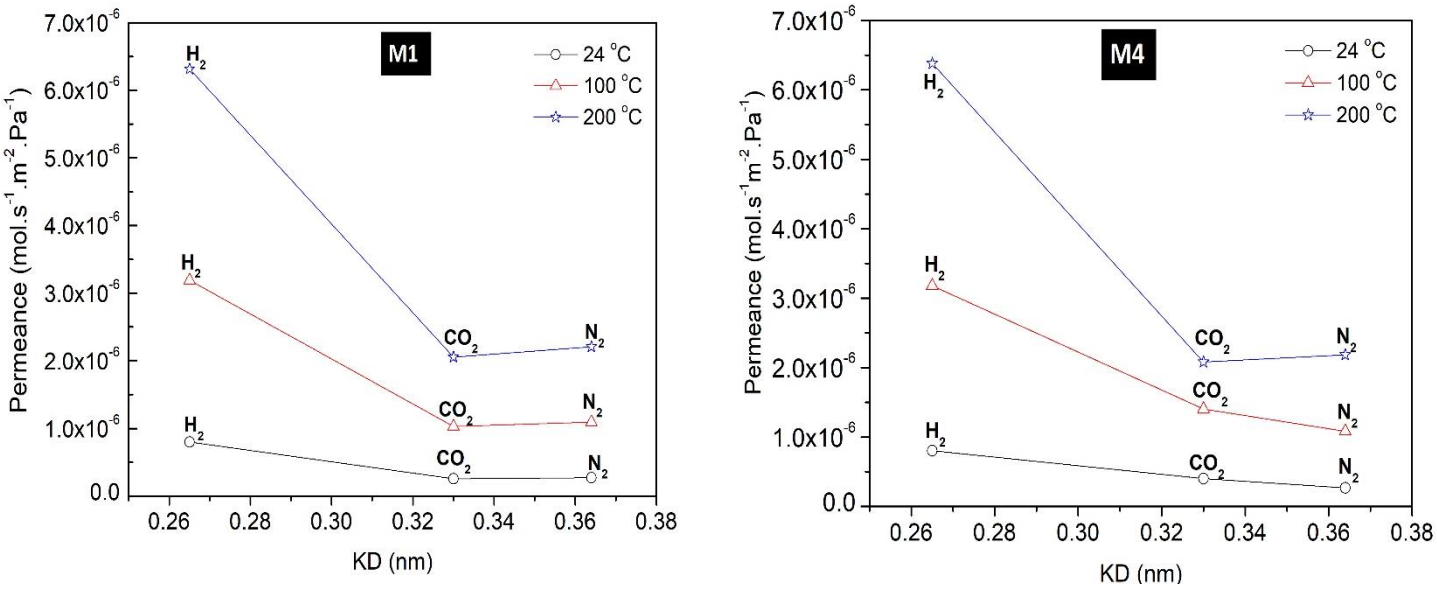

Figure 5. 5 Relationship between permeance and kinetic diameter

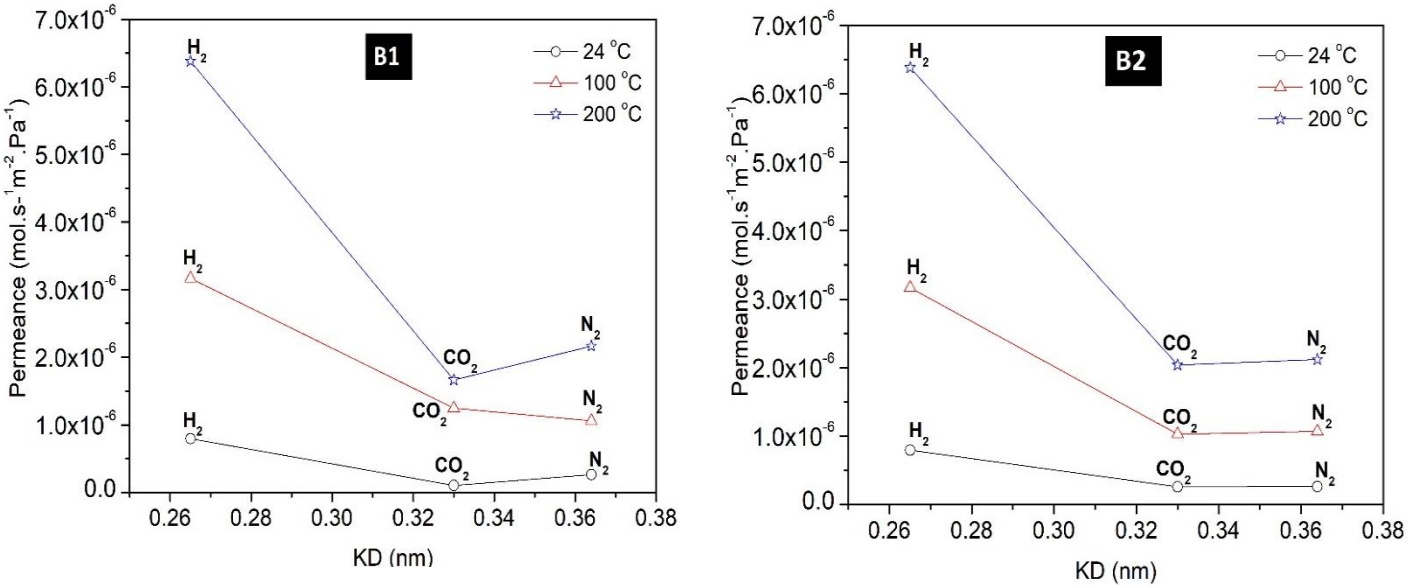

Figure 5. 6 Relationship between permeance and kinetic diameter

To further understand the performance of the as-synthesized membranes, the temperature dependence of its permeation property was plotted. The effect of permeation temperature on H_2, CO_2, and N_2 permeance at a feed pressure of 0.18 MPa is presented in Figure 5.7 and Figure 5.8. The plots show H_2 permeance exhibited a strong dependence with temperature. The mechanism of permeation for membranes synthesized in this study was analyzed keeping in mind single gas permeation behaviour with temperature (Coronas and Santamaría, 1999; Algieri et al., 2003). It was evident that at low temperature and ambient pressure, H_2 was only weakly absorbed on SOD zeolite as seen from Figure 5.7 and Figure 5.8. From these graphs, it can be observed also that the permeance of H_2 through SOD membrane increased fastest with increasing temperature. Hence, H_2 permeation through the membranes seemed to display activated diffusion behaviour (Shafie et al., 2012). Also, H_2 permeances do not show maxima in the range of temperature tested. A study by Kanezashi and Lin (2009) in which MFI membranes were synthesized on alumina support via secondary seeded growth method, the permeance of H_2 and CO_2 decreased with increasing temperature. The decrease in permeance was attributed to Knudsen-type temperature dependency display of the membrane up to 500 °C which was consistent with a study conducted by Hosseinzadeh Hejazi et al. (2011). Another study conducted by Zhou et al. (2014) using MFI membrane showed that both permeances of H_2 and CO_2 increased with temperature, although for

mixture gas components. Similar tendencies of a rise in permeance with temperature have also been reported for $AlPO_4$-type molecular sieving membranes formed on a porous alpha-alumina tube (Guan et al., 2003). Coronas et al. (1997) and Martínez Galeano et al. (2016) reported the same trend similar to this study for H_2, N_2 and CO_2 gas permeance. Each of these studies pointed to the fact that the increase in permeance with temperature suggested activated diffusion prevailed over Knudsen diffusion.

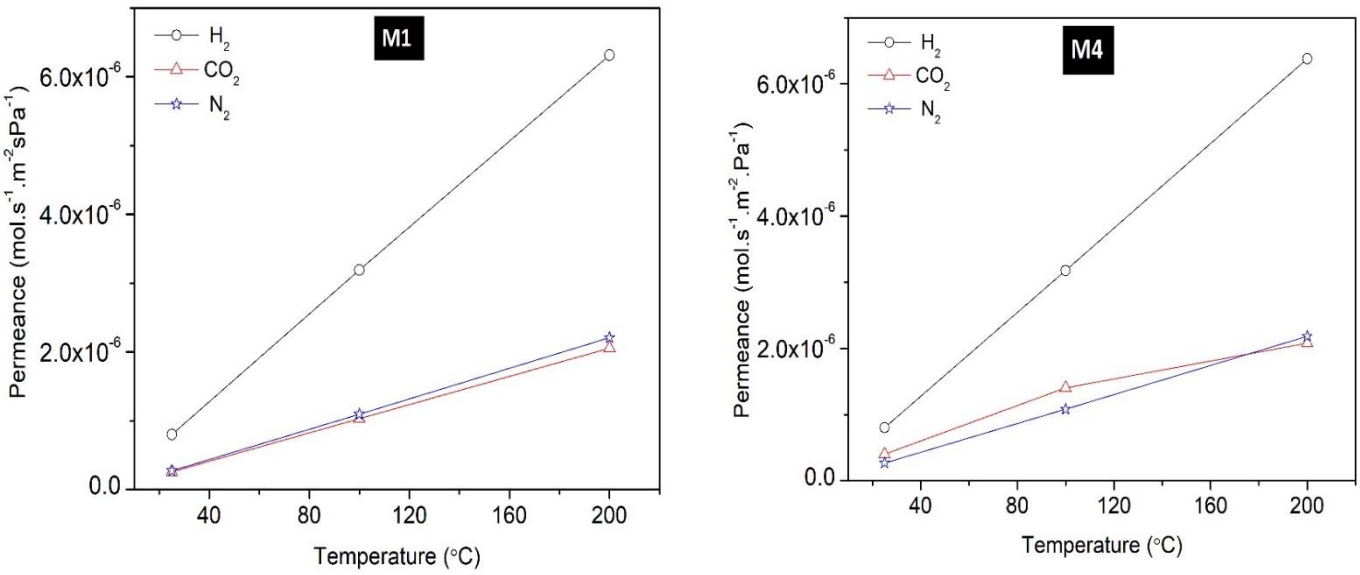

Figure 5. 7 Effect of permeation temperature on H_2, CO_2, and N_2 permeance

A clear increase of H_2 permeance with temperature could also suggest possibly there was a larger contribution of zeolite flux to total flux for H_2 flow. However, this may not be the case as H_2 is a small molecule capable of high permeation rates even through intercrystalline defects at the nanometer scale (Bernal et al., 2002). Even though permeate of H_2 in this study follows the general permeation pathway of microporous membrane of Algieri et al. (2003), we cannot conclude of a fact the membranes synthesized in this study were highly microporous or were of high quality using permeance-temperature dependency plots alone.

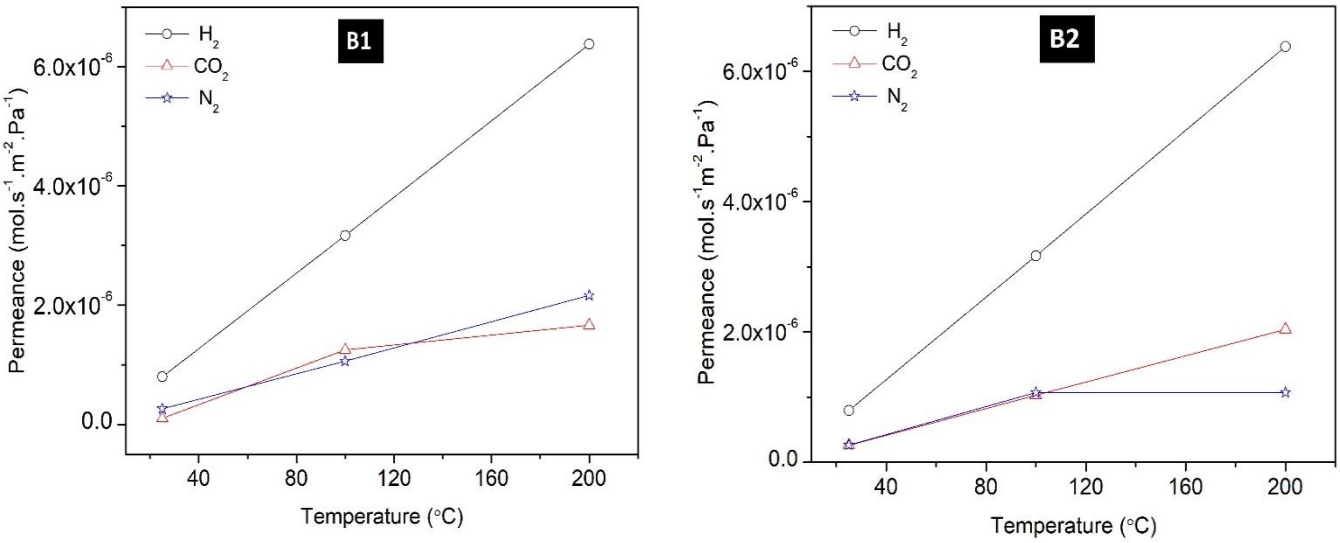

Figure 5. 8 Effect of permeation temperature on H_2, CO_2, and N_2 permeance

There are many good quality, polycrystalline zeolite membranes with zeolite pores, but also have intercrystalline gaps, which are microporous with pore size larger than the zeolite pores (Lin and Duke, 2013). In the field of zeolite membranes, synthesizing defect-free zeolite membranes especially on a large scale is an uphill task (Wang et al., 2017). However, a low concentration of defects is not undesired (Feng et al., 2015). The presence of large pore zeolitic phases such as Na-A (0.41 nm), Na-X (0.73 nm) type zeolite which formed alongside SOD zeolite as displayed in the XRD patterns (Figure 5.1), may have enhanced CO_2 permeance, especially in membrane M2 and M4. The CO_2 permeance for all the membranes synthesized was least reproducible and displayed only a slight increase in permeance as temperature increased, which could be attributed to its large size. Its strong absorption strength compared to H_2 and N_2 which are non-absorbing could also be a contributing factor. For zeolite coated stainless steel tubular membranes synthesized by Farjoo and coworker (Farjoo and Kuznicki, 2016), a constant trend of CO_2 permeance with temperature was attributed to the combined effects of zeolitic flux as an activated process and non-zeolitic flux.

The H_2, CO_2, and N_2 permeances (Figure 5.9 and Figure 5.10) were also found to be dependent on feed pressure for the whole range of temperature in this study. By varying operating pressure in the membrane, the test makes it possible to determine the contribution of viscous flux in the membrane. It was difficult to obtain high permeance at high pressures for all gases. Maximum H_2

permeance obtained for membrane M1 was 6.32 x 10^{-6} mol.s^{-1}.m^{-2}.Pa^{-1} at 200 °C and 0.18 MPa feed pressure which dropped to 1.58 x 10^{-6} mol.s^{-1}.m^{-2}.Pa^{-1} as pressure was increased. Moreso, CO_2 and N_2 permeance also decreased as the pressure was increased. The lowest N_2 permeance for membrane M1 was 6.83 x 10^{-8} mol.s^{-1}.m^{-2}.Pa^{-1} and 6.50 x 10^{-8} mol.s^{-1}.m^{-2}.Pa^{-1} for CO_2. These values were obtained at room temperature (25 °C) and 0.48 MPa. Whilst the lowest obtainable permeance for M4 was 6.63 x 10^{-8} mol.s^{-1}.m^{-2}.Pa^{-1} for N_2 and 4.03 x 10^{-8} mol.s^{-1}.m^{-2}.Pa^{-1} for CO_2 at 25 °C.

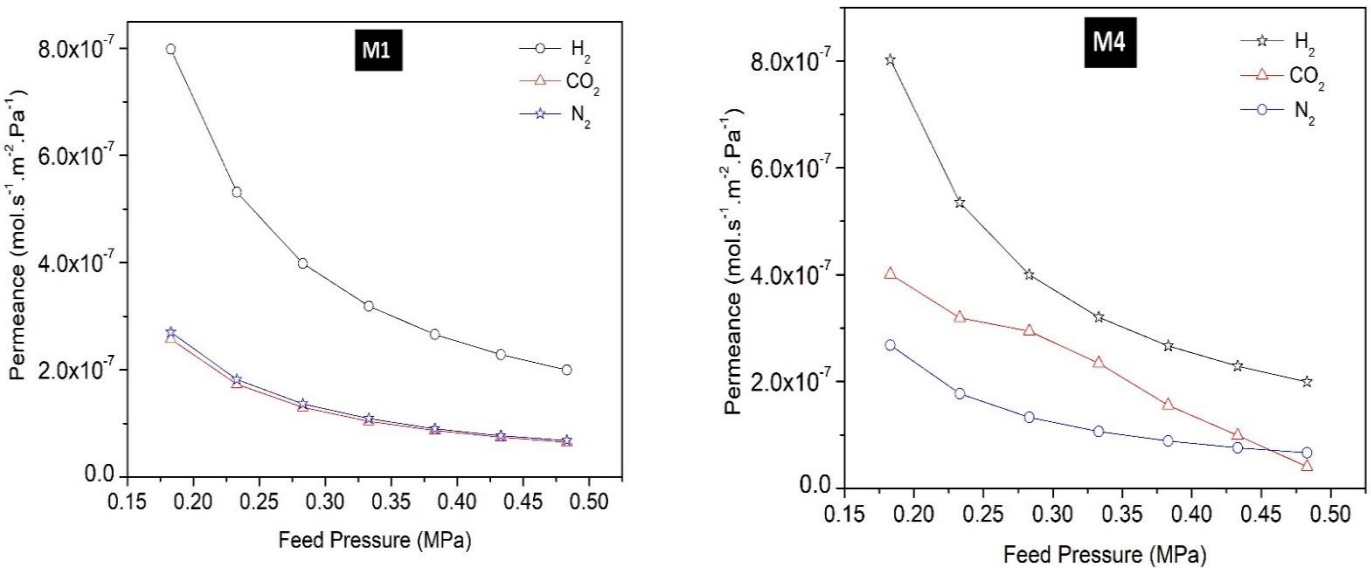

Figure 5. 9 H_2, CO_2, and N_2 permeances as a function of feed pressure at 25 °C

A study on the effect of dehydration temperature on H_2 potential of HSOD zeolite membrane by Vaezi and Babaluo, (2014) showed H_2 and CO_2 permeances slightly increased as a function of mean pressure which was attributed to the presence of impurities. These impurities provided larger pore sizes than the size of the HSOD membranes for the transport of smaller gases. For zeolite membranes, gas can transport through zeolite pores and non-zeolite pores. When these defects (non-zeolite pores) are relatively large, they provide non-selective pathways, and viscous flow becomes the predominant mechanism which will increase with pressure. Small defects will allow Knudsen mechanism to dominate the separation, thus making the membrane semi-selective and flux will remain almost constant as pressure increases (Farjoo and Kuznicki, 2016).

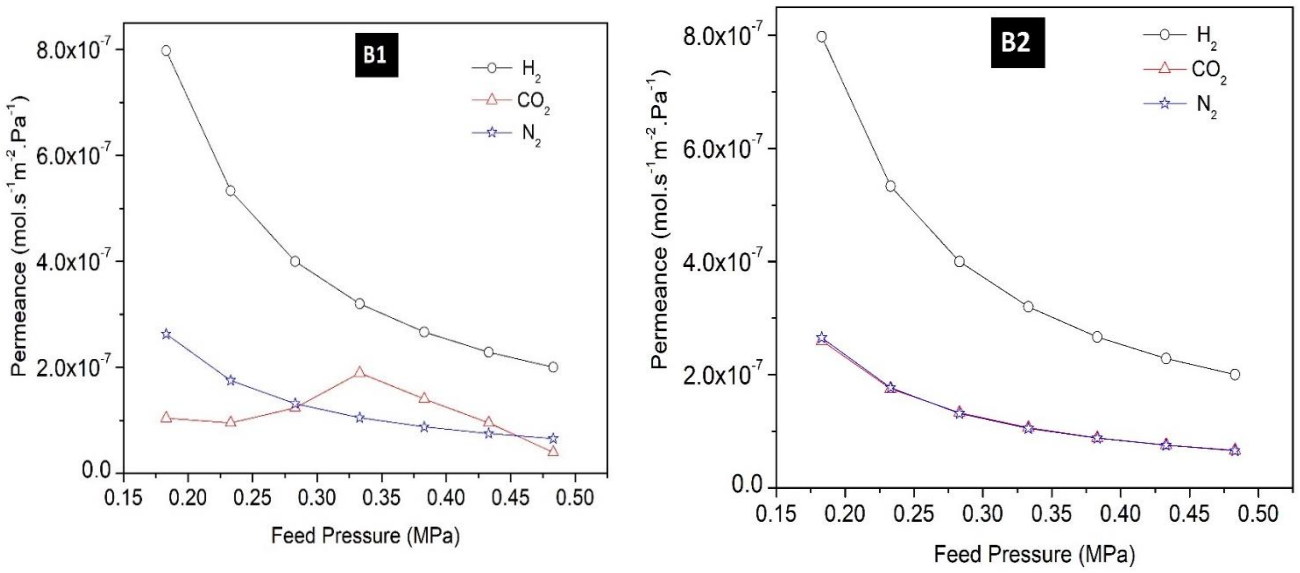

Figure 5. 10 H_2, CO_2, and N_2 permeances as a function of feed pressure at 25 °C (B1, B2)

According to Hosseinzadeh Hejazi et al. (2011), for pores greater than the kinetic diameter of the molecules and if the flow is through the zeolite pores, the flow should either be constant or decrease slightly with pressure. The decreasing trend of permeance with pressure as observed in this study indicates that the selective flow dominated in the membranes.

With permeance-pressure plots (Figure 5.9 and Figure 5.10), it was difficult using H_2 to probe for defect/dominant mechanism. Single gas H_2 permeance for the membranes prepared via each technique was neglected as the permeance of H_2 changed only slightly. CO_2 permeance-pressure curve (Figure 5.9 and Figure 5.10) was therefore used to give an additional indication of the quality and transport mechanisms displayed by these membranes. The observation that CO_2 permeance increased for membrane M2 over membrane M1 established an increase in non-selective SOD zeolite pathways in membrane M2 over membrane M1. This finding agrees with the permeance-kinetic diameter plot in Figure 5.5 and Figure 5.6. Likewise, a decrease in CO_2 permeance as observed over the pressure range tested for membrane M4 over membrane M3 established a decrease in non-selective SOD zeolite pathways in membrane M4. Membrane M2 and M3 have been discarded as poor-quality membranes in the early part of this section.

To give a reliable indicator of the presence of large defects, ideal selectivity was calculated for all the as-synthesized membranes. Figure 5.11 presents a plot of ideal selectivities of membranes as a function of feed pressure. Membrane M1 and B2 displayed a near-constant ideal selectivity of 3.10 for the range of feed pressure investigated at 25 °C. This value is lower than the predicted theoretical H_2/CO_2 Knudsen selectivity of 4.7, suggesting zeolite contributed little to permeation in these two membranes. The selectivity of these membranes did not improve when the temperature was increased to 200 °C. Membrane M2 and M3 had the smallest ideal selectivity value of 1.52 which supported the claim made prior that these membranes were of very poor quality. At high temperatures, CO_2 adsorption on the surface of the zeolite pores of M2 and M3 weakened dramatically and its mobility increased, resulting in membranes M2 and M3 possessing the lowest H_2/CO_2 selectivity. In other words, these membranes did not show molecular sieving abilities rather, the presence of large non-selective pores far greater than the KD of H_2 and CO_2 allowed for viscous flow through the pores of the membranes.

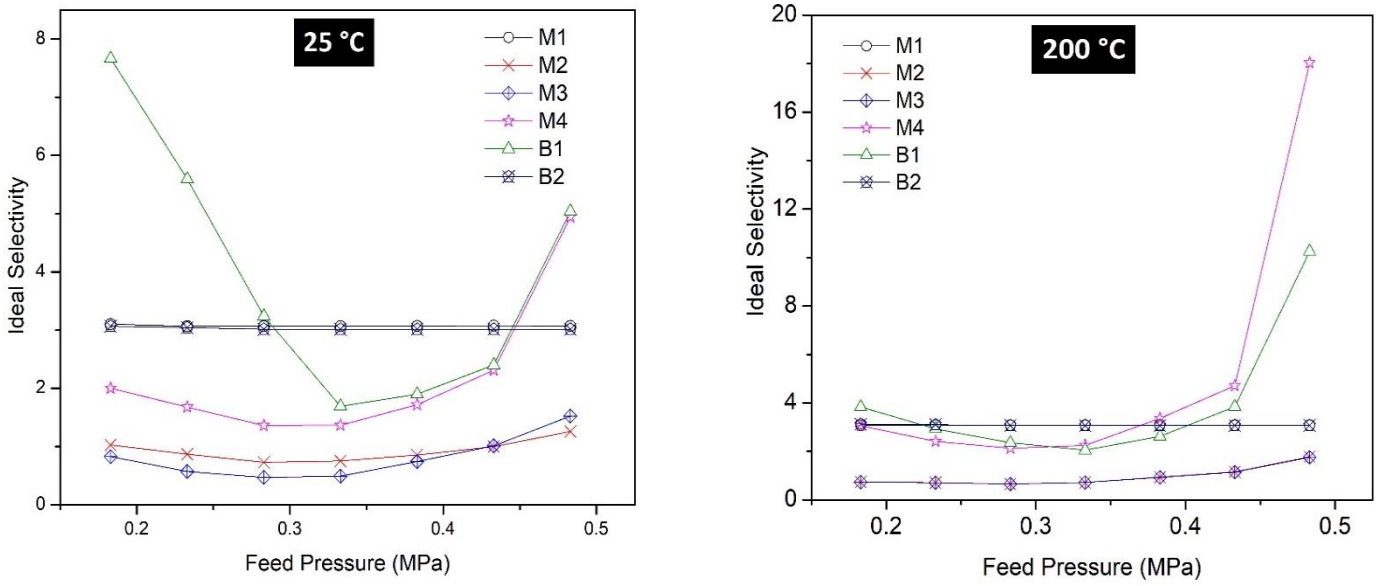

Figure 5. 11 Ideal selectivity of H_2/CO_2 as a function of feed pressure

Membrane B1 displayed high H_2/CO_2 selectivity of 7.66 at 0.18 MPa and 10.25 at 0.48 MPa which suggested that zeolite contributed to separation and that there was a decrease in the number and size of the non-selective pores. The ideal selectivity of membrane M1 exceeds H_2/CO_2 Knudsen

selectivity of 4.67. However, the selectivity decreased to 3.24 as pressure was increased to 0.33 MPa, suggesting an increase in non-selective flow through non-zeolitic pores in the membrane at these conditions. Membrane prepared via the pore-plugging hydrothermal synthesis using two interruptions steps of 1 hour each (membrane M4) produced the best selective membrane. The membrane displayed ideal selectivity of 4.94 at 25 °C and 18.03 at 200 °C, at a feed pressure of 0.48 MPa (Figure 5.12). The high selectivity achieved can be attributed to the much stronger adsorption of CO_2 restricting its diffusion on the membrane pore surface. Another contribution to high selectivity, in this case, may possibly be due to the enhanced pore-plugging effect of SOD zeolite in the pores of the support after the second interruption step.

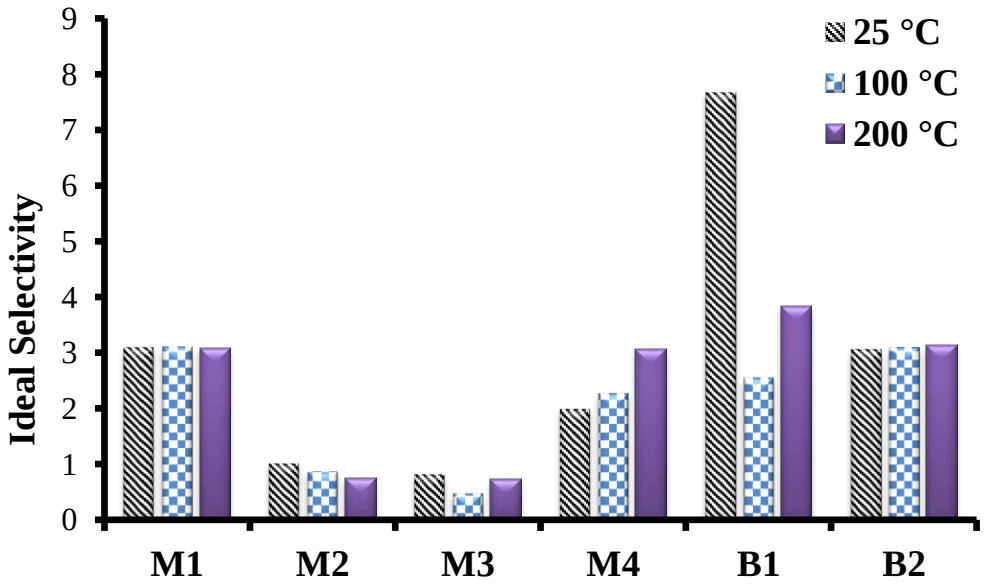

Figure 5. 12 Ideal selectivity of H_2/CO_2 as a function of temperature at 0.18 MPa

It can be concluded that the fraction of "non-selective" viscous flux in Membrane M4 was very minimal, hence decrease the concentration of defects and increase the concentration of active zeolite pores. A decrease in selectivity with increasing pressure suggests gas transport flow through non-zeolitic regions and macroporous defects (viscous flow contribution) (Julbe et al., 2003; Hosseinzadeh Hejazi et al., 2011).

For membrane prepared via the direct hydrothermal synthesis technique, the highest selectivity obtained was 10.25 (Figure 5.13) at 0.48 MPa feed pressure and 25 °C (i.e. membrane B1). This suggests at these conditions; the pore size of the membranes was very close to the kinetic diameter of the permeating molecules and gas separation was controlled by activated diffusion and/or Knudsen diffusion. Gas flow through real microporous membranes i.e. membranes with a small concentration of mesoporous defects may include the contribution of permeation through the micropores and mesopores (Gkanas et al., 2015). An ideal selectivity of 10 at high pressure has been reported for HSOD prepared on tubular alumina support via the direct hydrothermal technique (Vaezi and Babaluo, 2014). The ideal selectivity values obtained in this study are found to be similar to those in the literature (see Table 5.3).

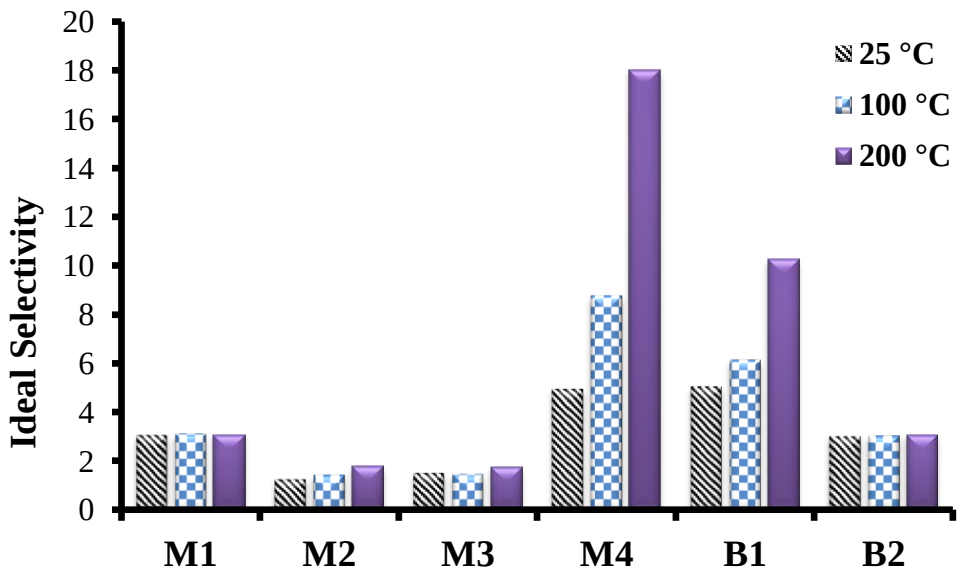

Figure 5. 13 Ideal selectivity of H_2/CO_2 as a function of temperature at 0.48 MPa

Table 5. 3 Comparison of membranes tested in this work compared to literature under relatively similar test condition

Zeolite	Support	Synthesis technique	T (°C)	Permeance (10^{-8} mol.s^{-1}.m^{-2}.Pa^{-1})			H_2/CO_2 selectivity	Ref.
				H_2	CO_2	N_2		
SOD (M1)	α- Al_2O_3 tube	PPH	25	7.99	2.58	2.71	3.10	This study
SOD (M4)	α- Al_2O_3 tube	PPH	200	15.9	0.88	5.46	18.07	This study
SOD (B1)	α- Al_2O_3 tube	DHS	200	16	1.56	5.36	10.25	This study
SOD (B2)	α- Al_2O_3 tube	DHS	25	7.97	2.60	2.65	3.07	This study
$AlPO_4$	α- Al_2O_3 tube	DHS	37	3.36	-	2.53	23.9	Guan et al. (2003)
LTA-Type ($AlPO_4$)	α- Al_2O_3 disk	SSG	20	2.63	0.24	-	11	Huang et al. (2010a)
NaA	Stainless steel disk	SSG	100	1.81	-	0.45	-	Martínez Galeano et al. (2016)
Silicalite-1	α- Al_2O_3 tube	SSG	25	79.1	43	46	-	Algieri et al. (2003)
NaA	α- Al_2O_3 tube	SSG	25	8.02		1.25		Zah et al. (2007)
ZIf-7	α- Al_2O_3 disk	SSG	25	0.46	0.035	0.022	13	Li et al. (2010)

SSG: secondary seeded growth; PPH: pore-plugging hydrothermal; DHS: direct hydrothermal synthesis; W-K: Wicke–Kallenbach method

5.3.3 Mixture gas separation

The best H_2/CO_2 ideal selectivity membranes (M4, B1), was then used for separating H_2/CO_2 (60/40) mixture. As expected, there was a significant difference between the permeance of H_2 as pure gas and that of H_2 in the gas mixture for both membranes. The mixture H_2 permeance obtained was 1.19×10^{-7} mol.s^{-1}.m^{-2}.Pa^{-1} (membrane B1) and 1.06×10^{-7} mol.s^{-1}.m^{-2}.Pa^{-1} (membrane M4) at 25 °C and 0.18 MPa feed pressure. Because of the strong impact of competitive adsorption, membrane performance was impacted by fluctuations in operating parameters. Figure 5.14 and Figure 5.15 show pressure dependence of permeance through SOD membrane, M4 and B1 tested in H_2/CO_2 mixture at 25 °C, permeate pressure kept at atmospheric.

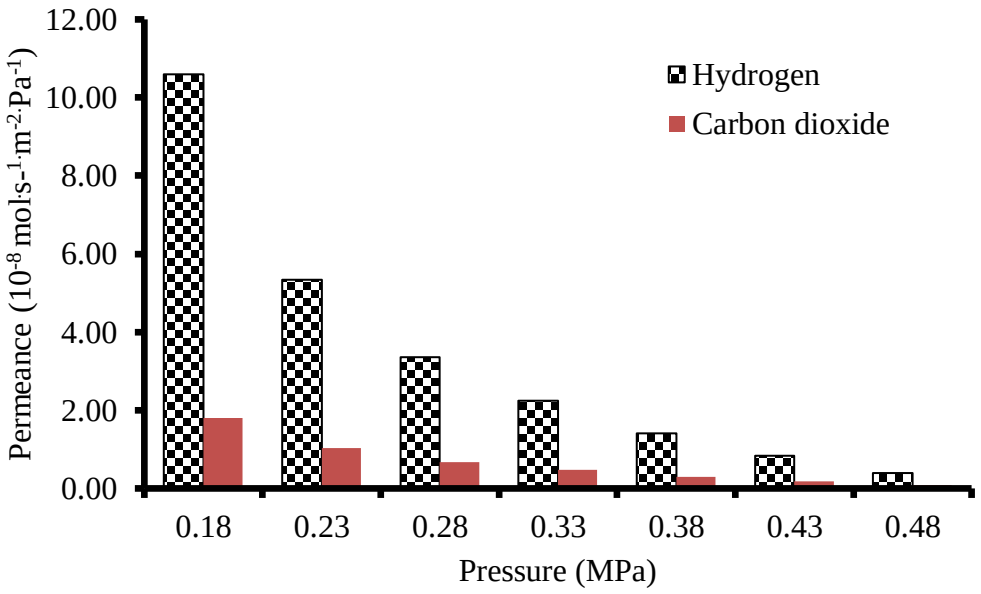

Figure 5. 14 Pressure dependence of permeance through SOD membrane M4 in H_2/CO_2 mixture at 25 °C

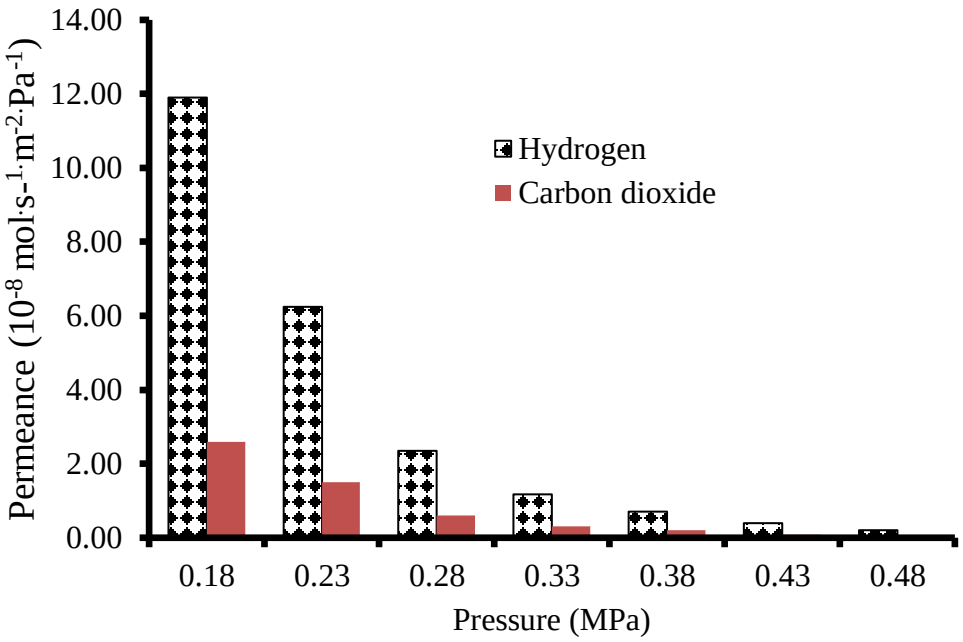

Figure 5. 15 Pressure dependence of permeance through SOD membrane B1 in H_2/CO_2 mixture at 25 °C

From Figure 5.14 and Figure 5.15, it was observed that the permeance of the weakly adsorbed H_2 is reduced much more than the strongly adsorbing CO_2. According to Lindmark and Hedlund, (2010), this suggests that the effective pore size of the membrane prepared in this study approaches the size of the permeating molecules. The H_2 and CO_2 gas permeance observed at the same temperature, 25 °C, for both single and mixture gas experiment show that H_2 permeance was 6-7 times lower in mixture experiment compared to its pure gas permeance. This is probably explained by a combination of the strong adsorption of CO_2 blocking the permeation of H_2 and concentration polarization.

Table 5. 4 H_2/CO_2 mixture separation factor of sodalite membrane M4 and B1

Feed pressure (MPa)	0.18	0.23	0.28	0.33	0.38	0.43	0.48
M4 Separation factor (-)	3.26	3.58	3.84	3.87	4.10	4.20	4.24
B1 Separation factor (-)	2.84	3.04	3.25	3.50	3.78	4.10	4.13

The mixture H_2 and CO_2 permeance decreased with an increase in feed pressure. And thus, H_2/CO_2 selectivities increased with feed pressure (see Table 5.4). Table 5.5 compares H_2/CO_2 separation performances for an H_2/CO_2 (60/40) mixture through the SOD membranes prepared in this study. To the best of my knowledge, no study using SOD membranes for the separation of H_2/CO_2 mixtures has been reported. The differences in the separation performance of both membranes can be attributed to the difference in preparation protocols. Membrane M4 prepared via pore-plugging hydrothermal synthesis technique using two interruption steps displayed higher H_2/CO_2 separation factor (4.24) obtained at a high feed pressure of 0.48 MPa and 25 °C. The separation factor increased as feed pressure increased from 0.18 MPa to 0.48 MPa. The separation factor for membranes prepared in this work tested at 25 °C is lower than the H_2/CO_2 separation factor of 7.2 at 50 °C for ZIF-22 in LTA topology membranes reported by Huang et al. (2010b). The pore size of zeolitic imidazolate framework (ZIF-22) is about 0.3 nm so it can be expected to display high molecular sieving performance for separation of H_2 from CO_2. Also, 1:1 binary mixtures of H_2 with CO_2 was used, and measurements were by the Wicke–Kallenbach technique using a sweep gas. Yin et al. (2007) prepared zeolite NaX composite membrane by the secondary seeded growth method to separate a 50:50 mixture of H_2/CO_2. The authors obtain a separation selectivity of 4.57 for a 1:1 binary mixture of H_2 with CO_2. NaX is a zeolite with polar sites and has strong electrostatic interactions with polar gas like CO_2 which contributed to H_2/CO_2 separation. SAPO-34 zeolite membrane prepared on chitosan modified support for H_2/CO_2 separation was reported by Das et al. (2012). It was found that the selectivity for H_2/CO_2 binary mixture increased to 4.2 by increasing CO_2 concentration. By synthesizing a unique bilayer membrane structure with intermediate macroporous yttria-stabilized zirconia (YSZ), Wang et al. (2014) reported an H_2/CO_2 separation factor of 25.3 at 450 °C. Huang and co-workers Huang et al. (2010c) prepared LTA zeolite membranes in the presence of covalent linkers via the direct hydrothermal synthesis method on disk support. A separation factor of 5.5 and CO_2 permeance of 6.8×10^{-8} $mol.s^{-1}.m^{-2}.Pa^{-1}$ was obtained. Considering the comparable test conditions, the different supports used, and the different synthesis techniques applied by these authors, H_2/CO_2 separation factor for SOD membrane in the range of 4.13-4.24 obtained in this study is very similar. Though the mixture separation factor is reasonable, the mixture separation factors obtained in this study were lower than the theoretical value of Knudsen diffusion (4.7). Thus, suggested that gases permeated through grain boundaries rather than molecular sieving through the regular zeolite pores.

Table 5. 5 Comparison of mixture gas separation data of the SOD membrane in this study with other membranes in the literature

Zeolite	Support	Preparation Technique	Temp (°C)	TMP (KPa)	H_2: CO_2	Permeance (10^{-8} mol.s^{-1}.m^{-2}.Pa^{-1})		SF	Ref.
						H_2	CO_2		
LTA	α-Al_2O_3 disk	DH	20	W-K	50:50	30	6.80	5.3	Huang et al. (2010c)
ZIF-22	TiO_2 disk	SR	50	100 W-K	50:50	16.6	2.30	7.2	Huang et al. (2010b)
ZIF-7	α-Al_2O_3 disk	SSG	220	W-K, N_2 sweep	50:50	4.55	0.33	13.6	Li et al. (2010a)
NaX	Stainless-steel net	SSG	16	-	50:50	10.1	-	4.57	Yin et al. (2007)
SAPO-34	Clay- Al_2O_3 tube	SSG	25	200	70:30	-	-	4.2	Das et al. (2012
MFI	α-Al_2O_3 disk	SSG	100	100	50:50	174	-	1.02	Wang et al. (2014)
LTA/$AlPO_4$	α-Al_2O_3 disk	SSG	20	100	50:50	24	3.17	7.6	Huang et al. (2010a)
SOD (M4)	α-Al_2O_3 tube	PPH	25	220	60:40	10.6	1.79	4.24	This study
SOD (B1)	α-Al_2O_3 tube	DH	25	220	60:40	11.9	2.55	3.90	This study

W-K: Wicke–Kallenbach technique; DH: Direct hydrothermal; SSG: Secondary Seeded Growth; PPH: Pore-Plugging Hydrothermal; SF: Separation Factor

Concluding Remarks

In conclusion, SOD/ceramic membranes via the pore-plugging using one interruption, two-interruption steps and via direct hydrothermal synthesis (Teflon around the support) were successfully synthesized. Nanocomposite membrane M4, synthesized via pore-plugging hydrothermal synthesis using two interruption steps had the best ideal selectivity of 18.03. The hydrogen permeance of this membrane was 1.59×10^{-6} $mol.s^{-1}.m^{-2}.Pa^{-1}$ at 200 °C and 0.48 MPa, performed quite well under a single component gas experiment. When tested at room temperature using a binary gas mixture of H_2/CO_2 in the ratio of 60:40, the H_2 permeance decreased to 1.06×10^{-7} $mol.s^{-1}.m^{-2}.Pa^{-1}$. The reduced H_2 permeance was attributed to the much stronger adsorption of CO_2 which restricted its diffusion in the membrane pore surface. Further optimizing the pore-plugging hydrothermal synthesis variables to synthesize nanocomposite SOD/ceramic membranes could potentially result in the development of practical, robust H_2 separation membranes showing strong molecular sieving properties.

Chapter 6: Conclusions and Recommendations

6.1 Overall Conclusions

The global consumption of fossil fuel energy will increase especially in developing nations. In a country like South Africa, coal is abundant, hence, provides a stable and cheap energy source. However, this fuel is the most carbon-intensive fuel, and a major contributor to rising energy-related carbon dioxide (CO_2) emissions. One of the main issues addressed globally is CO_2 emissions, which form the core of the climate change mitigation debate. Deployment of the carbon capture and storage (CCS) technology has been proposed as one of the solutions to reduce net CO_2 emissions from fossil-fueled power plants. Commercial state-of-the-art absorption technology which is the technology been implemented for the separation of CO_2 is associated with a high cost of capture. Research into membrane technology for gas separations is on the rise as the technology delivers a promise of lower energy penalties, cost and smaller footprint.

On this note, this study aimed to optimize the pore-plugging hydrothermal synthesis preparation of hydroxy sodalite crystals. The optimization step was important to developing high-quality sodalite/ceramic membranes applicable in pre-combustion capture. High purity sodalite crystals obtained by optimizing the pore-plugging hydrothermal synthesis technique was employed in the synthesis of high-quality nanocomposite SOD/ceramic membranes. Nanocomposite membranes were then compared with thin-film membranes synthesized via the direct hydrothermal synthesis technique. Overall performance of as-synthesized membranes was evaluated using single gas permeation of H_2, CO_2, N_2 and mixture gas separation of H_2/CO_2 under the same operating conditions. Major findings of each experimental chapter in this study are summarized as follows:

1. Sodalite crystals of different quality were successfully synthesized and evaluated. The optimization results demonstrated that ageing sodalite precursor under stirring for long hours before pore-plugging hydrothermal synthesis led to the formation of impurities with sodalite crystals.

2. The results from this study also confirmed that by ageing the sodalite precursor for 4 hours and varying conditions of the pore-plugging hydrothermal synthesis such as synthesis temperature,

pre-interruption time and post-interruption time, the quality of the as-produced sodalite crystals can positively or negatively impacted.

3. The covering of the outer surface of the support of the membrane prepared via the direct hydrothermal synthesis technique produced membrane with good reproducibility.

4. The results obtained in this study showed sodalite membrane supported on ceramic prepared via the pore-plugging hydrothermal synthesis using two interruption steps produced the best ideal selectivity (18.03) with H_2 permeance of 1.59×10^{-6} mol.$^{-1}$s-^{1}.m^{-2}.pa^{-1} at 200 °C and feed pressure of 0.48 MPa. The H_2 permeance decreased from 7.97×10^{-7} mol.$^{-1}$s-^{1}.m^{-2}.pa^{-1} to 1.06×10^{-7} mol.$^{-1}$s-^{1}.m^{-2}.pa^{-1} in a binary mixture of H_2/CO_2 (60/40) when tested at 25 °C and a feed pressure of 0.18 MPa.

6.2 Recommendations

Based on the observations from experiments carried out in this study, the following suggestions may be considered for future research.

1) Optimization effort should target pore-plugging hydrothermal synthesis in the presence of the support. The support would play an important role during sodalite growth to reduce defect formation.

2) The sealing of both ends of the support with Teflon cap to stop the growth of synthesis solution in the lumen of the support and to suppress pore-plugging growth of zeolite crystals from the outer surface to the inside of the pore of the support might lead to the fabrication of membrane with improve selectivity and gas separation abilities.

3) The use of a programmable oven equipped with ramping and cooling rate is recommended to ensure minimization of thermal shock to the membrane.

4) A sweep gas could be applied on the permeate side to keep the concentration of the permeate gas as low as possible. By so doing, the driving force for permeation could be enhanced and subsequently, the separation performance of the membrane could improve.

5) Synthesis of sodalite membrane in a rotating autoclave could help to remove little air bubbles on the surface of the support by the continuous rotation, as these bubbles contribute to defects in the zeolite layer. Effective mixing of the synthesis in a rotating autoclave can improve both mass and heat transfer.

6) The configuration of the permeation module and the flow conditions of the permeation measurement can affect the separation factor for mixture species. As such different flow arrangement like co-current, cross-flow arrangements should be considered which might improve selectivity.

References

Abanades, J.C., Arias, B., Lyngfelt, A., Mattisson, T., Wiley, D.E., Li, H., Ho, M.T., Mangano, E., and Brandani, S. (2015). Emerging CO_2 capture systems. International Journal of Greenhouse Gas Control 40, 126–166.

Adhikari, S., and Fernando, S. (2006). Hydrogen membrane separation techniques. Ind. Eng. Chem. Res. 45, 875–881.

Akhtar, F., Sjöberg, E., Korelskiy, D., Rayson, M., Hedlund, J., and Bergström, L. (2015). Preparation of graded silicalite-1 substrates for all-zeolite membranes with excellent CO_2/H_2 separation performance. J. Membr. Sci. 493, 206–211.

Albarracin Zaidiza, D., Belaissaoui, B., Rode, S., Neveux, T., Makhloufi, C., Castel, C., Roizard, D., and Favre, E. (2015). Adiabatic modelling of CO_2 capture by amine solvents using membrane contactors. Journal of Membrane Science 493, 106–119.

Algieri, C., Bernardo, P., Golemme, G., Barbieri, G., and Drioli, E. (2003). Permeation properties of a thin silicalite-1 (MFI) membrane. J. Membr. Sci. 222, 181–190.

Allwood, J.M., Cullen, J.M., and Milford, R.L. (2010). Options for achieving a 50% cut in industrial carbon emissions by 2050. Environ. Sci. Technol. 44, 1888–1894.

Alshebani, A., Pera-Titus, M., Landrivon, E., Schiestel, Th., Miachon, S., and Dalmon, J.-A. (2008a). Nanocomposite MFI-ceramic hollow fibers: Prospects for CO_2 separation. Microporous Mesoporous Mater. 115, 197–205.

Alshebani, A., Pera-Titus, M., Yeung, K.L., Miachon, S., and Dalmon, J.-A. (2008b). Influence of desorption conditions before gas separation studies in nanocomposite MFI–alumina membranes. J. Membr. Sci. 314, 143–151.

Al-Mufachi, N.A., Rees, N.V., and Steinberger-Wilkens, R. (2015). Hydrogen selective membranes: A review of palladium-based dense metal membranes. Renewable and Sustainable Energy Reviews 47, 540–551.

Anderson, T.R., Hawkins, E., and Jones, P.D. (2016). CO_2, the greenhouse effect and global warming: from the pioneering work of Arrhenius and Callendar to today's Earth System Models. Endeavour 40, 178–187.

Aresta, M., Dibenedetto, A., and Angelini, A. (2014). Catalysis for the valorization of exhaust carbon: from CO_2 to chemicals, materials, and fuels. Technological Use of CO_2. Chem. Rev. 114, 1709–1742.

Armor, J.N. (1998). Applications of catalytic inorganic membrane reactors to refinery products. J. Membr. Sci. 147, 217–233.

Avci, G., Velioglu, S., and Keskin, S. (2019). In-silico design of MOFs with enhanced CO_2 separation performances: Role of metal sites. J. Phys. Chem. C.

Bai, C., Jia, M.-D., Falconer, J.L., and Noble, R.D. (1995). Preparation and separation properties of silicalite composite membranes. Journal of Membrane Science 105, 79–87.

Ball, M., and Wietschel, M. (2009). The future of hydrogen – opportunities and challenges. International Journal of Hydrogen Energy 34, 615–627.

Basile, A., Iulianelli, A., Longo, T., Liguori, S., and De Falco, M. (2011). Pd-based selective membrane state-of-the-art. in membrane reactors for hydrogen production processes, M. De De Falco, L. Marrelli, and G. Iaquaniello, eds. London: Springer London, pp. 21–55.

Bayati, B., Babaluo, A.A., Karimi, R., (2008). Hydrothermal synthesis of nanostructure NaA zeolite: The effect of synthesis parameters on zeolite seed size and crystallinity. Journal of the European Ceramic Society 28, 2653–2657.

Bedard, R., and Liu, C. (2018). Recent advances in zeolitic membranes. Annual Review of Materials Research 48, 83–110.

Bernardo, P., Drioli, E., Golemme, G., (2009). Membrane gas separation: A review/state of the art. Ind. Eng. Chem. Res. 48, 4638–4663.

Bernal, M.P., Coronas, J., Menéndez, M., and Santamaría, J. (2002). Characterization of zeolite membranes by temperature programmed permeation and step desorption. J. Membr. Sci. 195, 125–138.

Bonilla, G., Tsapatsis, M., Vlachos, D.G., and Xomeritakis, G. (2001). Fluorescence confocal optical microscopy imaging of the grain boundary structure of zeolite MFI membranes made by secondary (seeded) growth. Journal of Membrane Science 182, 103–109.

Bose, A., Sen, M., Kishore Das, J., and Das, N. (2014). Sonication mediated hydrothermal process – an efficient method for the rapid synthesis of DDR zeolite membranes. RSC Advances 4, 19043–19052.

Bowen, T.C., Noble, R.D., and Falconer, J.L. (2004). Fundamentals and applications of pervaporation through zeolite membranes. J. Membr. Sci. 245, 1–33.

BP Statistical Review of World Energy 2017.

BP p.l.c., BP Energy Outlook, London, United Kingdom, 2019.

Brunetti, A., Scura, F., Barbieri, G., and Drioli, E. (2010). Membrane technologies for CO_2 separation. J. Membr. Sci. 359, 115–125.

Bryan, N., Lasseuguette, E., van Dalen, M., Permogorov, N., Amieiro, A., Brandani, S., and Ferrari, M.-C. (2014). Development of mixed matrix membranes containing zeolites for post-combustion carbon capture. Energy Procedia 63, 160–166.

Budinis, S., Krevor, S., Dowell, N.M., Brandon, N., and Hawkes, A. (2018). An assessment of CCS costs, barriers and potential. Energy Strategy Reviews 22, 61–81.

Buhl, J.-C., Schuster, K., and Robben, L. (2011). Nanocrystalline sodalite grown from superalkaline NaCl bearing gels at low temperature (333K) and the influence of TEA on crystallization process. Microporous and Mesoporous Materials 142, 666–671.

Busca, G. (2017). Acidity and basicity of zeolites: A fundamental approach. Microporous and Mesoporous Materials 254, 3–16.

Caro, J., Noack, M., Kölsch, P., and Schäfer, R. (2000). Zeolite membranes – state of their development and perspective. Microporous and Mesoporous Materials 38, 3–24.

Camus, O., Perera, S., Crittenden, B., Delft, Y.C. van, Meyer, D.F., Pex, P.P.A.C., Kumakiri, I., Miachon, S., Dalmon, J.-A., Tennison, S., et al. (2006). Ceramic membranes for ammonia recovery. AIChE Journal 52, 2055–2065.

Čejka, J. (2007) Introduction to Zeolite Science and Practice; Elsevier Science & Technology Books: Amsterdam

Ciavarella, P., Casanave, D., Moueddeb, H., Miachon, S., Fiaty, K., and Dalmon, J.-A. (2001). Isobutane dehydrogenation in a membrane reactor: Influence of the operating conditions on the performance. Catalysis Today 67, 177–184.

Ciferno J, Litynski J, Brickett L, Murphy J, Munson R, Zaremsky C, Marano J, Strock J

(2011) DOE/NETL advanced carbon dioxide capture R&D program: technology update. National Energy Technology Laboratory, USA, 516 pp (May 2011) Available from: http://www.netl.doe.gov/technologies/coalpower/ewr/pubs/CO2Handbook/

Clippel, F. de, Khan, A.L., Cano-Odena, A., Dusselier, M., Vanherck, K., Peng, L., Oswald, S., Giebeler, L., Corthals, S., Kenens, B., et al. (2012). CO_2 reverse selective mixed matrix membranes for H_2 purification by incorporation of carbon–silica fillers. J. Mater. Chem. A 1, 945–953.

Colella, C., and Wise, W.S. (2014). The IZA Handbook of Natural Zeolites: A tool of knowledge on the most important family of porous minerals. Microporous and Mesoporous Materials 189, 4–10.

Coronas, J., and Santamaría, J. (1999). Separations Using Zeolite Membranes. Separation and Purification Methods 28, 127–177.

Coronas, J., Falconer, J.L., and Noble, R.D. (1997). Characterization and permeation properties of ZSM-5 tubular membranes. AIChE Journal 43, 1797–1812.

Cuéllar-Franca, R.M., and Azapagic, A. (2015). Carbon capture, storage and utilisation technologies: A critical analysis and comparison of their life cycle environmental impacts. Journal of CO_2 Utilization 9, 82–102.

Cundy, C.S., and Cox, P.A. (2003). The hydrothermal synthesis of zeolites: History and development from the earliest days to the present time. Chem. Rev. 103, 663–702.

Cundy, C.S., and Cox, P.A. (2005). The hydrothermal synthesis of zeolites: Precursors, intermediates and reaction mechanism. Microporous and Mesoporous Materials 82, 1–78.

Czyperek, M., Zapp, P., Bouwmeester, H.J.M., Modigell, M., Ebert, K., Voigt, I., Meulenberg, W.A., Singheiser, L., and Stöver, D. (2010). Gas separation membranes for zero-emission fossil power plants: MEM-BRAIN. Journal of Membrane Science 359, 149–159.

D'Alessandro, D.M., Smit, B., and Long, J.R. (2010). Carbon dioxide capture: Prospects for new materials. Angewandte Chemie International Edition 49, 6058–6082.

Danaei Kenarsari, S., Yang, D., Jiang, G., Zhang, S., Wang, J., G. Russell, A., Wei, Q., and Fan, M. (2013). Review of recent advances in carbon dioxide separation and capture. RSC Advances 3, 22739–22773.

Daramola, M.O., Burger, A.J., Pera-Titus, M., Giroir-Fendler, A., Miachon, S., Lorenzen, L., and Dalmon, J.-A. (2009). Nanocomposite MFI–ceramic hollow fibre membranes via pore-plugging synthesis: Prospects for xylene isomer separation. Journal of Membrane Science 337, 106–112.

Daramola, M.O., Burger, A.J., Giroir-Fendler, A., Miachon, S., and Lorenzen, L. (2010a). Extractor-type catalytic membrane reactor with nanocomposite MFI-alumina membrane tube as separation unit: Prospect for ultra-pure para-Xylene production from m-Xylene isomerization over Pt-HZSM-5 catalyst. Applied Catalysis A: General 386, 109–115.

Daramola, M.O., Deng, Z., Pera-Titus, M., Giroir-Fendler, A., Miachon, S., Burger, A.J., Lorenzen, L., and Guo, Y. (2010b). Nanocomposite MFI–alumina membranes prepared via pore-pugging synthesis: Application as packed-bed membrane reactors for m-xylene isomerization over a Pt-HZSM-5 catalyst. Catalysis Today 156, 261–267.

Daramola, M.O., Aransiola, E.F., and Ojumu, T.V. (2012). Potential applications of zeolite membranes in reaction coupling separation processes. Materials 5, 2101–2136.

Daramola, M.O., Silinda, B., Masondo, S., and Oluwasina, O.O. (2015a). Polyethersulphone-sodalite (PES-SOD) mixed-matrix membranes: Prospects for acid mine drainage (AMD) treatment. Journal of the Southern African Institute of Mining and Metallurgy 115, 1221–1228.

Daramola, M.O., Dinat, A., and Hasrod, S. (2015b). Synthesis and Characterization of Nanocomposite Hydroxy-sodalite/ceramic membrane via pore-plugging hydrothermal synthesis technique. Journal of Membrane and Separation Technology 4, 1-7–7.

Daramola, M.O., Oloye, O., and Yaya, A. (2017). Nanocomposite sodalite/ceramic membrane for pre-combustion CO_2 capture: synthesis and morphological characterization. Int J Coal Sci Technol 4, 60–66.

Das, J.K., Das, N., and Bandyopadhyay, S. (2012). Highly selective SAPO 34 membrane on surface modified clay–alumina tubular support for H_2/CO_2 separation. International Journal of Hydrogen Energy 37, 10354–10364.

Das, R., Aich, S., and Naskar, M.K. (2017). One pot non-emulsion based hydrothermal synthesis of urchin-shaped hydroxy sodalite using waste coal fly ash. Indian Journal of Chemistry Section A-Inorganic Bio-Inorganic Physical Theoretical & Analytical Chemistry 56, 394–398.

Davidson, R. (2011). Pre-combustion capture of CO_2 in IGCC plants (2011) [Online]. Available: http://www.iea-coal.org.uk/documents/82847/8346/Pre-combustion-capture-of-CO_2-in-IGCC-plants-CCC/191. Last assessed 30th September (2019).

de Coninck, H., and Benson, S.M. (2014). Carbon dioxide capture and storage: Issues and prospects. Annual Review of Environment and Resources 39, 243–270.

Deichmann, U., Meisner, C., Murray, S., and Wheeler, D. (2011). The economics of renewable energy expansion in rural Sub-Saharan Africa. Energy Policy 39, 215–227.

Dinçer, F. (2011). The analysis on photovoltaic electricity generation status, potential and policies of the leading countries in solar energy. Renewable and Sustainable Energy Reviews 15, 713–720.

DOE/NETL Advanced Carbon Dioxide Capture R&D Program: Technology Update, September 2010.

Dong, J., Lin, Y.S., Hu, M.Z.-C., Peascoe, R.A., and Payzant, E.A. (2000). Template-removal-associated microstructural development of porous-ceramic-supported MFI zeolite membranes. Microporous and Mesoporous Materials 34, 241–253.

Dong, J., Lin, Y.S., Kanezashi, M., and Tang, Z. (2008). Microporous inorganic membranes for high temperature hydrogen purification. Journal of Applied Physics 104, 121301.

Dyk, L. van, Lorenzen, L., Miachon, S., and Dalmon, J.-A. (2005). Xylene isomerization in an extractor type catalytic membrane reactor. Catalysis Today 104, 274–280.

EIA (Energy Information Administration). International energy outlook 2016: with projections to 2040. Available from: http://wds.iea.org/wds/pdf/ele_documentation.pdf. Last assessed 5th January (2019).

EIA (Energy Information Administration) (April 2015). "South Africa" http://www.eia.gov/beta/international/analysis.cfm?iso=ZAF. Last assessed 9th November (2019).

Engelhardt G., Felsche J., Sieger P. The sodalite system $Na_{6+x}[SiAlO_4]_6(OH)_x \cdot nH_2O$ J. Am. Chem. Soc., 114 (1992), pp. 1173-1182.

Esaifan, M., Hourani, M., Khoury, H., Rahier, H., and Wastiels, J. (2017). Synthesis of hydroxysodalite zeolite by alkali-activation of basalt powder rich in calc-plagioclase. Advanced Powder Technology 28, 473–480.

Eskom, "Coal in South Africa," http://www.eskom.co.za/AboutElectricity/FactsFigures/Pages/Facts_Figures.aspx. Last assessed 23rd October (2019).

Fan, S., Liu, J., Zhang, F., Zhou, S., and Sun, F. (2013). Fabrication of zeolite MFI membranes supported by α-Al_2O_3 hollow ceramic fifibers for CO_2 separation. Journal of Materials Research 28, 1870–1876.

Fan, W., Morozumi, K., Kimura, R., Yokoi, T., and Okubo, T. (2008). Synthesis of nanometer-sized sodalite without adding organic additives. Langmuir 24, 6952–6958.

Farjoo, A., and Kuznicki, S.M. (2016). H_2 separation using tubular stainless steel supported natural clinoptilolite membranes. The Canadian Journal of Chemical Engineering 94, 2219–2224.

Fasolin, S., Romano, M., Boldrini, S., Ferrario, A., Fabrizio, M., Armelao, L., and Barison, S. (2019). Single-step process to produce alumina supported hydroxy-sodalite zeolite membranes. J Mater Sci 54, 2049–2058.

Favre, E. (2007). Carbon dioxide recovery from post-combustion processes: Can gas permeation membranes compete with absorption? Journal of Membrane Science 294, 50–59.

Favre, E. (2011). Membrane processes and post-combustion carbon dioxide capture: Challenges and prospects. Chemical Engineering Journal 171, 782–793.

Felsche, J., Luger, S., and Baerlocher, Ch. (1986). Crystal structures of the hydro-sodalite $Na_6[AlSiO_4]_6$ $8H_2O$ and of the anhydrous sodalite $Na_6[AlSiO_4]_6$. Zeolites 6, 367–372.

Feng, C., Khulbe, K.C., Matsuura, T., Farnood, R., and Ismail, A.F. (2015). Recent progress in zeolite/zeotype membranes. Journal of Membrane Science and Research 1, 49–72.

Figueroa, J.D., Fout, T., Plasynski, S., McIlvried, H., and Srivastava, R.D. (2008). Advances in CO_2 capture technology—The U.S. Department of Energy's Carbon Sequestration Program. International Journal of Greenhouse Gas Control 2, 9–20.

Franz, J., Maas, P., and Scherer, V. (2014). Economic evaluation of pre-combustion CO_2-capture in IGCC power plants by porous ceramic membranes. Applied Energy 130, 532–542.

Fu, C., and Gundersen, T. (2012). Carbon capture and storage in the power industry: challenges and opportunities. Energy Procedia 16, 1806–1812.

Gallucci, F., Fernandez, E., Corengia, P., and van Sint Annaland, M. (2013). Recent advances on membranes and membrane reactors for hydrogen production. Chemical Engineering Science 92, 40–66.

García, S., Gil, M.V., Martín, C.F., Pis, J.J., Rubiera, F., and Pevida, C. (2011). Breakthrough adsorption study of a commercial activated carbon for pre-combustion CO_2 capture. Chemical Engineering Journal 171, 549–556.

Gazzani, M., Turi, D.M., and Manzolini, G. (2014). Techno-economic assessment of hydrogen selective membranes for CO_2 capture in integrated gasification combined cycle. International Journal of Greenhouse Gas Control 20, 293–309.

Georgiev, D., Bogdanov, B., Angelova, K., Markovska, I., and Hristov, Y. (2009). Synthetic zeolites–Structure, classification, current trends in zeolite synthesis review. In Economics and Society Development on the Base of Knowledge: International Scientific Conference, Volume VII Technical studies.

Ghadimi, A., Amirilargani, M., Mohammadi, T., Kasiri, N., and Sadatnia, B. (2014). Preparation of alloyed poly (ether block amide)/poly (ethylene glycol diacrylate) membranes for separation of CO_2/H_2 (syngas application). Journal of Membrane Science 458, 14–26.

Gibbins, J., and Chalmers, H. (2008). Carbon capture and storage. Energy Policy 36, 4317–4322.

Gilron, J., and Soffer, A. (2002). Knudsen diffusion in microporous carbon membranes with molecular sieving character. Journal of Membrane Science 209, 339–352.

Giroir-Fendler, A., Peureux, J., Mozzanega, H., and Dalmon, J.-A. (1996). Characterization of a zeolite membrane for catalytic membrane reactor application. In Studies in Surface Science and Catalysis, J.W. Hightower, W. Nicholas Delgass, E. Iglesia, and A.T. Bell, eds. (Elsevier), pp. 127–136.

Gkanas, E.I., Steriotis, T.A., Stubos, A.K., Myler, P., and Makridis, S.S. (2015). A complete transport validated model on a zeolite membrane for carbon dioxide permeance and capture. Applied Thermal Engineering 74, 36–46.

Glazewski, J., Gilder, A. & Swanepoel, E. (2012). Carbon Capture and Storage (CCS): Towards a regulatory and legal regime in South Africa. Institute of Marine and Environmental Law (IMEL) and African Climate and Development Initiative (ACDI), University of Cape Town, Cape Town.

(GCI) Global CCS Institute (2009), Strategic Analysis of the Global Status of Carbon Capture and Storage Report 4: Existing Carbon Capture and Storage Research and Development Networks around the World Final Report, Canberra ACT 2601 Australia.

(GCI) Global CCS Institute (2012). CO_2 capture technologies: Technology option for CO_2 capture. Available from: http://www.flainox.com/blog/wp-content/uploads/2012/02/GCCSI-Tecnologie-di-cattura-0112.pdf. Last assessed 16th September (2019).

(GCI) Global CCS Institute, Fact sheet-capturing CO_2, 2015. Available at https://www.globalccsinstitute.com/wp-content/uploads/2018/12/Global-CCS-Institute-Fact-Sheet_Capturing-CO2.pdf. Last assessed 30th September (2019).

(GCI) Global CCS Institute, 2016. The Global Status of CCS: 2016.Summary Report, Global CCS Institute Australia. Available at https://www.globalccsinstitute.com/wp-content/uploads/2018/12/Global-Status-Report-2016_Summary.pdf. Last assessed 30th September (2019).

Go, Y., Lee, J.H., Shamsudin, I.K., Kim, J., and Othman, M.R. (2016). Microporous ZIF-7 membranes prepared by in-situ growth method for hydrogen separation. International Journal of Hydrogen Energy 41, 10366–10373.

Grahn, M., and Hedlund, J. (2014). Maxwell–Stefan modeling of high flux tubular silicalite-1 membranes for CO_2 removal from CO_2/H_2 gas mixtures. Journal of Membrane Science 471, 328–337.

Grashoff, G.J., Pilkington, C.E., and Corti, C.W. (1983). The purification of hydrogen.

Gu, X., Tang, Z., and Dong, J. (2008). On-stream modification of MFI zeolite membranes for enhancing hydrogen separation at high temperature. Microporous and Mesoporous Materials 111, 441–448.

Guan, G., Tanaka, T., Kusakabe, K., Sotowa, K.-I., and Morooka, S. (2003). Characterization of $AlPO_4$-type molecular sieving membranes formed on a porous α-alumina tube. Journal of Membrane Science 214, 191–198.

Guan, L., Wang, Z., and Lu, D. (2019). Evolution of zeolite crystals in self-supporting faujasite blocks: Effects of hydrothermal conditions. Materials 12, 1965.

Guillou, F., Rouleau, L., Pirngruber, G., and Valtchev, V. (2009). Synthesis of FAU-type zeolite membrane: An original in situ process focusing on the rheological control of gel-like precursor species. Microporous and Mesoporous Materials 119, 1–8.

Günther, C., Richter, H., Voigt, I., Michaelis, A., Tzscheutschler, H., Krause-Rehberg, R., and Serra, J.M. (2015). Synthesis and characterization of a sulfur containing hydroxy sodalite without sulfur radicals. Microporous and Mesoporous Materials 214, 1–7.

Hammond, G.P., and Spargo, J. (2014). The prospects for coal-fired power plants with carbon capture and storage: A UK perspective. Energy Conversion and Management 86, 476–489.

Hashemifard, S.A., Ismail, A.F., and Matsuura, T. (2010). Prediction of gas permeability in mixed matrix membranes using theoretical models. Journal of Membrane Science 347, 53–61.

He, X., and Hägg, M.-B. (2012). Membranes for Environmentally Friendly Energy Processes. Membranes 2, 706–726.

Herm, Z.R., Swisher, J.A., Smit, B., Krishna, R., and Long, J.R. (2011). Metal-Organic Frameworks as adsorbents for hydrogen purification and pre-combustion carbon dioxide capture. Journal of the American Chemical Society 133, 5664–5667.

Herzog, H.J. (2011). Scaling up carbon dioxide capture and storage: From megatons to gigatons. Energy Economics 33, 597–604.

Hong, M., Falconer, J.L., and Noble, R.D. (2005). Modification of zeolite membranes for H_2 separation by catalytic cracking of methyldiethoxysilane. Ind. Eng. Chem. Res. 44, 4035–4041.

Hosseinzadeh Hejazi, S.A., Avila, A.M., Kuznicki, T.M., Weizhu, A., and Kuznicki, S.M. (2011). Characterization of natural zeolite membranes for H_2/CO_2 separations by single gas permeation. Ind. Eng. Chem. Res. 50, 12717–12726.

Huang, A., Liang, F., Steinbach, F., Gesing, T.M., and Caro, J. (2010a). Neutral and cation-free LTA-type aluminophosphates ($ALPO_4$) molecular sieve membrane with high hydrogen permselectivity. Journal of the American Chemical Society 132, 2140–2141.

Huang, A., Bux, H., Steinbach, F., and Caro, J. (2010b). Molecular-sieve membrane with hydrogen permselectivity: ZIF-22 in LTA topology prepared with 3-aminopropyltriethoxysilane as covalent linker. Angewandte Chemie International Edition 49, 4958–4961.

Huang, A., Liang, F., Steinbach, F., and Caro, J. (2010c). Preparation and separation properties of LTA membranes by using 3-aminopropyltriethoxysilane as covalent linker. Journal of Membrane Science 350, 5–9.

Huang, A., Chen, Y., Wang, N., Hu, Z., Jiang, J., and Caro, J. (2012). A highly permeable and selective zeolitic imidazolate framework ZIF-95 membrane for H_2/CO_2 separation. Chemical Communications 48, 10981.

Huisingh, D., Zhang, Z., Moore, J.C., Qiao, Q., and Li, Q. (2015). Recent advances in carbon emissions reduction: policies, technologies, monitoring, assessment and modeling. Journal of Cleaner Production 103, 1–12.

Hunt, A.J., Sin, E.H.K., Marriott, R., and Clark, J.H. (2010). Generation, capture, and utilization of industrial carbon dioxide. ChemSusChem 3, 306–322.

Hussain, A., Arif, S.M., and Aslam, M. (2017). Emerging renewable and sustainable energy technologies: State of the art. Renewable and Sustainable Energy Reviews 71, 12–28.

IEA (International Energy Agency) (2011), World Energy Outlook 2011, OECD Publishing, Paris, https://doi.org/10.1787/weo-2011-en. Last assessed 4th August (2019).

IEA (International Energy Agency) (2013a), World Energy Outlook 2013. Available from doi: https://doi.org/10.1787/weo-2013-en. Last assessed 30th September (2019).

IEA (International Energy Agency) (2013b). Technology Roadmap: Carbon Capture and Storage, OECD/IEA, Paris. Available from

https://www.iea.org/publications/freepublications/publication/TechnologyRoadmapCarbonCaptureandStorage.pdf. Last assessed 16th September (2019).

IEA (International Energy Agency) (2015). CO_2 emissions from fuel combustion: Highlights, OECD/IEA, Paris.

IEA (International Energy Agency) (2016). 20 years of carbon capture and storage: Accelerating future development, OECD/IEA, Paris. Available online at www.iea.org/t&c/. Last assessed 16th September (2019).

IEA (International Energy Agency) (2017), World Energy Outlook 2017. Available from https://webstore.iea.org/world-energy-outlook-2017. Last assessed 31st October (2019).

IEA (International Energy Agency) (2018). CO_2 Emissions from Fuel Combustion 2018 Overview.

IEA (International Energy Agency) (2019). Executive Summary of Coal 2018 - Analysis and Forecasts to 2O23 - Market Report © OECD/IEA. Available online at https://webstore.iea.org/market-report-series-coal-2018. Last assessed 1st November (2019).

IEAGHG (2014). CO_2 Capture at Coal Based Power and Hydrogen Plants, 2014/3, June 2014. Available online at https://ieaghg.org/docs/General_Docs/Reports/2014-03.pdf. Last assessed 30th September (2019).

IEAGHG (2018). Greenhouse gas emissions accounting for carbon dioxide capture and utilization (SSU) technologies-characterizing CCU technologies, policy support, regulation and emissions accounting. 2018-TR01, Cheltenham, Gloucestershire, UK, UKIEA Greenhouse Gas R&D Programme, 72 pp (Mar 2018).

IEO (International Energy Outlook) (2016). U.S. Energy Information Administration. Available online at www.eia.gov/forecasts/ieo/pdf/0484(2016).pdf. Last assessed 30th September (2019).

International Zeolite Association, (IZA). http://www.iza-structure.org/databases/. Last assessed 4th August (2019).

IPCC, (2005): Metz, B., O. Davidson, H. C. de Coninck, M. Loos, and L. A. Meyer (eds.). IPCC special report on carbon dioxide capture and storage. prepared by working group III of the Intergovernmental Panel on Climate Change. Cambridge University Press, Cambridge, United Kingdom and New York, NY, USA, 442 pp.

IPCC (2014): R.K. Pachauri and L.A. Meyer (eds.): Climate Change 2014: Synthesis Report Contribution of Working Groups I, II and III to the Fifth Assessment Report of the Intergovernmental Panel on Climate Change. IPCC, Geneva, Switzerland, 151 pp.

IPCC (2018): [Masson-Delmotte, V., P. Zhai, H.-O. Pörtner, D. Roberts, J. Skea, P.R. Shukla, A. Pirani, W. Moufouma-Okia, C. Péan, R. Pidcock, S. Connors, J.B.R. Matthews, Y. Chen, X. Zhou, M.I. Gomis, E. Lonnoy, T. Maycock, M. Tignor, and T. Waterfield (eds.)]. Global Warming of 1.5°C. An IPCC Special Report on the impacts of global warming of 1.5°C above pre-industrial levels and related global greenhouse gas emission pathways, in the context of strengthening the global response to the threat of climate change, sustainable development, and efforts to eradicate poverty

Ilić, B., and Wettstein, S.G. (2017). A review of adsorbate and temperature-induced zeolite framework flexibility. Microporous and Mesoporous Materials 239, 221–234.

Jansen, D., Gazzani, M., Manzolini, G., Dijk, E. van, and Carbo, M. (2015). Pre-combustion CO_2 capture. International Journal of Greenhouse Gas Control 40, 167–187.

Jareman, F., Hedlund, J., Creaser, D., and Sterte, J. (2004). Modelling of single gas permeation in real MFI membranes. Journal of Membrane Science 236, 81–89.

Jiang, G., Huang, Q., Kenarsari, S.D., Hu, X., Russell, A.G., Fan, M., and Shen, X. (2015). A new mesoporous amine-TiO_2 based pre-combustion CO_2 capture technology. Applied Energy 147, 214–223.

Julbe, A., Motuzas, J., Cazevielle, F., Volle, G., and Guizard, C. (2003). Synthesis of sodalite/αAl_2O_3 composite membranes by microwave heating. Separation and Purification Technology 32, 139–149.

Kalantari, N., Vaezi, M.J., Yadollahi, M., Babaluo, A.A., Bayati, B., and Kazemzadeh, A. (2015). Synthesis of nanostructure hydroxy sodalite composite membranes via hydrothermal method: support surface modification and synthesis method effects. Asia-Pacific Journal of Chemical Engineering 10, 45–55.

Kanezashi, M., and Lin, Y.S. (2009). Gas permeation and diffusion characteristics of MFI-type zeolite membranes at high temperatures.

Kanezashi, M., O'Brien-Abraham, J., Lin, Y.S., and Suzuki, K. (2008). Gas permeation through DDR-type zeolite membranes at high temperatures. AIChE Journal 54, 1478–1486.

Kanniche, M., Gros-Bonnivard, R., Jaud, P., Valle-Marcos, J., Amann, J.-M., and Bouallou, C. (2010). Pre-combustion, post-combustion and oxy-combustion in thermal power plant for CO_2 capture. Applied Thermal Engineering 30, 53–62.

Kapteijn, F., Moulijn, J.A., and Krishna, R. (2000). The generalized Maxwell–Stefan model for diffusion in zeolites: sorbate molecules with different saturation loadings. Chemical Engineering Science 55, 2923–2930.

Karimi, S., Korelskiy, D., Yu, L., Mouzon, J., Ali Khodadadi, A., Mortazavi, Y., Esmaeili, M., and Hedlund, J. (2015). A simple method for blocking defects in zeolite membranes. Journal of Membrane Science 489, 270–274.

Kayvani Fard, A., McKay, G., Buekenhoudt, A., Al Sulaiti, H., Motmans, F., Khraisheh, M., and Atieh, M. (2018). Inorganic membranes: Preparation and Application for water treatment and desalination. Materials (Basel) 11.

Kazemimoghadam, M., and Rigi, Z.A. (2018). Evaluation and synthesis of nano-pore hydroxysodalite (HS) zeolite membranes: Application to pervaporation of ethanol/water mixture. Journal of Water and Environmental Nanotechnology 3, 173–190.

Kenarsari, S.D., Yang, D., Jiang, G., Zhang, S., Wang, J., Russell, A.G., Wei, Q., and Fan, M. (2013). Review of recent advances in carbon dioxide separation and capture. RSC Adv. 3, 22739–22773.

Khajavi, S., Jansen, J.C., and Kapteijn, F. (2007a). Preparation and performance of H-SOD membranes: a new synthesis procedure and absolute water separation. In Studies in Surface Science and Catalysis, R. Xu, Z. Gao, J. Chen, and W. Yan, eds. (Elsevier), pp. 1028–1035.

Khajavi, S., Kapteijn, F., and Jansen, J.C. (2007b). Synthesis of thin defect-free hydroxy sodalite membranes: New candidate for activated water permeation. Journal of Membrane Science 299, 63–72.

Khajavi, S., Sartipi, S., Gascon, J., Jansen, J.C., and Kapteijn, F. (2010a). Thermostability of hydroxy sodalite in view of membrane applications. Microporous and Mesoporous Materials 132, 510–517.

Khajavi, S., Jansen, J.C., and Kapteijn, F. (2010b). Production of ultra-pure water by desalination of seawater using a hydroxy sodalite membrane. Journal of Membrane Science 356, 52–57.

Khalilpour, R., Mumford, K., Zhai, H., Abbas, A., Stevens, G., and Rubin, E.S. (2015). Membrane-based carbon capture from flue gas: a review. Journal of Cleaner Production 103, 286–300.

Kita, H., Horii, K., Ohtoshi, Y., Tanaka, K., and Okamoto, K.-I. (1995). Synthesis of a zeolite NaA membrane for pervaporation of water/organic liquid mixtures. J Mater Sci Lett 14, 206–208.

Kondo, M., Komori, M., Kita, H., and Okamoto, K. (1997). Tubular-type pervaporation module with zeolite NaA membrane. Journal of Membrane Science 133, 133–141.

Korelskiy, D., Grahn, M., Mouzon, J., and Hedlund, J. (2012). Characterization of flow-through micropores in MFI membranes by permporometry. Journal of Membrane Science 417–418, 183–192.

Koros, W.J. (2004). Evolving beyond the thermal age of separation processes: Membranes can lead the way. AIChE J. 50, 2326–2334.

Kosinov, N., Auffret, C., Gücüyener, C., M. Szyja, B., Gascon, J., Kapteijn, F., and M. Hensen, E.J. (2014). High flux high-silica SSZ-13 membrane for CO_2 separation. Journal of Materials Chemistry A 2, 13083–13092.

Kosinov, N., Gascon, J., Kapteijn, F., and Hensen, E.J.M. (2016). Recent developments in zeolite membranes for gas separation. Journal of Membrane Science 499, 65–79.

Koutsonikolas D., Kaldis S.P., Pantoleontos G.T., Zaspalis V.T., and Sakellaropoulos G.P. (2013). Techno-economic assessment of polymeric, ceramic and metallic membranes integration in an advanced IGCC process for H_2 production and CO_2 capture. Chemical Engineering Transactions 35, 715–720.

Ku, A.Y., Kulkarni, P., Shisler, R., and Wei, W. (2011). Membrane performance requirements for carbon dioxide capture using hydrogen-selective membranes in integrated gasification combined cycle (IGCC) power plants. Journal of Membrane Science 367, 233–239.

Kumakiri, I., Stange, M., Peters, T.A., Klette, H., Kita, H., and Bredesen, R. (2008). Membrane characterisation by a novel defect detection technique. Microporous and Mesoporous Materials 115, 33–39.

Kundu, D., Dey, B., Naskar, M.K., and Chatterjee, M. (2010). Emulsion-derived urchin-shaped hydroxy sodalite particles. Materials Letters 64, 1630–1633.

Lafleur, M., Bougie, F., Guilhaume, N., Larachi, F., Fongarland, P., and Iliuta, M.C. (2017). Development of a water-selective zeolite composite membrane by a new pore-plugging technique. Microporous and Mesoporous Materials 237, 49–59.

Lee, S.-R., Son, Y.-H., Julbe, A., and Choy, J.-H. (2006). Vacuum seeding and secondary growth route to sodalite membrane. Thin Solid Films 495, 92–96.

Li, G., Su, X., and Lin, R. (2007). Preparation of highly water-selective mordenite membranes via post-synthetic treatment with oxalic acid. Materials Letters 61, 4576–4578.

Li, H., Fam, W., Satrisna, P., Hou, J., and Chen, V. (2019). New generation high performance composite hollow fiber membranes for low cost CO_2 capture (Rochester, NY: Social Science Research Network).

Li, H., Wang, J., Xu, J., Meng, X., Xu, B., Yang, J., Li, S., Lu, J., Zhang, Y., He, X., et al. (2013). Synthesis of zeolite NaA membranes with high performance and high reproducibility on coarse macroporous supports. Journal of Membrane Science 444, 513–522.

Li, H., Haas-Santo, K., Schygulla, U., and Dittmeyer, R. (2015). Inorganic microporous membranes for H_2 and CO_2 separation—Review of experimental and modeling progress. Chemical Engineering Science 127, 401–417.

Li, Y., Pera-Titus, M., Xiong, G., Yang, W., Landrivon, E., Miachon, S., Dalmon, J.-A. (2008). Nanocomposite MFI-alumina membranes via pore-plugging synthesis: Genesis of the zeolite material. Journal of Membrane Science 325, 973–981.

Li, Y., Liang, F., Bux, H., Yang, W., and Caro, J. (2010). Zeolitic imidazolate framework ZIF-7 based molecular sieve membrane for hydrogen separation. Journal of Membrane Science 354, 48–54.

Lin, Y., and Duke, M.C. (2013). Recent progress in polycrystalline zeolite membrane research. Current Opinion in Chemical Engineering 2, 209–216.

Lin, H., He, Z., Sun, Z., Kniep, J., Ng, A., Baker, R.W., and Merkel, T.C. (2015). CO_2-selective membranes for hydrogen production and CO_2 capture – Part II: Techno-economic analysis. Journal of Membrane Science 493, 794–806.

Lin, Y.S., Kumakiri, I., Nair, B.N., and Alsyouri, H. (2002). Microporous inorganic membranes. Separation and Purification Methods 31, 229–379.

Lindmark, J., and Hedlund, J. (2010). Carbon dioxide removal from synthesis gas using MFI membranes. Journal of Membrane Science 360, 284–291.

Liu, B., Sun, H., Peng, T., and He, Q. (2018). One-Step Synthesis of hydroxy sodalite using natural bentonite at moderate temperatures. Minerals 8, 521.

Liu, Y., Yang, Z., Yu, C., Gu, X., and Xu, N. (2011). Effect of seeding methods on growth of NaA zeolite membranes. Microporous and Mesoporous Materials 143, 348–356.

Lockwood, T. (2014) IEA Clean Coal Centre – Developments in oxyfuel combustion of coal. IEA Clean Coal Centre Park House 14 Northfields, London SW18 1DD, United Kingdom, (August 2014).

Lockwood, T. (2016) IEA Clean Coal Centre – Next-generation carbon capture technologies for coal IEA Clean Coal Centre Park House 14 Northfields, London SW18 1DD, United Kingdom, (May 2016).

Luis, P., Van Gerven, T., and Van der Bruggen, B. (2012). Recent developments in membrane-based technologies for CO_2 capture. Progress in Energy and Combustion Science 38, 419–448.

Maghsoudi, H. (2016). Defects of zeolite membranes: Characterization, modification and post-treatment techniques. Separation & Purification Reviews 45, 169–192.

Martínez Galeano, Y., Cornaglia, L., and Tarditi, A.M. (2016). NaA zeolite membranes synthesized on top of APTES-modified porous stainless-steel substrates. Journal of Membrane Science 512, 93–103.

Masuda, T., Hara, H., Kouno, M., Kinoshita, H., and Hashimoto, K. (1995). Preparation of an A-type zeolite film on the surface of an alumina ceramic filter. Microporous Materials 3, 565–571.

McDonald, D.K., and Rogers, K.J. (2014). Segregated in-situ forced oxidation wet flue gas desulfurization for oxygen-fired fossil fuel combustion.

Mei, W., Du, Y., Wu, T., Gao, F., Wang, B., Duan, J., Zhou, J., and Zhou, R. (2018). High-flux CHA zeolite membranes for H2 separations. Journal of Membrane Science 565, 358–369.

Merkel, T.C., Lin, H., Wei, X., and Baker, R. (2010). Power plant post-combustion carbon dioxide capture: An opportunity for membranes. Journal of Membrane Science 359, 126–139.

Merkel, T.C., Zhou, M., and Baker, R.W. (2012). Carbon dioxide capture with membranes at an IGCC power plant. Journal of Membrane Science 389, 441–450.

Meulenberg, W.A. (2017). Ceramic ion-conducting membranes for a sustainable European energy system.

Miachon, S., Landrivon, E., Aouine, M., Sun, Y., Kumakiri, I., Li, Y., Prokopová, O.P., Guilhaume, N., Giroir-Fendler, A., Mozzanega, H., et al. (2006). Nanocomposite MFI-alumina membranes via pore-plugging synthesis: Preparation and morphological characterisation. Journal of Membrane Science 281, 228–238.

Miachon, S., Ciavarella, P., van Dyk, L., Kumakiri, I., Fiaty, K., Schuurman, Y., and Dalmon, J.-A. (2007). Nanocomposite MFI-alumina membranes via pore-plugging synthesis: Specific transport and separation properties. Journal of Membrane Science 298, 71–79.

Ming Leung, K., P. Edwards, P., Jones, E., and Sartbaeva, A. (2015). Microwave synthesis of LTN framework zeolite with no organic structure directing agents. RSC Advances 5, 35580–35585.

Mohammadi, T., and Maghsoodloorad, H. (2013). Synthesis and characterization of ceramic membranes (W-type zeolite membranes). International Journal of Applied Ceramic Technology 10, 365–375.

Mondal, M.K., Balsora, H.K., and Varshney, P. (2012). Progress and trends in CO_2 capture/separation technologies: A review. Energy 46, 431–441.

Musselman, I., Kenneth Balkus, J., and Ferraris, J. (2009). Mixed-Matric Membranes for CO_2 and H_2 gas separations using metal-organic framework and mesoporus hybrid silicas (University of Texas at Dallas).

Musyoka, N.M., Petrik, L.F., Balfour, G., Gitari, W.M., Hums, E., (2011). Synthesis of hydroxy sodalite from coal fly ash using waste industrial brine solution. Journal of Environmental Science and Health, Part A 46, 1699–1707.

Nabavi, M.S., Mohammadi, T., and Kazemimoghadam, M. (2014). Hydrothermal synthesis of hydroxy sodalite zeolite membrane: Separation of H_2/CH_4. Ceramics International 40, 5889–5896.

Naskar, M.K., Kundu, D., and Chatterjee, M. (2011a). Coral-like hydroxy sodalite particles from rice husk ash as silica source. Materials Letters 65, 3408–3410.

Naskar, M.K., Kundu, D., and Chatterjee, M. (2011b). An aqueous-based synthesis of flower-like hydroxy sodalite particles in the presence of cetyltrimethylammonium bromide. Journal of the American Ceramic Society 94, 1643–1646.

Naskar, M.K., Kundu, D., and Chatterjee, M. (2011c). Effect of process parameters on surfactant-based synthesis of hydroxy sodalite particles. Materials Letters 65, 436–438.

National energy technology laboratory. https://www.netl.doe.gov/coal/carbon-utilization/about. Last assessed 7th November (2019).

Nikolić, D.D., and Kikkinides, E.S. (2015). Modelling and optimization of hybrid PSA/membrane separation processes. Adsorption 21, 283–305.

Ockwig, N.W., and Nenoff, T.M. (2007). Membranes for Hydrogen Separation. Chem. Rev. 107, 4078–4110.

Olajire, A.A. (2010). CO_2 capture and separation technologies for end-of-pipe applications – A review. Energy 35, 2610–2628.

Oloye, O., Eterigho-Ikelegbe, O., and Daramola, M.O. (2019). Synthesis and evaluation of a nanocomposite hydroxy sodalite/ceramic (HS/ceramic) membrane for pre-combustion CO_2 capture: characterization and permeation test during CO_2/H_2 separation. Materials Science for Energy Technologies.

Pan, L., Liu, W., Chen, W., Yan, K., Yang, H., and Yu, J. (2016). Crystal structure and band gap studies of sodalite: experimental and calculated results. Journal of Molecular Structure 1106, 59–63.

Pandey, P., and Chauhan, R.S. (2001). Membranes for gas separation. Progress in Polymer Science 26, 853–893.

Park, H.B., Kamcev, J., Robeson, L.M., Elimelech, M., and Freeman, B.D. (2017). Maximizing the right stuff: The trade-off between membrane permeability and selectivity. Science 356.

Perez Pugatch, M. (2011). The Role of Intellectual Property Rights in the Transfer of Environmentally Sound Technologies. Global Challenges Report. Available from https://www.wipo.int/edocs/pubdocs/en/wipo_pub_gc_4.pdf. Last assessed 30th September (2019).

Petrov, I., and Michalev, T. (2012). Synthesis of zeolite A: A Review. 6.

Phan, A., Doonan, C.J., Uribe-Romo, F.J., Knobler, C.B., O'Keeffe, M., and Yaghi, O.M. (2010). Synthesis, structure, and carbon dioxide capture properties of zeolitic imidazolate frameworks. Acc. Chem. Res. 43, 58–67.

Popp, J., Lakner, Z., Harangi-Rákos, M., and Fári, M. (2014). The effect of bioenergy expansion: Food, energy, and environment. Renewable and Sustainable Energy Reviews 32, 559–578.

Porter, R.T.J., Fairweather, M., Pourkashanian, M., and Woolley, R.M. (2015). The range and level of impurities in CO_2 streams from different carbon capture sources. International Journal of Greenhouse Gas Control 36, 161–174.

Poshusta, J.C., Tuan, V.A., Falconer, J.L., and Noble, R.D. (1998). Synthesis and permeation properties of SAPO-34 tubular membranes. Ind. Eng. Chem. Res. 37, 3924–3929.

Pourali, S.M., and Samadi-Maybodi, A. (2015). Role of gel aging in template-free synthesis of micro and nano- crystalline sodalites. Chemistry of Solid Materials 2, 21–31.

Praetorius, B., and Schumacher, K. (2009). Greenhouse gas mitigation in a carbon constrained world: The role of carbon capture and storage. Energy Policy 37, 5081–5093.

Qi, H. (2011). Preparation of composite microporous silica membranes using TEOS and 1, 2-Bis(triethoxysilyl)ethane as precursors for gas separation. Chinese Journal of Chemical Engineering 19, 404–409.

Qian Zhu. (2018). Developments in CO_2 utilization technologies. IEA Clean Coal Centre-London, United Kingdom Available from https://www.iea-coal.org/the-latest-state-of-development-on-ccu-draft/. Last assessed 30th September (2019).

Rahman, F.A., Aziz, M.M.A., Saidur, R., Bakar, W.A.W.A., Hainin, M.R., Putrajaya, R., and Hassan, N.A. (2017). Pollution to solution: Capture and sequestration of carbon dioxide (CO_2) and its utilization as a renewable energy source for a sustainable future. Renewable and Sustainable Energy Reviews 71, 112–126.

Reyes, C.A.R., Williams, C., and Alarcón, O.M.C. (2013). Nucleation and growth process of sodalite and cancrinite from kaolinite-rich clay under low-temperature hydrothermal conditions. Materials Research 16, 424–438.

Rising global temperature and CO_2 (source: https://www.climatecentral.org/gallery/graphics/co2-and-rising-global-temperatures.

Robeson, L.M. (2008). The upper bound revisited. Journal of Membrane Science 320, 390–400.

Rossi, F., Nicolini, A., Palombo, M., Castellani, B., Morini, E., Filipponi, M., Rossi, F., Nicolini, A., Palombo, M., Castellani, B., et al. (2014). An innovative configuration for CO_2 capture by high temperature fuel cells. Sustainability 6, 6687–6695.

Roy, P., and Das, N. (2019). Synthesis of NaX zeolite-graphite amine fiber composite membrane: Role of graphite amine in membrane formation for H_2/CO_2 separation. Applied Surface Science 480, 934–944.

Rubin, E.S., Mantripragada, H., Marks, A., Versteeg, P., and Kitchin, J. (2012). The outlook for improved carbon capture technology. Progress in Energy and Combustion Science 38, 630–671.

Ruthven, D.M., DeSisto, W.J., and Higgins, S. (2009). Diffusion in a mesoporous silica membrane: Validity of the Knudsen diffusion model. Chemical Engineering Science 64, 3201–3203.

Sarfraz, M., and Ba-Shammakh, M. (2016). A novel zeolitic imidazolate framework based mixed-matrix membrane for efficient CO_2 separation under wet conditions. Journal of the Taiwan Institute of Chemical Engineers 65, 427–436.

Saidur, R., Abdelaziz, E.A., Demirbas, A., Hossain, M.S., and Mekhilef, S. (2011). A review on biomass as a fuel for boilers. Renewable and Sustainable Energy Reviews 15, 2262–2289.

Salim, W., Han, Y., Vakharia, V., Wu, D., Wheeler, D.J., and Ho, W.S.W. (2019). Scale-up of amine-containing membranes for hydrogen purification for fuel cells. Journal of Membrane Science 573, 465–475.

Sánchez-Laínez, J., Zornoza, B., Friebe, S., Caro, J., Cao, S., Sabetghadam, A., Seoane, B., Gascon, J., Kapteijn, F., Le Guillouzer, C., et al. (2016). Influence of ZIF-8 particle size in the performance of polybenzimidazole mixed matrix membranes for pre-combustion CO_2 capture and its validation through interlaboratory test. Journal of Membrane Science 515, 45–53.

Sanders, D.F., Smith, Z.P., Guo, R., Robeson, L.M., McGrath, J.E., Paul, D.R., and Freeman, B.D. (2013). Energy-efficient polymeric gas separation membranes for a sustainable future: A review. Polymer 54, 4729–4761.

Sathre, R., Chester, M., Cain, J., and Masanet, E. (2012). A framework for environmental assessment of CO_2 capture and storage systems. Energy 37, 540–548.

Scholes, C.A., Smith, K.H., Kentish, S.E., and Stevens, G.W. (2010). CO_2 capture from pre-combustion processes—Strategies for membrane gas separation. International Journal of Greenhouse Gas Control 4, 739–755.

Schwartz, J., Porter, J., Patki, N., Kelley, M., Stanislowski, J., Tolbert, S., Way, J.D., and Makuch, D. (2015). Advanced Hydrogen Transport Membrane for Coal Gasification (Praxair, Inc., Tonawanda, NY (United States)).

Sebastián, V., Kumakiri, I., Bredesen, R., and Menéndez, M. (2007). Zeolite membrane for CO_2 removal: Operating at high pressure. Journal of Membrane Science 292, 92–97.

Shafie, A.H., An, W., Hosseinzadeh Hejazi, S.A., Sawada, J.A., and Kuznicki, S.M. (2012). Natural zeolite-based cement composite membranes for H_2/CO_2 separation. Separation and Purification Technology 88, 24–28.

Shan, L., Shao, J., Wang, Z., and Yan, Y. (2011). Preparation of zeolite MFI membranes on alumina hollow fibers with high flux for pervaporation. Journal of Membrane Science 378, 319–329.

Shao, L., Low, B.T., Chung, T.-S., and Greenberg, A.R. (2009). Polymeric membranes for the hydrogen economy: Contemporary approaches and prospects for the future. Journal of Membrane Science 327, 18–31.

Shekhawat, D., Luebke, D.R., and Pennline, H.W. (2003). A review of carbon dioxide selective membranes: A Topical Report (National Energy Technology Laboratory (NETL), Pittsburgh, PA, Morgantown, WV, and Albany, OR (United States)).

Shoko, E., McLellan, B., Dicks, A.L., and da Costa, J.C.D. (2006). Hydrogen from coal: Production and utilisation technologies. International Journal of Coal Geology 65, 213–222.

Shrestha, S., and Dutta, P.K. (2019). Modification of a continuous zeolite membrane grown within porous polyethersulfone with Ag(I) cations for enhanced propylene/propane gas separation. Microporous and Mesoporous Materials 279, 178–185.

Simon, A., Richter, H., Reif, B., Schuelein, M., Sanwald, D., and Schwieger, W. (2019). Evaluation of a method for micro-defect sealing in ZSM-5 zeolite membranes by chemical vapor deposition of carbon. Separation and Purification Technology 219, 180–185.

Smart, S., C. Lin, C.X., Ding, L., Thambimuthu, K., and Costa, J.C.D. da (2010). Ceramic membranes for gas processing in coal gasification. Energy & Environmental Science 3, 268–278.

Smart, S., Beltramini, J., Diniz da Costa, J.C., Katikaneni, S.P., and Pham, T. (2013). 9 - Microporous silica membranes: fundamentals and applications in membrane reactors for hydrogen separation. In Handbook of Membrane Reactors, A. Basile, ed. (Woodhead Publishing), pp. 337–369.

Sreenivasulu, B., Gayatri, D.V., Sreedhar, I., and Raghavan, K.V. (2015). A journey into the process and engineering aspects of carbon capture technologies. Renewable and Sustainable Energy Reviews 41, 1324–1350.

Sumida, K., Rogow, D.L., Mason, J.A., McDonald, T.M., Bloch, E.D., Herm, Z.R., Bae, T.-H., and Long, J.R. (2012). Carbon dioxide capture in metal–organic frameworks. Chem. Rev. 112, 724–781.

Sutrisna, P.D., Hou, J., Li, H., Zhang, Y., and Chen, V. (2017). Improved operational stability of Pebax-based gas separation membranes with ZIF-8: A comparative study of flat sheet and composite hollow fiber membranes. Journal of Membrane Science 524, 266–279.

Tobia, K.J.A.H. (2007). Monolith hydroxysodalite from low grade kaolin and its application as an adsorbent for lead. Iraqi National Journal of Earth Science 7, 19–30.

Treacy, M.M.J., and Higgins, J.B. (2007). Collection of simulated XRD powder patterns for zeolites Fifth (5th) Revised Edition (Elsevier).

Tsapatsis, M., and Gavalas, G.R. (1999). Synthesis of porous inorganic membranes. MRS Bulletin 24, 30–35.

Vaezi, M., and Babaluo, A.A. (2014). Effect of dehydration temperature on the H_2 separation potential of hydroxy sodalite zeolite membranes. Iranian Journal of Hydrogen & Fuel Cell 1.

Van Niekerk, A., Zah, J., Breytenbach, J.C., and Krieg, H.M. (2007). Direct crystallization of a hydroxy sodalite membrane without seeding using a conventional oven. J. Membr. Sci. 300, 156–164.

Wall, T., Stanger, R., and Santos, S. (2011). Demonstrations of coal-fired oxy-fuel technology for carbon capture and storage and issues with commercial deployment. International Journal of Greenhouse Gas Control 5, S5–S15.

Walton, R.I., Millange, F., O'Hare, D., Davies, A.T., Sankar, G., and Catlow, C.R.A. (2001). An in-situ energy-dispersive x-ray diffraction study of the hydrothermal crystallization of zeolite a. 1. Influence of reaction conditions and transformation into sodalite. J. Phys. Chem. B 105, 83–90.

Wang, C., Liu, X., Cui, R., and Zhang, B. (2009). In situ evaluation of defect size distribution for supported zeolite membranes. Journal of Membrane Science 330, 259–266.

Wang, H., Dong, X., and Lin, Y.S. (2014). Highly stable bilayer MFI zeolite membranes for high temperature hydrogen separation. Journal of Membrane Science 450, 425–432.

Wang, M., Joel, A.S., Ramshaw, C., Eimer, D., and Musa, N.M. (2015a). Process intensification for post-combustion CO_2 capture with chemical absorption: A critical review. Applied Energy 158, 275–291.

Wang, N., Mundstock, A., Liu, Y., Huang, A., and Caro, J. (2015b). Amine-modified Mg-MOF-74/CPO-27-Mg membrane with enhanced H_2/CO_2 separation. Chemical Engineering Science 124, 27–36.

Wang, B., Hu, N., Wang, H., Zheng, Y., and Zhou, R. (2015c). Improved $AlPO_4$-18 membranes for light gas separation. J. Mater. Chem. A 3, 12205–12212.

Wang, R., Liu, S.L., Lin, T.T., and Chung, T.S. (2002). Characterization of hollow fiber membranes in a permeator using binary gas mixtures. Chemical Engineering Science 57, 967–976.

Wang, S., Li, X., Wu, H., Tian, Z., Xin, Q., He, G., Peng, D., Chen, S., Yin, Y., Jiang, Z., et al. (2016). Advances in high permeability polymer-based membrane materials for CO_2 separations. Energy Environ. Sci. 9, 1863–1890.

Wang, Y., Zhao, L., Otto, A., Robinius, M., and Stolten, D. (2017). A review of post-combustion CO_2 capture technologies from coal-fired power plants. Energy Procedia 114, 650–665.

Wang, B., Zheng, Y., Zhang, J., Zhang, W., Zhang, F., Xing, W., and Zhou, R. (2019). Separation of light gas mixtures using zeolite SSZ-13 membranes. Microporous and Mesoporous Materials 275, 191–199.

Xu, J., Wang, Z., Zhang, C., Zhao, S., Qiao, Z., Li, P., Wang, J., and Wang, S. (2015). Parametric analysis and potential prediction of membrane processes for hydrogen production and pre-combustion CO_2 capture. Chemical Engineering Science 135, 202–216.

Xu, X., Yang, W., Liu, J., and Lin, L. (2001a). Synthesis of NaA zeolite membranes from clear solution. Microporous and Mesoporous Materials 43, 299–311.

Xu, X., Yang, W., Liu, J., and Lin, L. (2001b). Synthesis and perfection evaluation of NaA zeolite membrane. Separation and Purification Technology 25, 475–485.

Xu, X., Bao, Y., Song, C., Yang, W., Liu, J., and Lin, L. (2004). Microwave-assisted hydrothermal synthesis of hydroxy-sodalite zeolite membrane. Microporous and Mesoporous Materials 75, 173–181.

Yamaura, M., and Fungaro, D.A. (2013). Synthesis and characterization of magnetic adsorbent prepared by magnetite nanoparticles and zeolite from coal fly ash. J Mater Sci 48, 5093–5101.

Yang, S., Cao, Z., Arvanitis, A., Sun, X., Xu, Z., and Dong, J. (2016). DDR-type zeolite membrane synthesis, modification and gas permeation studies. Journal of Membrane Science 505, 194–204.

Yao, J., Wang, H., Ratinac, K.R., and Ringer, S.P. (2006). Formation of colloidal hydroxy-sodalite nanocrystals by the direct transformation of silicalite nanocrystals. Chem. Mater. 18, 1394–1396.

Yeo, Z.Y., Chew, T.L., Zhu, P.W., Mohamed, A.R., and Chai, S.-P. (2012). Conventional processes and membrane technology for carbon dioxide removal from natural gas: A review. Journal of Natural Gas Chemistry 21, 282–298.

Yin, X., Zhu, G., Wang, Z., Yue, N., and Qiu, S. (2007). Zeolite P/NaX composite membrane for gas separation. Microporous and Mesoporous Materials 105, 156–162.

Yong, Z., Mata, V., and Rodrigues, A.E. (2002). Adsorption of carbon dioxide at high temperature—a review. Separation and Purification Technology 26, 195–205.

Zaarour, M., Dong, B., Naydenova, I., Retoux, R., and Mintova, S. (2014). Progress in zeolite synthesis promotes advanced applications. Microporous and Mesoporous Materials 189, 11–21.

Zah, J., Krieg, H.M., and Breytenbach, J.C. (2007). Single gas permeation through compositionally different zeolite NaA membranes: Observations on the intercrystalline porosity in an unconventional, semicrystalline layer. Journal of Membrane Science 287, 300–310.

Zerta, M., Schmidt, P.R., Stiller, C., and Landinger, H. (2008). Alternative World Energy Outlook (AWEO) and the role of hydrogen in a changing energy landscape. International Journal of Hydrogen Energy 33, 3021–3025.

Zhang, X., Tong, D., Zhao, J., and Li, X. (2013). Synthesis of NaX zeolite at room temperature and its characterization. Materials Letters 104, 80–83.

Zhao, S., Feron, P.H.M., Deng, L., Favre, E., Chabanon, E., Yan, S., Hou, J., Chen, V., and Qi, H. (2016). Status and progress of membrane contactors in post-combustion carbon capture: A state-of-the-art review of new developments. Journal of Membrane Science 511, 180–206.

Zheng, Z., Hall, A.S., and Guliants, V.V. (2008). Synthesis, characterization and modification of DDR membranes grown on α-alumina supports. J Mater Sci 43, 2499–2502.

Zheng, Z., Guliants, V.V., and Misture, S. (2009). Sodalites as ultramicroporous frameworks for hydrogen separation at elevated temperatures: thermal stability, template removal, and hydrogen accessibility. J Porous Mater 16, 343–347.

Zhong, S., Bu, N., Zhou, R., Jin, W., Yu, M., and Li, S. (2016). Aluminophosphate-17 and silicoaluminophosphate-17 membranes for CO_2 separations. Journal of Membrane Science 520, 507–514.

Zhou, M., Korelskiy, D., Ye, P., Grahn, M., and Hedlund, J. (2014). A uniformly oriented MFI membrane for improved CO_2 separation. Angewandte Chemie 126, 3560–3563.

Zhu, M., Liang, L., Wang, H., Liu, Y., Wu, T., Zhang, F., Li, Y., Kumakiri, I., Chen, X., and Kita, H. (2019). Influences of acid post-treatment on high silica SSZ-13 zeolite membrane. Ind. Eng. Chem. Res. 58, 14037–14043.

Appendix A: Experimental Equipment



Figure A. 1 A 45 mL capacity autoclave (left) and LABOTEC EcoTherm® oven (right)



Figure A. 2 A 250 mL capacity autoclave

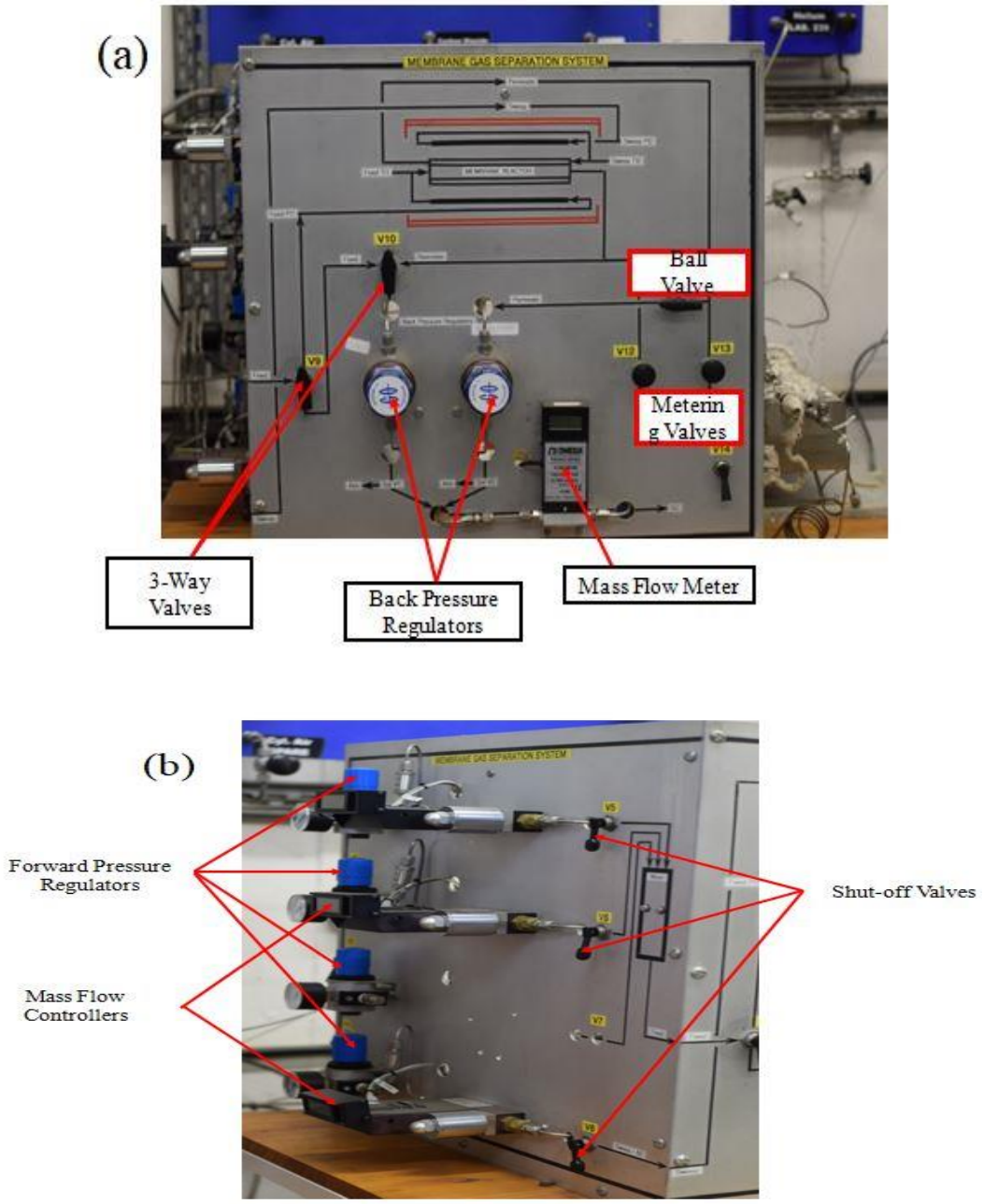

Figure A. 3 Membrane testing rig (a) front view (b) side view



Figure A. 4 Picture of feeding cylinders to the membrane gas separation testing rig



Figure A. 5 Picture of Bruker 430-GC used in this study

Appendix B: Membrane Equipment Process Flow Diagram

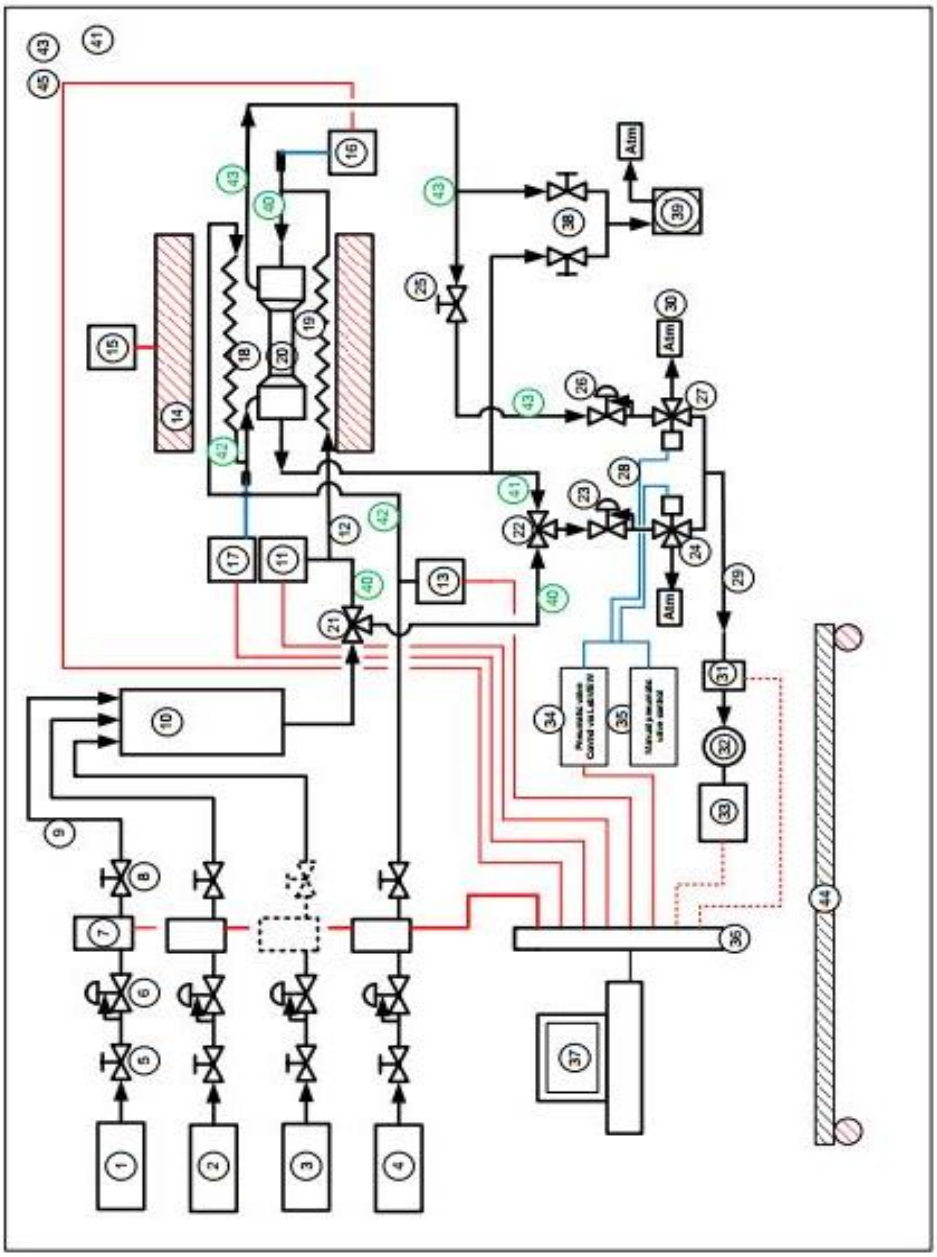

Figure B. 1 Detailed process flow diagram with component list

Table B. 1 Components of the membrane gas separation system

No	Description
1	Main feed gas: CO2
2	Make-up gas: N2
3	Secondary feed gas: CH4, etc.
4	Sweep gas: N2
5	Shut-off valves; 4x
6	Single-stage in-line regulators + 1/8” BSP fittings; 4x
7	Mass Flow Controllers + 1/8” BSP fittings; 3x
8	1/8” shut-off valves
9	1/8” SS tubing and Swagelok fittings
10	Gas mixer unit + 1/8” fittings
11	**Feed gas** electronic pressure transducer + 1/8” fittings + display + connector to NI LabVIEW DAC system.
12	**Feed gas** mixture gas line; 1/8” SS tubing + fittings.
13	**Sweep gas** electronic pressure transducer + 1/8” fittings + display + connector to NI LabVIEW DAC system.
14	Split level, ceramic band, clamp-on heater; ambient - 500°C.
15	Temperature control unit for heater.
16	Digital thermometer + type-K thermocouple (TC1) + DAC unit

17	Digital thermometer + type-K thermocouple (TC2) + DAC unit
18	Sweep gas heat exchanger.
19	Feed gas heat exchanger.
20	Membrane reactor + insert/membrane + seals.
20	Residue gas line + 1/8” fittings for easy access and membrane change.
21	1/8” Swagelok SS 3-way valve.
22	1/8” Swagelok SS 3-way valve.
23	GO Back-pressure regulator for feed/retentate gas line + fittings.
24	ASCO 3-way electro-pneumatic valve.
25	1/8” Swagelok SS ball valve.
26	GO Back-pressure regulator for permeate gas line + fittings.
27	ASCO 3-way electro-pneumatic valve.
28	Electric lines to the manual operation switch and the NI LabVIEW control system
29	1/8” SS gas line to the MFM, GC and column.
30	Exhaust to atmosphere.
31	Mass flow meter (MFM).
32	GC gas sampling valve + 1/8” fittings
33	GC
34	NI 240 VAC relay module to control the 3-way electro-pneumatic valves.
35	Manual valve control system.
36	NI LabVIEW DAC interface modules for recording temperature, pressure, and pneumatic valves.
37	PC/Laptop with LabVIEW customized software.
38	1/8” Swagelok SS metering valves.
39	Vacuum pump + fittings.

40 **Feed** gas mixture gas lines.

41 **Retentate** gas mixture gas lines.

42 **Sweep** mixture gas lines

43 **Permeate** gas mixture gas lines

44 Custom built trolley, instrument panels, support framework, power supplies, gas couplings, etc.

Appendix C: Procedures for Operating the Membrane Gas Separation Equipment

Five stages are involved to successfully operate the membrane gas separation system, which are highlighted below.

✓ Warming up of Mass Flow Meter (MFM) and Mass Flow Controller (MFC)

1. Close all forward pressure regulator (completely counter clockwise)
2. Open valves (V5, V6 & V8) connecting lines to the mixer
3. Set valve V9 to the back-pressure regulator line
4. Set valve V10 to the feed line
5. Set valve V11 to the back-pressure line
6. Close valve V12 and V13
7. Ensure that the two back pressure regulators are open
8. Turn the power on both 19'' instrument racks to ON
9. Set the electro-pneumatic valves control to Manual
10. Set the electro-pneumatic valve selection switch to OFF
11. Switch the power to the MFCs and MFM ON
12. Allow 10-15 minutes for the instruments to warm up and stabilize

✓ Setting the gas lines pressure and flow

1. Open laboratory main gas supplies and set to desired pressures
2. Open valves (V1, V2 & V4)
3. Adjust the individual gas inlet pressures to the desired pressure by adjusting the forward pressure regulators.
4. Adjust the mass flow control by turning carefully the right-hand screw of the MFC

✓ Loading and preparing the membrane module

1. Carefully place the membrane in the module, ensuring the membrane align with the module
2. Fix the graphite O-ring at both ends of the membrane module
3. Carefully screw in both end of the membrane to ensure it is gas-tight.
4. Position the membrane module in the oven and ensure that gas lines are leak proof

✓ **Setting the gas lines back pressures and reactor / furnace temperature**

1. Set valve V9 to the reactor
2. Set valve V10 to Retentate
3. Set valve V11 to Permeate
4. Adjust the pressure in the feed gas line by turning the GO back pressure regulator clockwise
5. Repeat the above for the sweep gas line

✓ **Analyzing the gas mixtures by GC, with manual or NI DAC & LabVIEW Control**

For the feed gas mixture

1. Switch valve V9 to the back-pressure regulator
2. Switch valve V10 to the feed position
3. Switch the gas line selector switch to FEED/RETENTATE
4. Trap the gas from the GC line and analyze with the GC until statistically repeatable results are obtained.

For the permeate gas

1. Switch valve V9 to the reactor
2. Switch valve V10 to the retentate position
3. Switch the gas line selector switch to FEED/RETENTATE
4. Trap the gas from the GC line and analyze with the GC until statistically repeatable results are obtained.
5. Repeat the above till the desired results are obtained

Appendix D: Published Works

KeAi

Materials Science for Energy Technologies

Available online 23 October 2019

In Press, Journal Pre-proof



Synthesis and evaluation of a nanocomposite hydroxy sodalite/ceramic (HS/ceramic) membrane for pre-combustion CO_2 Capture: characterization and permeation test during CO_2/H_2 separation

O. Oloye, O. Eterigho-Ikelegbe, M.O. Daramola

Show more

https://doi.org/10.1016/j.mset.2019.10.005

Get rights and content

Under a Creative Commons license

open access

Highlights

- Nanocomposite HS/ceramic membrane was prepared via one-stage and two-stage pore-plugging hydrothermal (PPH) synthesis technique.
- Two-stage PPH prepared membranes displayed an improved quality compared to one obtained via the one-stage PPH synthesis.
- Maxwell-Stefan model describes well H_2 permeation behaviour through the membrane prepared via the two-stage PPH synthesis.
- The findings in this study could serve as a platform for R & D in membrane materials for pre-combustion CO_2 capture.

Abstract

Greenhouse gases (GHGs), secondary products from combustion of fossil fuel, have been instrumental to global warming which causes climate change. However, carbon capture, storage and utilization (CCSU) is one of the promising ways to reducing CO_2 emission from large point sources via pre-combustion CO_2 capture. Membrane technology has been identified as one of the promising technologies for

Applied Nanoscience - Submission Confirmation Synthesis of high purity hydroxy sodalite nanoparticles via pore-plugging hydrothermal method for inorganic membrane development: Effect of synthesis variables on crystallinity, crystal size and morphology for co-author

Inbox x

Applied Nanoscience (APNA) <em@editorialmanager.com>

Sat, 2 Nov, 14:56 (3 days ago)

to me

Re: "Synthesis of high purity hydroxy sodalite nanoparticles via pore-plugging hydrothermal method for inorganic membrane development: Effect of synthesis variables on crystallinity, crystal size and morphology"
Full author list: Orevaoghene Eterigho-Ikelegbe; Samson Bada, PhD; Michael Daramola, PhD; Rosemary Falcon, PhD

Dear mr Orevaoghene Eterigho-Ikelegbe,

We have just received the submission entitled: "Synthesis of high purity hydroxy sodalite nanoparticles via pore-plugging hydrothermal method for inorganic membrane development: Effect of synthesis variables on crystallinity, crystal size and morphology" for possible publication in Applied Nanoscience, and you are listed as one of the co-authors.

The manuscript has been submitted to the journal by Prof Michael Daramola who will be able to track the status of the paper through his/her login.

If you have any objections, please contact the editorial office as soon as possible. If we do not hear back from you, we will assume you agree with your co-authorship.

Thank you very much.

With kind regards,

Springer Journals Editorial Office
Applied Nanoscience

(Ctrl)

Appendix E: Plagiarism Report

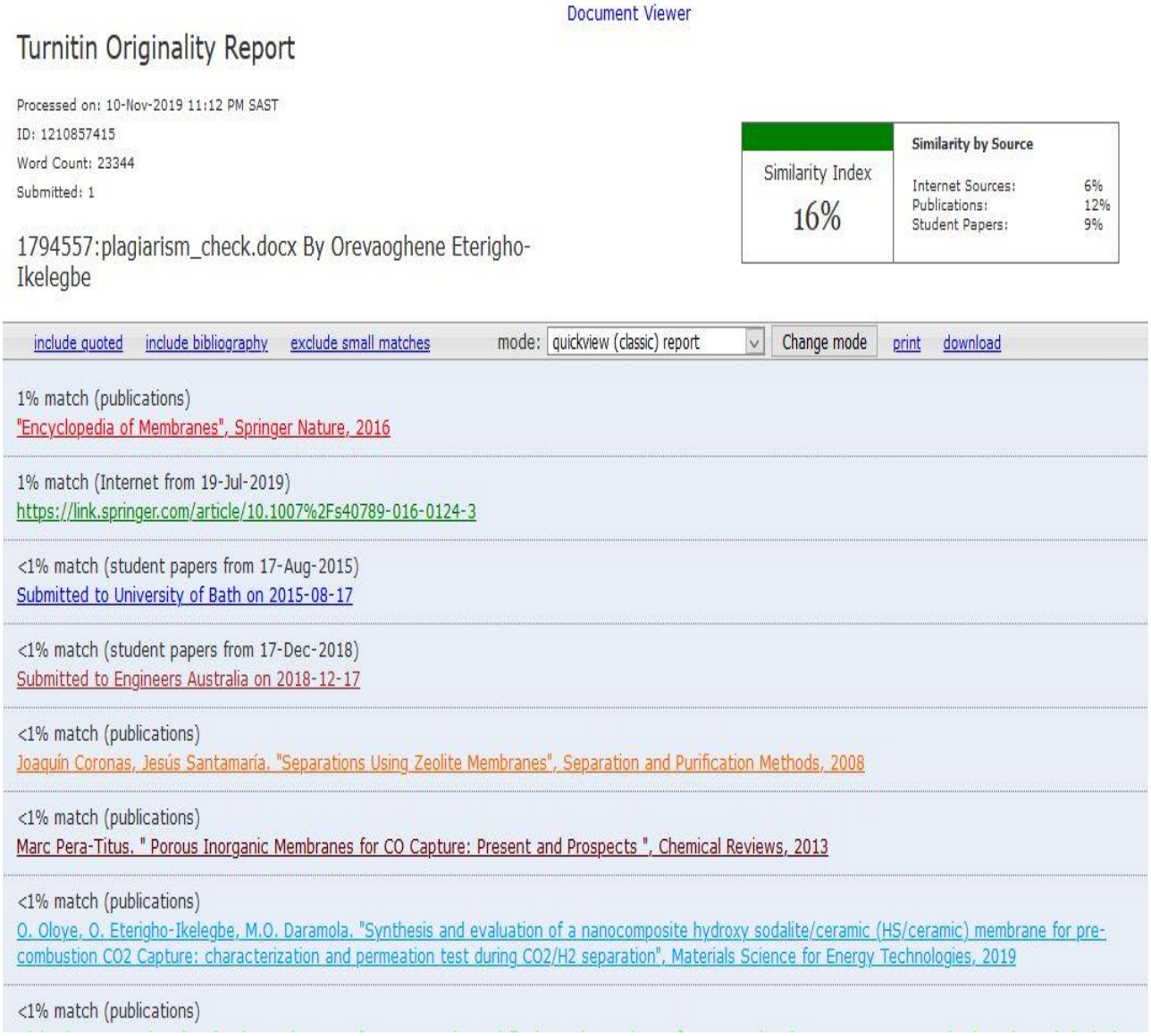

Document Viewer

Turnitin Originality Report

Processed on: 10-Nov-2019 11:12 PM SAST
ID: 1210857415
Word Count: 23344
Submitted: 1

1794557:plagiarism_check.docx By Orevaoghene Eterigho-Ikelegbe

Similarity Index	Similarity by Source	
16%	Internet Sources:	6%
	Publications:	12%
	Student Papers:	9%

include quoted | include bibliography | exclude small matches | mode: quickview (classic) report | Change mode | print | download

1% match (publications)
"Encyclopedia of Membranes", Springer Nature, 2016

1% match (Internet from 19-Jul-2019)
https://link.springer.com/article/10.1007%2Fs40789-016-0124-3

<1% match (student papers from 17-Aug-2015)
Submitted to University of Bath on 2015-08-17

<1% match (student papers from 17-Dec-2018)
Submitted to Engineers Australia on 2018-12-17

<1% match (publications)
Joaquín Coronas, Jesús Santamaría. "Separations Using Zeolite Membranes", Separation and Purification Methods, 2008

<1% match (publications)
Marc Pera-Titus. " Porous Inorganic Membranes for CO Capture: Present and Prospects ", Chemical Reviews, 2013

<1% match (publications)
O. Oloye, O. Eterigho-Ikelegbe, M.O. Daramola. "Synthesis and evaluation of a nanocomposite hydroxy sodalite/ceramic (HS/ceramic) membrane for pre-combustion CO2 Capture: characterization and permeation test during CO2/H2 separation", Materials Science for Energy Technologies, 2019

<1% match (publications)